WCAP-14168

CONDENSATION IN THE PRESENCE OF NONCONDENSIBLE GASES: AP600 CONTAINMENT SIMULATION

September 1994

AP600 DOCUMENT COVER SHEET

TDC: _____ IDS: I _____ S _____

Form 58202G(5/94) [t:\xxxx.wpt:1x]
0058.FRM

AP600 CENTRAL FILE USE ONLY:

RFS#: RFS ITEM #:

AP600 DOCUMENT NO.	REVISION NO.		ASSIGNED TO
PCS-T2R-040	0	Page 1 of ___	

ALTERNATE DOCUMENT NUMBER: WORK BREAKDOWN #: 2.6.6.3

DESIGN AGENT ORGANIZATION: Westinghouse Electric Corporation

TITLE: Condensation in the Presence of Noncondensable Gases: AP600 Containment Simulation

ATTACHMENTS:	DCP #/REV. INCORPORATED IN THIS DOCUMENT REVISION:
CALCULATION/ANALYSIS REFERENCE:	

ELECTRONIC FILENAME	ELECTRONIC FILE FORMAT	ELECTRONIC FILE DESCRIPTION
N/A	N/A	

☐ WESTINGHOUSE PROPRIETARY CLASS 2
This document contains information proprietary to Westinghouse Electric Corporation; it is submitted in confidence and is to be used solely for the purpose for which it is furnished and returned upon request. This document and such information is not to be reproduced, transmitted, disclosed or used otherwise in whole or in part without prior written authorization of Westinghouse Electric Corporation, Energy Systems Business Unit, subject to the legends contained hereof.

☐ WESTINGHOUSE PROPRIETARY CLASS 2C
This document is the property of and contains Proprietary Information owned by Westinghouse Electric Corporation and/or its subcontractors and suppliers. It is transmitted to you in confidence and trust, and you agree to treat this document in strict accordance with the terms and conditions of the agreement under which it was provided to you.

☒ WESTINGHOUSE CLASS 3 (NON PROPRIETARY)

COMPLETE 1 IF WORK PERFORMED UNDER DESIGN CERTIFICATION OR COMPLETE 2 IF WORK PERFORMED UNDER FOAKE.

1 ☒ DOE DESIGN CERTIFICATION PROGRAM - GOVERNMENT LIMITED RIGHTS STATEMENT [See page 2]

Copyright statement: A license is reserved to the U.S. Government under contract DE-AC03-90SF18495.

☒ DOE CONTRACT DELIVERABLES (DELIVERED DATA)
Subject to specified exceptions, disclosure of this data is restricted until September 30, 1995 or Design Certification under DOE contract DE-AC03-90SF18495, whichever is later.

EPRI CONFIDENTIAL: NOTICE: 1 ☐ 2 ☐ 3 ☐ 4 ☐ 5 ☐ CATEGORY: A ☐ B ☐ C ☐ D ☐ E ☐ F ☐

2 ☐ ARC FOAKE PROGRAM - ARC LIMITED RIGHTS STATEMENT [See page 2]

Copyright statement: A license is reserved to the U.S. Government under contract DE-FC02-NE34267 and subcontract ARC-93-3-SC-001.

☐ ARC CONTRACT DELIVERABLES (CONTRACT DATA)
Subject to specified exceptions, disclosure of this data is restricted under ARC Subcontract ARC-93-3-SC-001.

ORIGINATOR	SIGNATURE/DATE	
E. F. Peters	[signature] 8/29/94	
AP600 RESPONSIBLE MANAGER	SIGNATURE*	APPROVAL DATE
E. J. Piplica	E. J. Piplica	8/30/94

*Approval of the responsible manager signifies that document is complete, all required reviews are complete, electronic file is attached and document is released for use.

AP600 DOCUMENT COVER SHEET

Form 58202G(5/94)

LIMITED RIGHTS STATEMENTS

DOE GOVERNMENT LIMITED RIGHTS STATEMENT

(A) These data are submitted with limited rights under government contract No. DE-AC03-90SF18495. These data may be reproduced and used by the government with the express limitation that they will not, without written permission of the contractor, be used for purposes of manufacturer nor disclosed outside the government; except that the government may disclose these data outside the government for the following purposes, if any, provided that the government makes such disclosure subject to prohibition against further use and disclosure:

(I) This "Proprietary Data" may be disclosed for evaluation purposes under the restrictions above.

(II) The "Proprietary Data" may be disclosed to the Electric Power Research Institute (EPRI), electric utility representatives and their direct consultants, excluding direct commercial competitors, and the DOE National Laboratories under the prohibitions and restrictions above.

(B) This notice shall be marked on any reproduction of these data, in whole or in part.

ARC LIMITED RIGHTS STATEMENT:

This proprietary data, furnished under Subcontract Number ARC-93-3-SC-001 with ARC may be duplicated and used by the government and ARC, subject to the limitations of Article H-17.F. of that subcontract, with the express limitations that the proprietary data may not be disclosed outside the government or ARC, or ARC's Class 1 & 3 members or EPRI or be used for purposes of manufacture without prior permission of the Subcontractor, except that further disclosure or use may be made solely for the following purposes:

This proprietary data may be disclosed to other than commercial competitors of Subcontractor for evaluation purposes of this subcontract under the restriction that the proprietary data be retained in confidence and not be further disclosed, and subject to the terms of a non-disclosure agreement between the Subcontractor and that organization, excluding DOE and its contractors.

DEFINITIONS

CONTRACT/DELIVERED DATA — Consists of documents (e.g. specifications, drawings, reports) which are generated under the DOE or ARC contracts which contain no background proprietary data.

EPRI CONFIDENTIALITY / OBLIGATION NOTICES

NOTICE 1: The data in this document is subject to no confidentiality obligations.

NOTICE 2: The data in this document is proprietary and confidential to Westinghouse Electric Corporation and/or its Contractors. It is forwarded to recipient under an obligation of Confidence and Trust for limited purposes only. Any use, disclosure to unauthorized persons, or copying of this document or parts thereof is prohibited except as agreed to in advance by the Electric Power Research Institute (EPRI) and Westinghouse Electric Corporation. Recipient of this data has a duty to inquire of EPRI and/or Westinghouse as to the uses of the information contained herein that are permitted.

NOTICE 3: The data in this document is proprietary and confidential to Westinghouse Electric Corporation and/or its Contractors. It is forwarded to recipient under an obligation of Confidence and Trust for use only in evaluation tasks specifically authorized by the Electric Power Research Institute (EPRI). Any use, disclosure to unauthorized persons, or copying this document or parts thereof is prohibited except as agreed to in advance by EPRI and Westinghouse Electric Corporation. Recipient of this data has a duty to inquire of EPRI and/or Westinghouse as to the uses of the information contained herein that are permitted. This document and any copies or excerpts thereof that may have been generated are to be returned to Westinghouse, directly or through EPRI, when requested to do so.

NOTICE 4: The data in this document is proprietary and confidential to Westinghouse Electric Corporation and/or its Contractors. It is being revealed in confidence and trust only to Employees of EPRI and to certain contractors of EPRI for limited evaluation tasks authorized by EPRI. Any use, disclosure to unauthorized persons, or copying of this document or parts thereof is prohibited. This Document and any copies or excerpts thereof that may have been generated are to be returned to Westinghouse, directly or through EPRI, when requested to do so.

NOTICE 5: The data in this document is proprietary and confidential to Westinghouse Electric Corporation and/or its Contractors. Access to this data is given in Confidence and Trust only at Westinghouse facilities for limited evaluation tasks assigned by EPRI. Any use, disclosure to unauthorized persons, or copying of this document or parts thereof is prohibited. Neither this document nor any excerpts therefrom are to be removed from Westinghouse facilities.

EPRI CONFIDENTIALITY / OBLIGATION CATEGORIES

CATEGORY "A" — (See Delivered Data) Consists of CONTRACTOR Foreground Data that is contained in an issued reported.

CATEGORY "B" — (See Delivered Data) Consists of CONTRACTOR Foreground Data that is not contained in an issued report, except for computer programs.

CATEGORY "C" — Consists of CONTRACTOR Background Data except for computer programs.

CATEGORY "D" — Consists of computer programs developed in the course of performing the Work.

CATEGORY "E" — Consists of computer programs developed prior to the Effective Date or after the Effective Date but outside the scope of the Work.

CATEGORY "F" — Consists of administrative plans and administrative reports.

x

Executive Summary

The Westinghouse Electric Corporation has designed an advanced pressurized light water reactor, AP600. This reactor is designed with a passive cooling system to remove sensible and decay heat from the containment. The heat removal path involves condensation heat transfer, aided by natural convective forces generated by buoyancy effects. A one-twelfth scale slice of the proposed upper region of the reactor containment has been constructed at the University of Wisconsin to simulate conditions anticipated from transients and accidents that may occur in a full scale containment vessel under a variety of conditions. Similitude of the test facility was obtained by considering the appropriate dimensionless group for the natural convective process (modified Froude number) and the aspect ratio (H/R) of the containment vessel.

The support structure was constructed of steel and aluminum with a front and back face of clear polycarbonate plates to allow visualization of the developed flow patterns in the cavity. The test section incorporates the ability to vary the flow rate of pressurized steam through a steam injection port located at the bottom of the facility over a wide range of conditions, allowing appropriate quasi-steady state conditions to develop at atmospheric pressure. Previous investigations have been conducted to measure the heat transfer coefficients of a condensing surface in the presence of non-condensable gases, however they primarily consist of small cavities with one fixed orientation of the cooled condensing surface. The present test facility has been designed with a horizontal and a vertical condensing surface made of two 3.81cm thick aluminum 2024 plates positioned in the corner of a (152.4 cm x 228.6 cm x 30.48 cm) rectangular cavity. The aluminum condensing surface was coated with a 0.0095cm thick layer of inorganic zinc paint similar to the actual AP600 surface treatment. This promoted filmwise condensation and simulated the actual containment vessel surface wetting conditon.

An experimental investigation to determine the heat transfer coefficient associated with the condensing surfaces, along with axial temperature profiles of the test section at several different inlet steam mass flow rates and test section temperatures was conducted. In this series of experiments the air mass fraction varied between (0.9 - 0.4) with corresponding mixture temperatures of 60-90 °C. The heat transfer coefficient associated with the top horizontal surface varied from (82 - 296) W/m^2K and the vertical side plate heat transfer coefficient varied from (70 - 268) W/m^2K. The heat transfer coefficients were found and compared using two independent methods, an energy balance on the coolant used to cool the condensing plates and a differential temperature measurement at various locations in the aluminum plate. The heat transfer coefficients for various test section temperatures were measured with the two different methods of measurement (Type E thermocouples were used in both measurements and the millivolt readings were collected by a Keithley 500 Data Acquisition System). Several tests were conducted to ensure reproducibility of the facility. Results were found to yield values of the heat transfer coefficients to within a few percent of any given test, at each of the various conditions. The results were then compared to previously published studies of smaller scale similar configurations and were found to be consistent with past reported results [1]. The report discusses this data in some detail along with the effect of various steam inlet flow patterns and gas compositions.

This facility differs from previous studies in that it has a similar aspect ratio to the AP600. In past tests this was not the case and some of the important aspects of heat transfer phenomena may have been overlooked. Among these effects is the possible enhancement of the overall heat transfer rate due to mixed convection effects as the length scale increases. The design of the facility allows possible visual observation of gas mixture flow patters as well as velocities. One major draw back to the present facility is the inability to acquire data at higher pressures (2-4 bar absolute). A similar test section design has been proposed to handle these higher pressures.

Nomenclature

A	Area
C_d	Discharge coefficient
C_g	Vapor Concentration of bulk
C_w	Vapor Concentration at Wall
C_p	Heat Capacity
D_o	Diffusion Coefficient
h	Heat Transfer Coefficient
i	Enthalpy
k	Conductivity
L	Length
M	Molecular Weight
m	mass
p	Pressure
q''	Heat Flux
T_{back}	Back of Condensing Plate Temperature
T_{bulk}	Bulk gas Temperature
T_{cool}	Coolant Temperature
T_{mix}	Mixture Temperature
T_{wall}	Coolant Wall Temperature
V	Volume Flow Rate
V_a	Atomic Volume of air
V_b	Atomic Volume of H_2O
x	mass fraction

Dimensionless Numbers

Gr	Grashoff Number
Fr	Froude Number
Nu	Nusselt Number
Pr	Prandlt Number
Sc	Schmidt Number

Greek Symbols

κ_m	Mass Transfer Coefficient
ρ	Density
σ	Error in Value
Σ	Summation of Elements
θ	Correction Factor for Mass Transfer Correlation

Table of Contents

List of Figures

List of Tables

Chapter 1

Introduction

A primary concern involved in the safety of nuclear power generation is the prevention or mitigation of an accident occurring in which radioactive by-products may be released into the atmosphere. To mitigate such an accident it is necessary to provide a containment system sufficient to contain these materials , under several accidental scenarios. One such event is a primary system pipe break, in which a large amount of primary system water discharges and flashes into steam. This will cause an increase in pressure and temperature in the containment atmosphere. This increase in the pressure and temperature must be controlled by some mechanism before the containment structural integrity is compromised. The mechanisms which are currently in use for operating light water reactors rely principally on active safety systems to spray cold water into the containment to condense this steam. These active systems require the use of AC power to drive the injection pumps, which must be supplied by either backup diesel generators or off-site power. This not only adds further cost to the plant construction but also more mechanical components whose reliability must be considered in the event of an accident. New advanced reactor designs have included the use of passive cooling techniques which seek to take advantage of the natural circulation processes within containment eliminating costly

mechanical components and adding improved reliability. The Westinghouse Electric Corporation has designed a 600 MWe pressurized light water reactor (AP600) that utilizes these concepts integrated into the passive safety systems.

The AP600 utilizes a passive containment cooling system (PCCS) to transfer sensible and core decay heat from within the reactor containment to the atmosphere in the case of an accident without compromising the containment vessel. The PCCS incorporates large water reservoirs situated above the containment vessel that are opened and allowed to flow by gravity over the containment shell, assisting natural circulation in removing heat primarily during the initial hours of an accident when the core decay heat is high. Figure 1.1 shows the layout of the AP600's proposed design. A water film is developed from the flow of water over the outer surface of the steel containment which provides evaporative cooling thus increasing the heat transfer coefficient on the outside of containment. As a result of the cooled steel containment shell, the steam inside the containment condenses on the inner containment wall, which can increase the heat removal ability to the containment structure. The energy transferred and steam condensed on the inside of the containment is controlled by the presence of noncondensable gases in the containment volume, which forms a barrier that the steam must diffuse through before condensing. It is the combination of these heat transfer coefficients which determine the overall heat removal rate; each being a significant heat transfer resistance. It is vital to have good estimates of the heat removal rate associated with the evaporation of the water film on the outside of the containment and the energy transferred by condensation of the steam in the presence of noncondensable gases [1] on the inside of containment, to ensure that the reactor containment will be able to remove the necessary energy required to keep the containment intact, during the various stages of an accident

A series of experiments investigating the condensation of steam in the presence of noncondensable gas was conducted to model such accident scenarios and to measure the resulting heat transfer coefficient from steam condensation on the inner wall of containment. Several tests were

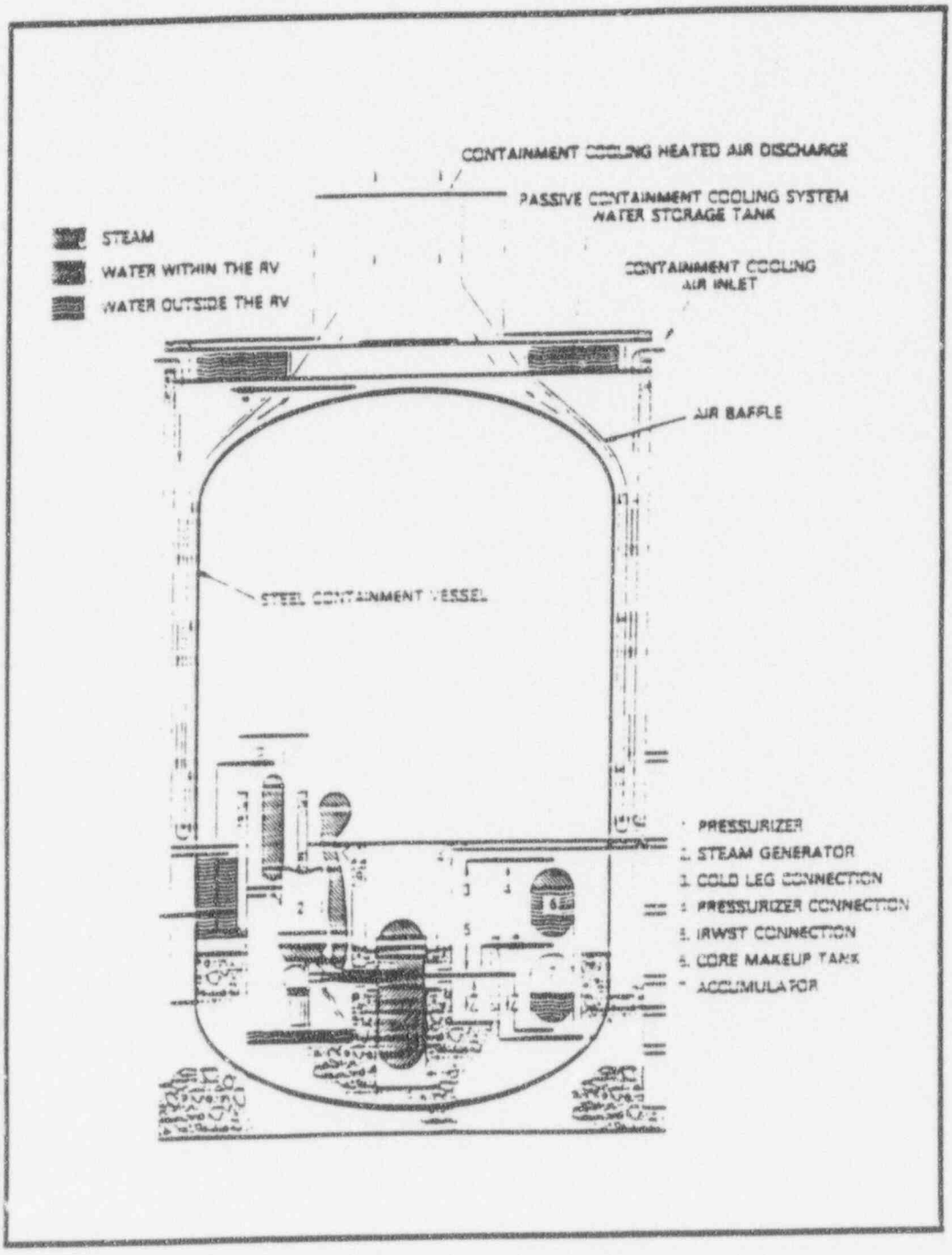

Fig.1.1: Passive Safety Fueatures of Westinghouse AP-600 Design

preformed with differing ratios of air, helium, and steam to quantify the effects of noncondensable gas that may be present in the containment during an accident.

The effect of the noncondensable gas barrier may also be related to the position and the location of the injected steam therefore, tests varying the location of steam injections were conducted. In an effort to understand the heat transfer coefficients found during the experiments it is necessary to obtain data on the natural circulation velocity field developed in the test section, so methods are being developed to measure and quantify the associated velocities near the condensing walls. Some preliminary data is provided in this area.

1.1 Air/Steam Experiments

To investigate the condensation of steam in the presence of the noncondensible gas we explored the effects of the heat transfer coefficient on a horizontal and a vertical cooled wall in an environment of varying concentrations of air and steam. The tests were conducted at atmospheric pressure and various temperatures of saturated steam. These scoping tests provide the heat transfer coefficients under a range of conditions where a break in a pipe would cause an influx of steam to rise and condense on the cooled steel containment structure. The experimental observations were then compared with previous experiments of the same nature [1,2,3] and used as a reference to compare tests with varying light gas concentrations and more prototypic geometries.

1.2 Helium/Air/Steam Experiments

In the event that primary system cooling water is lost and temperatures in the reactor core rise to levels high enough for water to start reacting with the fuel cladding of zircaloy metal, hydrogen gas may be produced. Oxidation of the cladding due to the presence of water may introduce hydrogen in bulk concentrations of 0-10% molar. This production of a light noncondensable gas may alter the rate of

steam condensation on the containment structure not only by increasing the layer of noncondensible gas the steam must diffuse through, but also due to the small molecular weight of hydrogen which may preferentially collect near the upper condensing surfaces. Therefore, it is necessary to examine the effects on the heat transfer coefficient due to the introduction of a light weight noncondensable gas.

Tests were conducted to study these effects using helium gas instead of hydrogen. This was chosen due to the obvious hazards of working with hydrogen and the close similarities between the two gases. In these experiments air and helium were mixed so the helium molar concentrations varied from 3-32% prior to the injection of steam. Then steam was injected at mass flow rates which would produce steady state temperatures of 60-90 °C.

1.3 Steam Injection

Two different steam injection configurations have been considered. The majority of tests were conducted with a uniform steam injection system located at the bottom of the test section. This consisted of a 1" IPS aluminium pipe with 19 uniformly spaced injection nozzles with an inside opening of 3/16". This injection produced a uniform distribution of steam into the test section with mass flow rates between (0.0012 kg/sec - 0.0058 kg/sec). The second steam inlet configuration was constructed to model a pipe rupture in the steam generator room of the AP600 containment. In this scenario steam would enter the containment atmosphere at a level of approximately 4 meters above the operating deck of the AP600 through an opening of about 25 sq.m. The position of the steam generator can be seen in the schematic in Figure 1.1. This steam injection system consisted of 1" IPS pipe formed in a configuration that would represent a scaled version of a steam generator rupture.

Chapter 2

Literature Review

A complete review of earlier works was discussed in detail by Huhtiniemi in 1991 and updated by Pernsteiner in 1993. The following review of work in the area of condensation heat transfer was adapted from Pernsteiner. Two separate classifications of the research were formed to allow for a consistent way to present the different studies.

1. *Separate Effects Experiments*

   In this classification a simple relatively small test geometry is used to isolate one or a few of the effects of condensation. Typically, time dependence is eliminated, and the tests are conducted at steady state temperatures to simplify the measurement procedure.

2. *Intergral/Large Scale Experiments*

   This classification includes large facilities that are designed to study realistic flow geometries along with transient behavior to simulate actual containment situations. Generally these tests are too complex to obtain much information about individual factors that contribute to the heat transfer.

An investigation of these two different classifications is given in Reference [2]. Table 2.1 gives some of the measurements found in different separate effects tests.

Parameter	Barry[18]	Dallmeyer[19]	Debhi[20]	Gerstmann[21]	Henderson[22]
Gas	air	air	air,He	air	air
Vapor	steam	CCL_4,C_6H_6	steam	freon-113	steam
T_{max}[°C]	51.3-88.2	95	sat	NA	NA
m_{air}/m_{tot}	0.47-0.92	0.02-0.16	0.25-0.9	trace	0.1-0.83
v_{mix}[m/s]	2.1-6.9	1-13	0	0	NA
ϕ[°]	180	90	90	0-90	180
P[MPa]	0.1	sat	0.15-0.45	0.1	Na
ΔT [°C]	26.3-63.2	55-85	10-65	4.3-39.4	Na
Geom	plate	plate	tube	plate	tube
L/D	610	410	3500/38	457.2	1220/29

Cho[23]	Kroger[24]	Kutsuna[25]	Robinson[26]	Slegers[27]	Spencer[28]
air	Ar,He	air	air	air	N_2,Co_2,He
steam	potassium	steam	steam	steam	freon-113
sat	598-768	85-90	sat	26.7-65.6	sat
0-1.4e5	Na	0.42-0.55	0.16-0.87	0-0.01	0-0.03
0	0	4-5.3	<2m/s,Na	0	0
0	0	180	90	90	90
0.31-1.24	sat	0.1	0.27-6.2	0.004-0.03	Na
35-100	2.3-733	5.0-15	4.0-10	1.4-20.8	Na
disk	disk	plate	disk	plate	tube
137	101.6	800	46	127	Na/Na

Table 2.1 Summary of Previous Investigations

2.1 Recent work

2.1.1 Separate Effects Studies

Since the extensive review by Huhtiniemi there has been some new and relevant work done in the area of condensation heat transfer. A summary of some of the separate effects results is given in Table 2.2. The following summary of previous investigations into condensation heat transfer was adapted form Pernsteiner Ref. [3], with the addition of a short description of his work.

Lu and Suryanarayana [14] investigated vapor flow inside a horizontal rectangular duct. The vapors used in the study were R-113 and its proposed replacement FC-72™. The heat transfer coefficient was found to increase with increasing inlet vapor velocity, and an enhancement of the heat transfer coefficient was observed upon the appearance of interfacial waves. These effects have been observed before, and were verified here for the CFC R-113 and its replacement. The results were correlated by two separate equations for the wave free regime, and another for the wavy regime.

Fox et. al. [15] studied steam-helium and steam-air mixtures inside a reflux condenser tube. It was found that transport phenomena were greatly affected by the stability of the component combinations used in the condenser. In general, stable flow patterns were observed when helium gas, with a molecular weight less than that of vapor, was used in the condenser, and unstable flow patterns developed for the cases when a noncondensable gas heavier than the vapor was implemented. Stable conditions were observed for both noncondensable gas loadings at high vapor mass fractions (0.95). It was found that certain unstable conditions exist which result in oscillatory recirculation regions which exhibit small temporal fluctuations. The results indicate that simple models which assume a stable gas/temperature front are not valid when using noncondensables with a molecular weight greater than the condensing vapor.

Siddique et. al [16] measured the local condensation heat transfer coefficient of steam, in the presence of air, in a vertical tube, with a downward flow. The experiment was developed to model condensation heat transfer inside the isolation condenser, a component of the General Electric SBWR passive cooling

Parmeter	LU [14]	Fox[15]	Siddique[16]	Kang/Kim[17]
Gas	none	air,He	air	air
Vapor	R-113/FC-72	steam	steam	steam
T_{max}[°C]	50/60	sat	100-140	Na
m_{ga}/m_{tot}	----	0.75-0.95	0.10-0.35	0-1.0
v_{max}[m/s]	0.3-4.4	0.2	Na	3
ϕ [°]	180	90	90	184.1
P[Mpa]	sat	0.1	sat	0.1
Geom	plate	tube	tube	plate
L/D	40	8.1	55	15.2

Table 2.2 Summary of Recent Work

system. The inlet air mass fraction ranged from 0.10 to 0.35, with mixture inlet temperatures of 100, 120 and 140°C. The local Nusselt number increased with the mixture Reynolds number and decreased with increased noncondensable mass fraction. A model was developed to predict local heat transfer coefficients on the inside of the tubes, for the range of condition studied in the test series.

Kang and Kim [17] investigated the effect of noncondensable gas and a wavy water film on condensation heat transfer. A water film was injected into a 1.52 m long rectangular channel, at steady state thermal conditions, to produce a wavy film condition. Data was collected for varying air mass fractions (0-0.78), mixture velocities (1-7 m/s), and film flow rates. Even small amounts of noncondensable gas were seen to greatly affect condensation heat transfer rates. The waviness of the condensate film also increased the heat transfer as listed previously.

Pernsteiner [3] investigated a series of forced flow tests with a horizontal, downward facing condensing plate coated with inorganic zinc paint. The tests were conducted with variable mass fractions varying from 0.65-0.78, velocities ranging from 1.0 to 2.1 m/s and helium concentrations between 0 and 39 percent of the total noncondensible content. A second series of investigations was conducted to study the effects of natural convection. These tests were conducted with the condensing plate in a vertical position. The mass fraction of noncondensables was varied from 0.33 to 0.92 with helium molar fractions ranging from 0 to 30 percent. It was found that the previously reported inhibiting effects of the light noncondensable gas (helium) was not observed except when helium concentrations became greater than 30%. Figure 2.1 is a diagram of the experimental facility used.

2.1.2 Integral Experiments

Separate effects tests provide increasing knowledge of the processes of condensation heat transfer, however they may not always be scaled to larger facilities. This leads to the importance of large scale tests to investigate effects not seen by the separate effects studies, ie mixed convection, gas

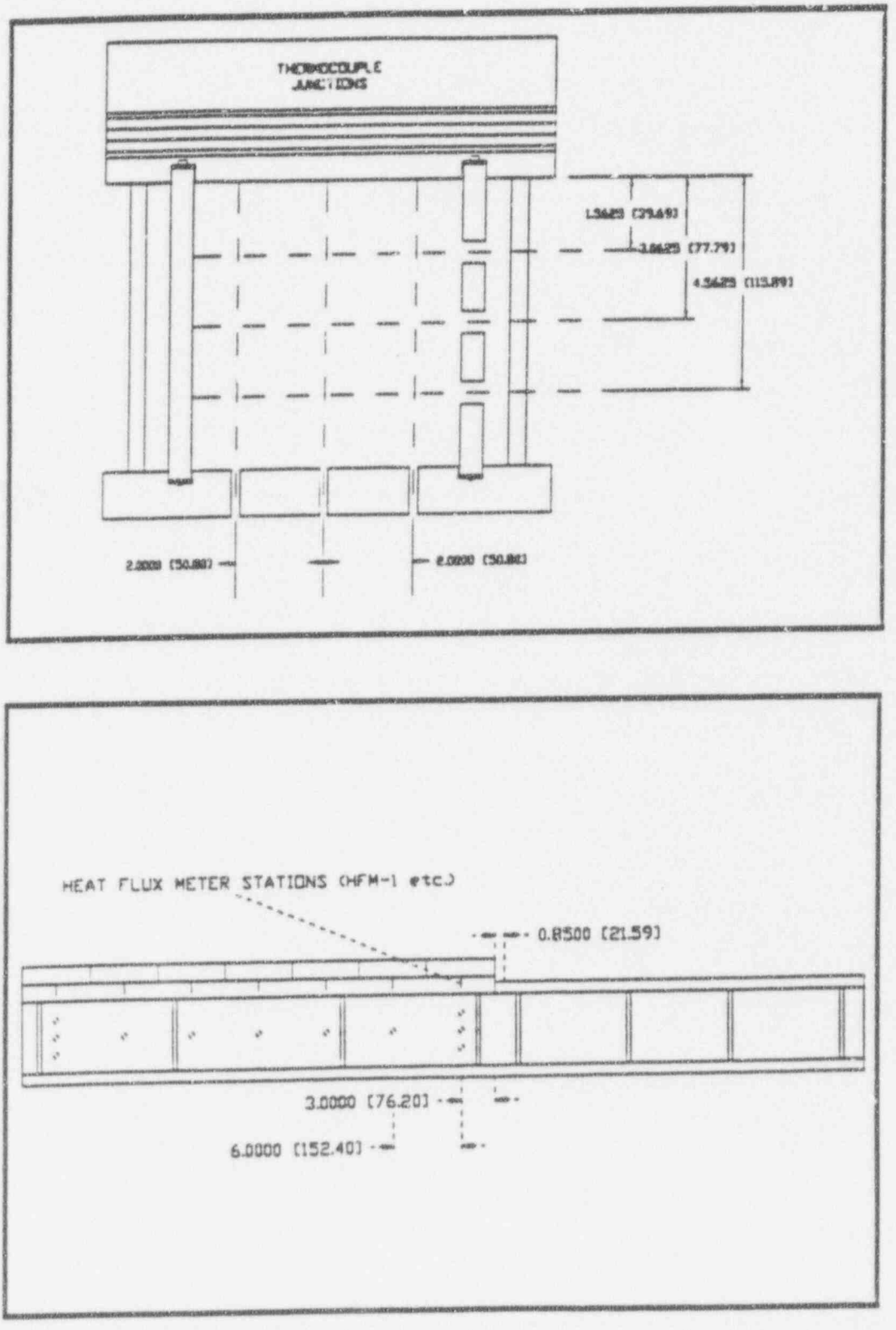

Figure 2.1 Schematic of Pernsteiner's Experimental Apparatus

concentrations, temperatures, flow fields, and system pressure that would occur in containment during an accident.

Westinghouse has carried out several large scale tests involving an externally cooled containment structure similar to that proposed for the AP600. The testing of an 1/8th scale facility allows measurements of local heat fluxes and heat transfer rates at both the inside and outside of containment. They have studied the effects of steam injection location and noncondensable mixture mole fractions on the total heat transfer along with several other investigations.

A second series of large scale integral tests is being performed at the Paul Scherrer Institute, which is very similar to the work being done by Westinghouse, except for the SBWR . They have constructed a 1/10 linear scale SBWR at full height to provide experiments to General Electric on the performance characteristics of their new simplified boiling water reactor and its passive containment system.

2.2 Justification for Current Study

The major motivation behind the current experiments is to find representative values for the condensation heat transfer coefficient under a wide variety of conditions from a facility similar to the Westinghouse AP600. Westinghouse has employed a combination of separate effects experiments along with integral experiments to try to document the effects of the heat and mass transfer phenomena. The University of Wisconsin has shared in this effort by conducting several separate effects tests over the years. Barry, Kim, Huhtiniemi, and Pernsteiner have investigated the heat transfer rate on metal surfaces with similar finishes as the AP600 containment (see Appendix 5 for bibliography). They have investigated several different parameters that effect this heat transfer (ie. temperature, mass ratio, gas composition, pressure, and cold wall orientation). One of the major limitations to the previous studies conducted is the representation of only a small portion of the cooled containment wall. This limitation was necessary to evaluate some of the previously mentioned parameters, however it may have also

caused them to overlook important aspects of the heat transfer phenomena. One major aspect is the enhancement of the heat transfer due to mixed convection effects. This was first noted by Huhtiniemi in his experimental results [2].

The present investigation is an effort to gain additional understanding of the heat and mass transfer phenomena in this mixed convection regime. Therefore, the experimental facility was constructed with a similar aspect ratio to that of the AP600 containment. The design of the facility is such that velocity fields, which are imperative to the understanding of the heat and mass transfer can be observed through clear polycarbonate sheets on the front and back of the test section and measured at particular locations.

Chapter 3

Experimental Scaling Considerations

3.1 Governing Dimensionless Groups

The experiments were designed to represent a two-dimensional slice of the upper dome of the AP600 containment; i.e., from the radial center to the wall of the relatively open region above the operating deck in the containment. This representation assumes that any flow patterns are axisymmetric along the center of containment. In addition, the size of the experiment is small enough (1:12 linear scale) that we must consider how the governing dimensionless groups are affected by these geometric distortions. In the past, our method of investigation of the condensation heat transfer upon the cooled surfaces similar to the AP600 walls indicated that for a large number of conditions a mixed convection regime may be present in the containment for low forced convective velocities; i.e., less than 1-3 m/s. Based on this analysis it seems that the most appropriate dimensionless group to preserve in our experiments is a modified Froude Number given by the expression:

$$Fr = \rho v^2 / \Delta\rho g L \qquad (1)$$

where ρ is the density of the gas mixture, $\Delta\rho$ is the difference in density between the bulk gas and the gas mixture near the interface with the cold wall, v is the bulk gas velocity, g is the gravitational acceleration

and L is the characteristic length. For our analysis we have assumed that the gas velocity can be represented by the steam velocity entering the upperdome containment from a compartment below the operating deck up to the top of containment. This dimensionless group is felt to be the most important because it is the ratio of the natural convection forces to the forced convection inertial forces in the volume.

To give an illustration of the quantitative magnitude of this grouping consider an accident sequence in the AP600 where due to some pipe rupture and initial blowdown, a quasi-steady state is established in which steam is injected into containment at a rate which matches the condensation on the cold walls at a particular pressure. This is similar to the situation developed in the 1/8th scale containment experiments conducted at Westinghouse. Let us assume that the characteristic velocity for steam injection is 1 meter/sec, which corresponds to the mass flow of steam generated from core decay heat and entering the containment through an area similar to the steam generator compartments. For a containment pressure of 3 bar, with saturated steam present, the Froude number is about 0.0043. If we assume the same velocity the minimum Froude number is about 0.055 for our experimental apparatus. This value is higher in direct proportion to the smaller length scale of our facility. However, this distortion can be reduced by decreasing the input flow velocity while holding all other parameters constant. This reduction must be realistically balanced by the quasi-steady conditions attainable within the apparatus. Although this is a distortion in the dimensionless group, it is of similar magnitude.

3.2 Modeling Analysis

In an effort to compare the experimental results to boundary layer heat and mass transfer theory we took an approach similar to Westinghouse [11] which we found to be appropriate for heat transfer modeling. The scale on the experimental facility is such that the heat and mass transfer may be governed

by turbulent free convection. Therefore, the use of McAdams correlation for free convection would approximate the heat transfer from the test section atmosphere to the cooled walls by:

$$Nu = 0.13 Gr^{1/3} Pr^{1/3} \qquad (2)$$

To obtain a similar correlation for the mass transfer which accounts for the majority of the total heat transfer the McAdams correlation was used with the momentum, heat and mass transfer analogy, thus the Nusselt Number is replaced with the Sherwood Number and the Prandlt Number with the Schimidt Number.

$$Sh = 0.13 Gr^{1/3} Sc^{1/3} \qquad (3)$$

The above correlations which were developed from similarity arguments are dimensionless and independent of the length scale. The above correlations were arrived at using the Grashoff Number based on thermal expansion rather than the Grashoff Number based on the total density difference. In our case, the density is a function of both the temperature difference and the steam concentration which would result in an increase of the driving force for heat transfer. Because of this increased density difference, it is more appropriate to use the Grashoff Number based on the total density difference, rather than just the thermal differences. The mixture properties of the bulk were used along with the properties at the wall in both the calculation of the convection heat transfer coefficient and the condensation heat transfer coefficient. The convection heat transfer coefficient can be determined directly by the definition of the Nusselt Number:

$$Nu = \frac{hL}{k} \qquad (4)$$

It is first necessary to calculate the mass transfer coefficient κ_m to obtain the condensation heat transfer coefficient from the Sherwood Number. The Sherwood Number is defined as:

$$Sh = \frac{\kappa_m L}{D_0} \qquad (5)$$

where D_0 is the diffusion coefficient, and κ_m is the mass transfer coefficient. An approximation of the diffusion coefficient of steam in air was calculated from the following equation recommended by Rohsenow et.al (Ref 10).

$$D_o = 0.0069 \frac{T^{3/2}}{P(V_a^{1/3}+V_b^{1/3})^2}\sqrt{\frac{1}{M_a}+\frac{1}{M_b}} \qquad (6)$$

Where T is in Rankine, V_a and V_b are atomic volumes given in table 14.1 of reference 5, and P is in atmosphere. The mass flow rate can then be calculated by the following equation:

$$\dot{m} = \kappa_m(C_g - C_w) \qquad (7)$$

where c_g and c_w are the local vapor concentrations of the bulk gas and the wall respectively. The condensation heat transfer coefficient is then found by substituting the previous equation into the expression:

$$h_{cond} = \frac{\dot{m}(i_{v,bulk}-i_{f,wall})}{T_{bulk}-T_{wall}} \qquad (8)$$

The total heat transfer from the bulk to the wall is the sum of the contributions from the convection heat transfer and the condensation heat transfer ($h_{tot} = h_{conv} + h_{cond}$). The above mass transfer correlation was

developed considering tangential flow across a plate neglecting normal flow. In our situation there is an additive effect due to the normal component of the velocity. This will result in an increase in the heat transfer coefficient due to condensation. To take into account these effects Bird et.al. [4] suggests the addition of a correction factor to the mass transfer correlation.

$$Sh = 0.13 Gr^{1/3} Sc^{1/3} \theta \qquad (9)$$

where θ is a correction factor for the effect of mass transfer on the transfer coefficients :

$$\theta = \frac{\ln(R+1)}{R} \qquad (10)$$

$$R = \frac{x_r - x_b}{1 - x_i} \qquad (11)$$

and varies between 1.5 and 1 for the conditions of our tests. Chapter 5 and 6 of the report indicate that the above correlations produce good agreement with the uniform injection experiments.

Chapter 4

Experimental Apparatus

4.1 Summary Description of experimental facilities

The facility for testing the effectiveness of the AP600's PCCS heat removal capabilities consisted of a rectangular cavity 8 ft. (243.84 cm) tall, 6 ft. (182.88 cm) wide and 1.04 ft. (31.75 cm) in depth. Air or air/helium mixtures are initially in the test section at atmospheric pressure, then steam supplied by a Sussman model ES-7L boiler is added through a steam injection configuration at the bottom of the test section. The 72kW boiler which is able to produce 0.027kg/sec of steam is equipped with a Mercoid Da 531 Bourdon tube pressure switch, which has a dead band of 3psi so that the boiler pressure fluctuations are minimized resulting in a minimal variation of the steam temperature. Energy is removed by horizontal and vertical oriented condensing plates located in the right hand corner of the test section. The aluminum condensing plate was held at a temperature of approximately 30°C by cooling plates located on the back side. Coolant water, supplied by a Neslab HX-150 constant temperature water bath able to provide 4500W of cooling power at 20°C, passes through a series of Dwyer RMC-141 flow meters into the cooling plates. The steam flow rate from the boiler was then controlled by a needle valve until a steady state

temperature of 60,70,80,85, or 90 °C was achieved. Figure 4.1 is a schematic of the essential components of the experiment.

4.2 Test Facility

Figure 4.2 is a schematic diagram of the test facility. It consists of a front and back sheet of 1/2" thick polycarbonate (Lexan™). The sides, top, and bottom are also made of Lexan with the exception of the aluminum condensing plates. The bottom and left side are entirely Lexan while the top and right side house the aluminum condensing plates. The condensing plates are attached to the Lexan sheet with a butt joint and a 1" x 2" phenolic coupling piece used to seal the joint. The two condensing plates are also connected in the corner with a 2" x 2" phenolic coupling joint. Nylon screws were used to connect the phenolic pieces to both the condensing plates and the Lexan. This was done to reduce any changes in the properties of the materials. The aluminum condensing plates were 12" wide as compared to 12.5" wide Lexan sides so that a thermal insulator could be placed between the plates and the carbon steel frame which held the structure together. A 1/8" rubber gasket and a 3/16" thick piece of G-10 phenolic were used to seal and insulate the condensing plate from the frame. The Lexan sheets were then pinned into place with 3/16" x 3/4" dowel pins that went through the steel frame and into the cross section of the Lexan. 5/16" x 1" dowel pins were used to hold the condensing plates in position. These pins went through the steel support structure through the phenolic insulation and into a nylon insert placed in the condensing plate (Figure 4.3). This construction insured that the condensing plates were thermally isolated from any significant mode of conduction heat transfer to the rest of the test section. The sides were then sealed with silicon sealant on both the inside and outside of the test section. The front and back faces were sealed to the steel frame with silicone sealant, and a second frame made of 1/4" thick 2" aluminium angle was placed over the front and back surfaces. The whole test section was sandwiched together with a series of 3/8" threaded rod positioned 6" apart around the perimeter of the

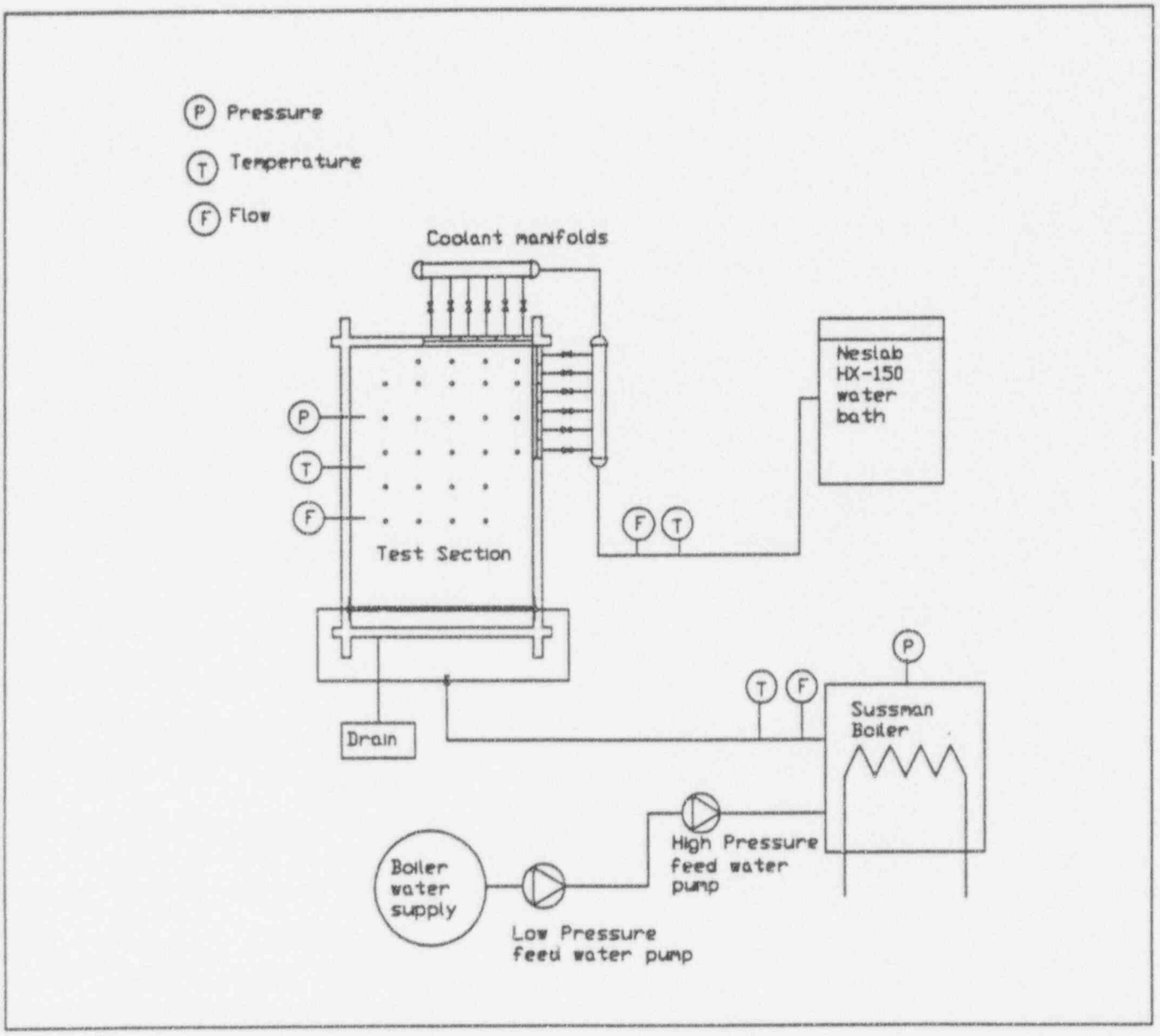

Figure 4.1 Essential Components of Experimental Facility

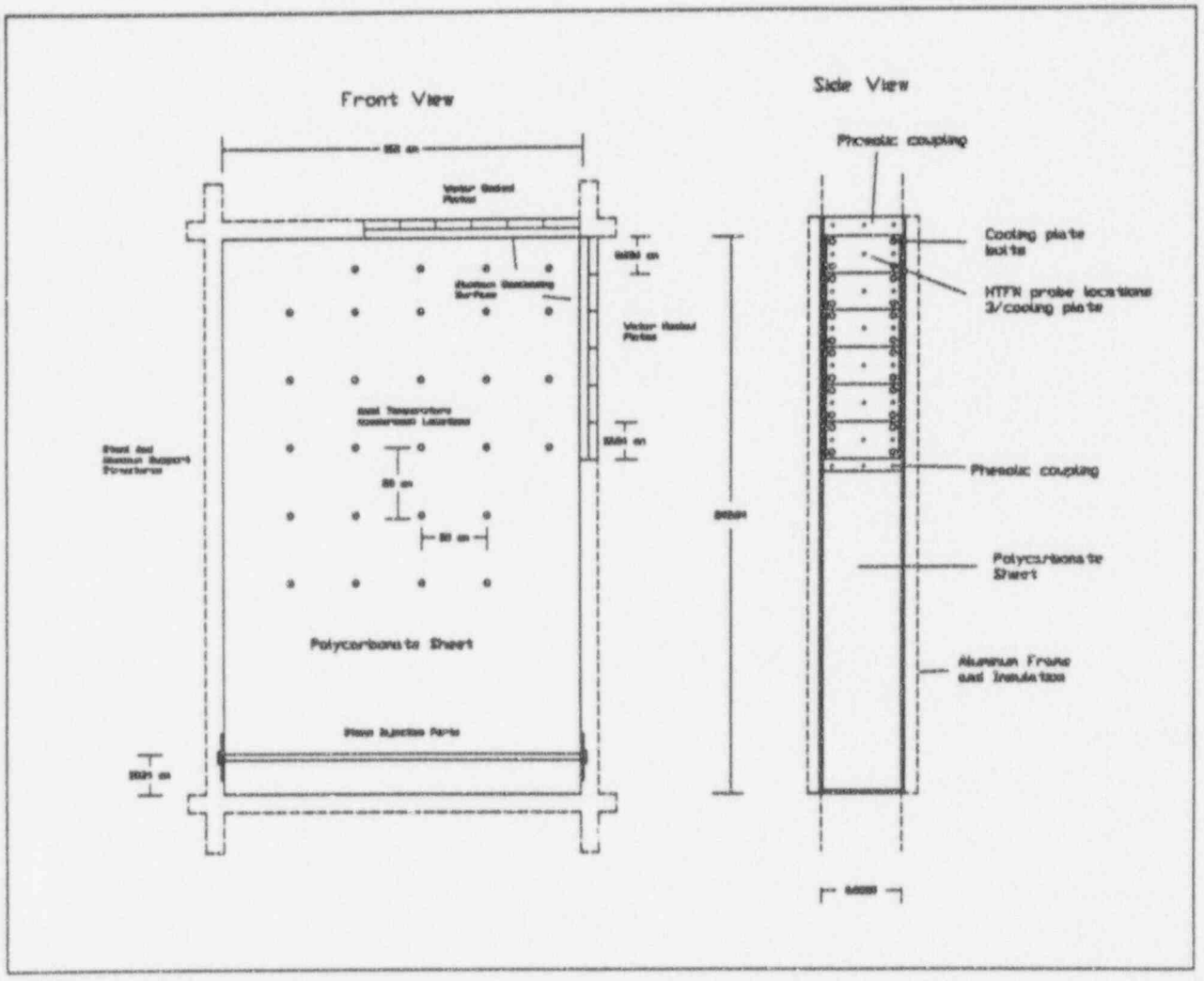

Figure 4.2 Schematic of Test Section

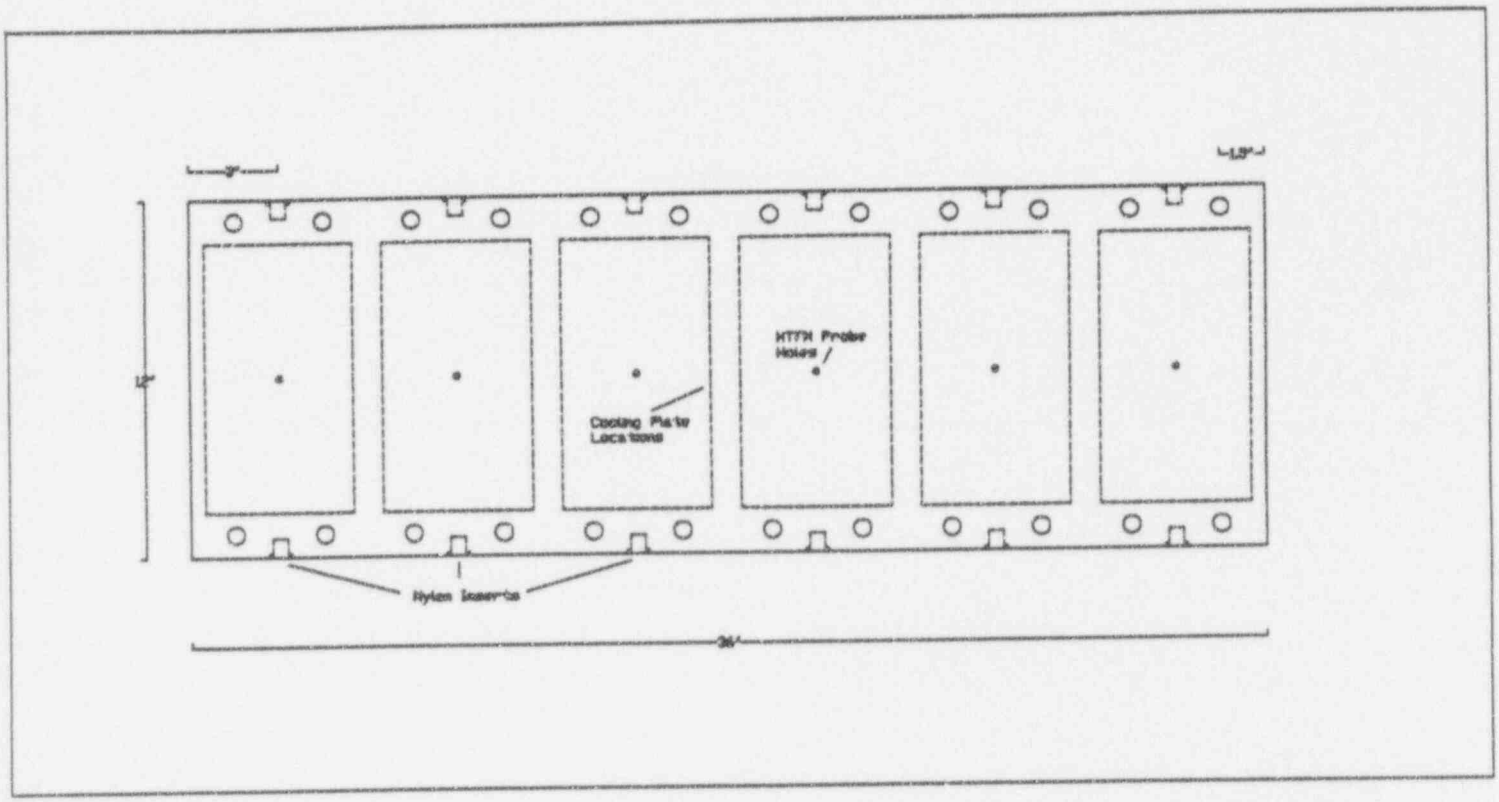

Figure 4.3 Condensing Plates with Nylon Inserts

aluminum frame. Two 7.5" diameter access holes were placed in each side of the test section with the center of the hole located 6" above the bottom plate to provide mountings for the steam injection system. Aluminum flanges were constructed to house the steam injection system and seal the access holes Figure 4.4. The entire test section was supported by a Unistrut support structure and insulated with 2" thick R-12 polystyrene foam insulation, so that the only form of energy removal was from the condensing surface.

4.3 Condensing Plates

The two condensing plates consisted of 2024 aluminum plates with dimensions 3'x1'x1.5". The test plates thermophysical properties, needed in the calculation of the heat transfer coefficient, were measured by Purdue University Themophysical Properties Research Laboratory (TPRL) and a summary of there findings are given in Appendix 1 , The plates were sand-blasted then coated with a 3.75 +/- 0.25 mils thick coat of inorganic zinc paint as measured by a KTA-Tator, Inc Posi-tector 3000 dry film detector. This self curing, inorganic zinc primer contains 85% zinc when dry and has a thermal conductivity of 0.0209 w/cm K. Westinghouse uses the primer to protect the inner and outer surface of the containment facility. It was demonstrated to have good film wetting characteristics at several angles and to prevent corrosion to the vessels [1]. Each condensing plate was fitted with six coolant plates so that coolant flow through each plate could be controlled and monitored separately by the flow meters. A schematic of the cooling plate is shown in Figure 4.5. The 6" x 12" x 1.5" cooling plates were bolted onto the condensing plates with four 1/2 -13 x 2.5" allen head cap screws. It was found that the use of the carbon steel bolts imbedded in the aluminum would not effect the measurements more than one percent. Three sets of holes were drilled through each coolant plate and into the condensing plate to allow for the insertion of heat flux probes. This was done to study any fluctuations of the heat transfer coefficient on positions varying from the center of the test section.

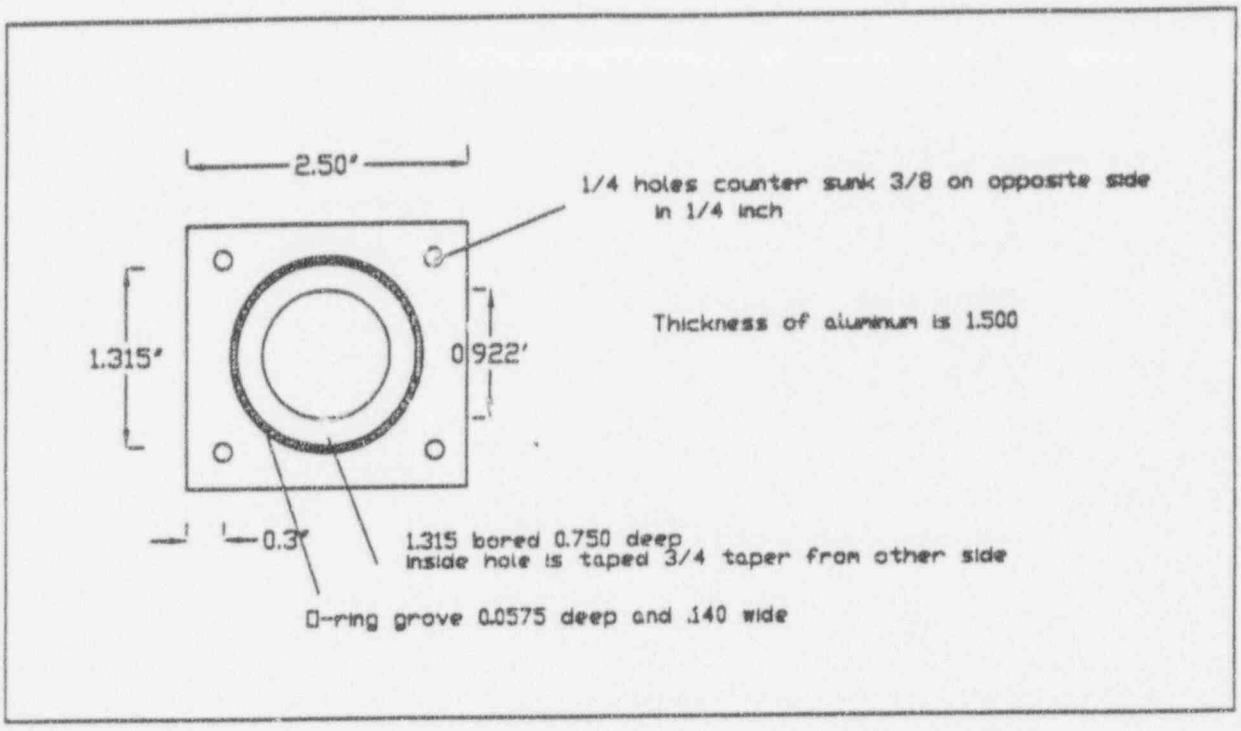

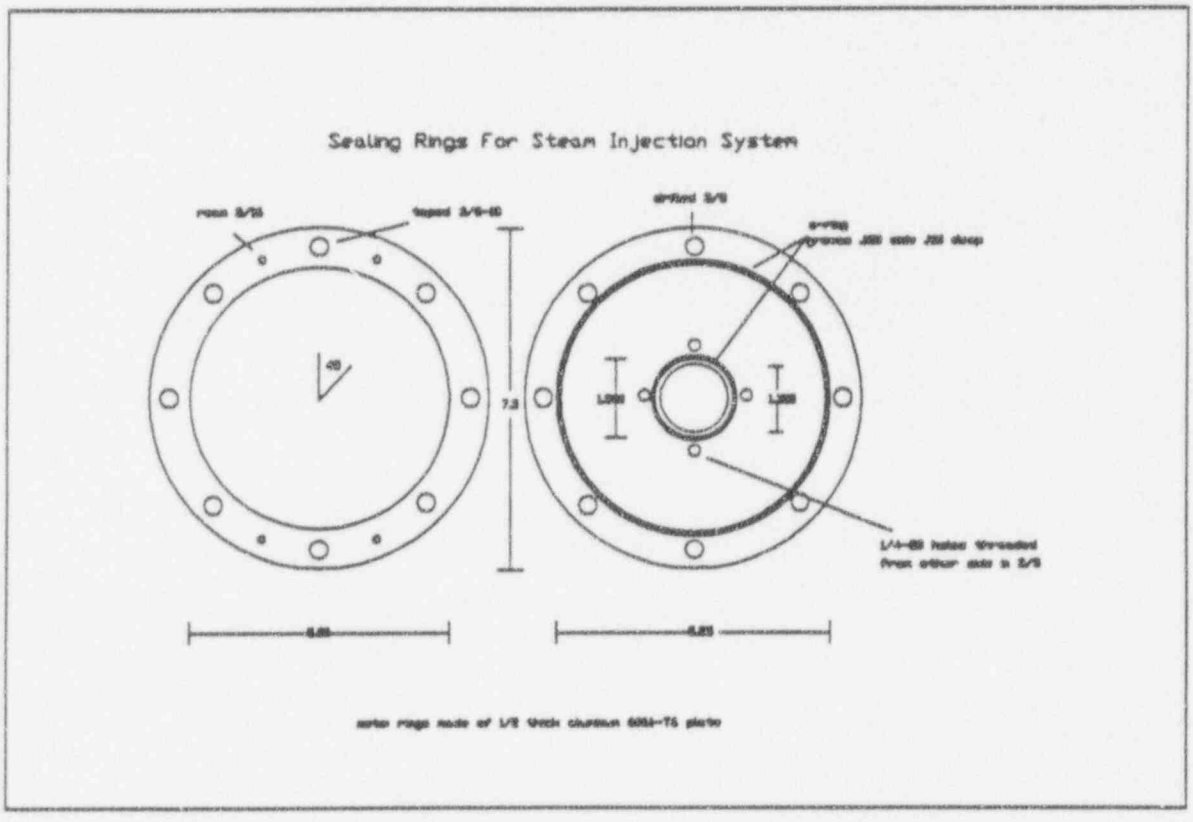

Figure 4.4 Steam Injection Flanges

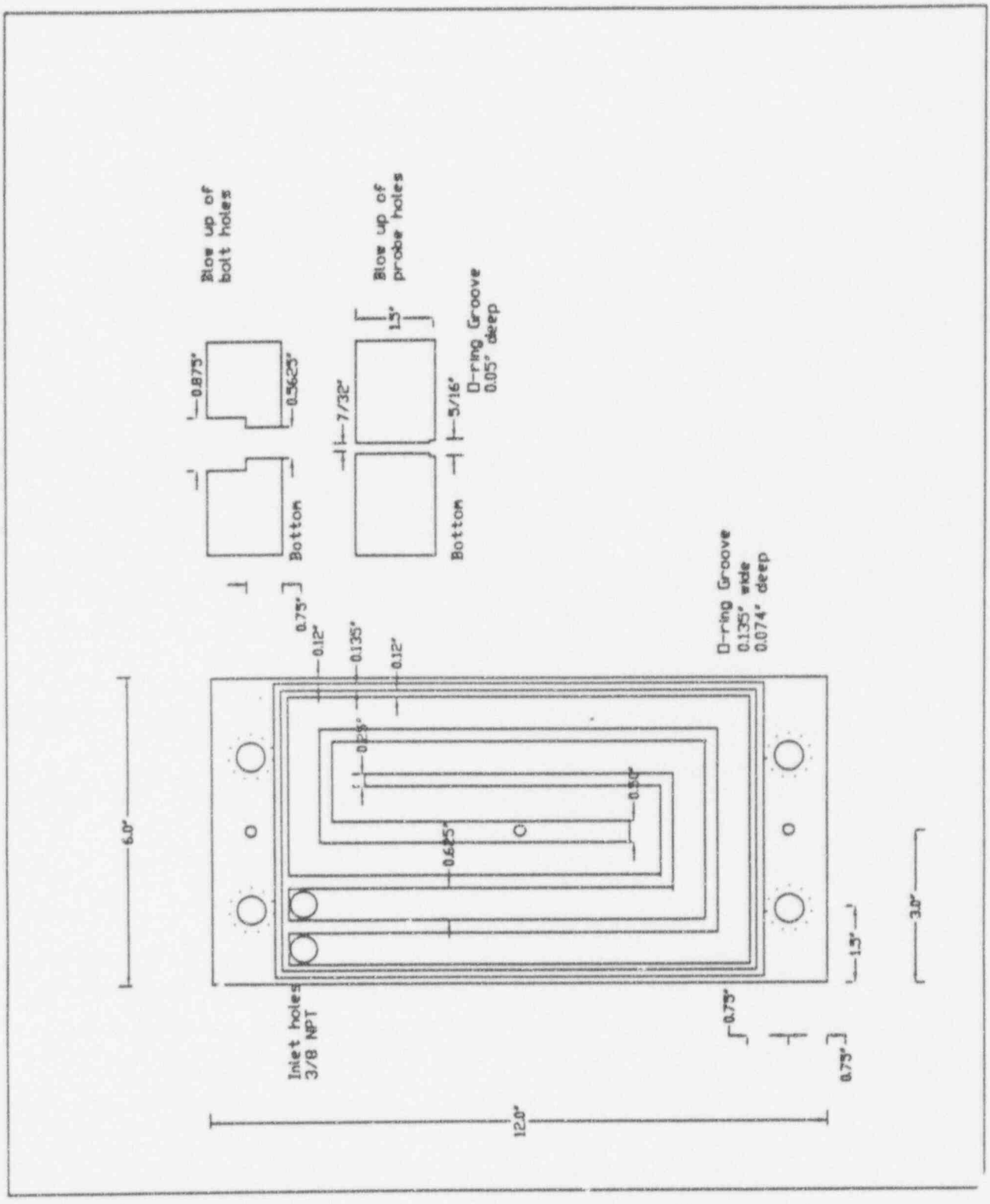

Figure 4.5 Cooling Plates

3.4 Steam Injection System

The first of the two steam injection systems was a uniform distribution of steam. It was constructed of 1" IPS aluminum pipe and is shown in Figures 4.6. A blow up of the injection nozzels is given Figure 4.7. Nineteen evenly spaced Swadgelock fittings, with a minimum opening of 3/16 inch, were used as the injection nozzles for the steam. A small hole was also drilled in the bottom of the pipe to allow any condensed liquid to flow out of the tube. Steam was supplied on both ends of the pipe to create a uniform injection from each nozzle.

The second steam injection system was designed to act as if there were a rupture in a steam generator pipe Figure 4.8. The size and position of the injection was determined by calculating a 1:12 ratio of the actual steam generator. The steam flow rate was scaled by the ratio of the volumes of the actual containment to the test facility. In this arrangement steam enters through one side and passes through a 1" pipe which has 90° turn at a distance of 25 7/8" from the left side and then a 8" high vertical inlet section.

4.5 Measurement Techniques

Two separate methods of determination of the heat transfer coefficients were used. The first was a local heat flux measurement using thermocouple heat flux meters (HTFM) and the second was an area averaged heat transfer coefficient that was determined from a coolant energy balance (CEB). The heat flux meters are shown in Figure 4.9. They consist of a set of four E-type thermocouples incased in a 3/16" O.D. stainless steel tube (E-type thermocouple grade wire was chosen because both elements have a low thermal conductivity, good resistance to corrosion and a high Seebeck coefficient) . Four 0.039" precision holes were drilled in the side of the stainless steel sheath. Thermocouples with a bead of no more than 0.025" were inserted into the hole and a silicon sealant was injected into the end of the tube to hold the thermocouples in place. Each probe was then independently measured and the location of the

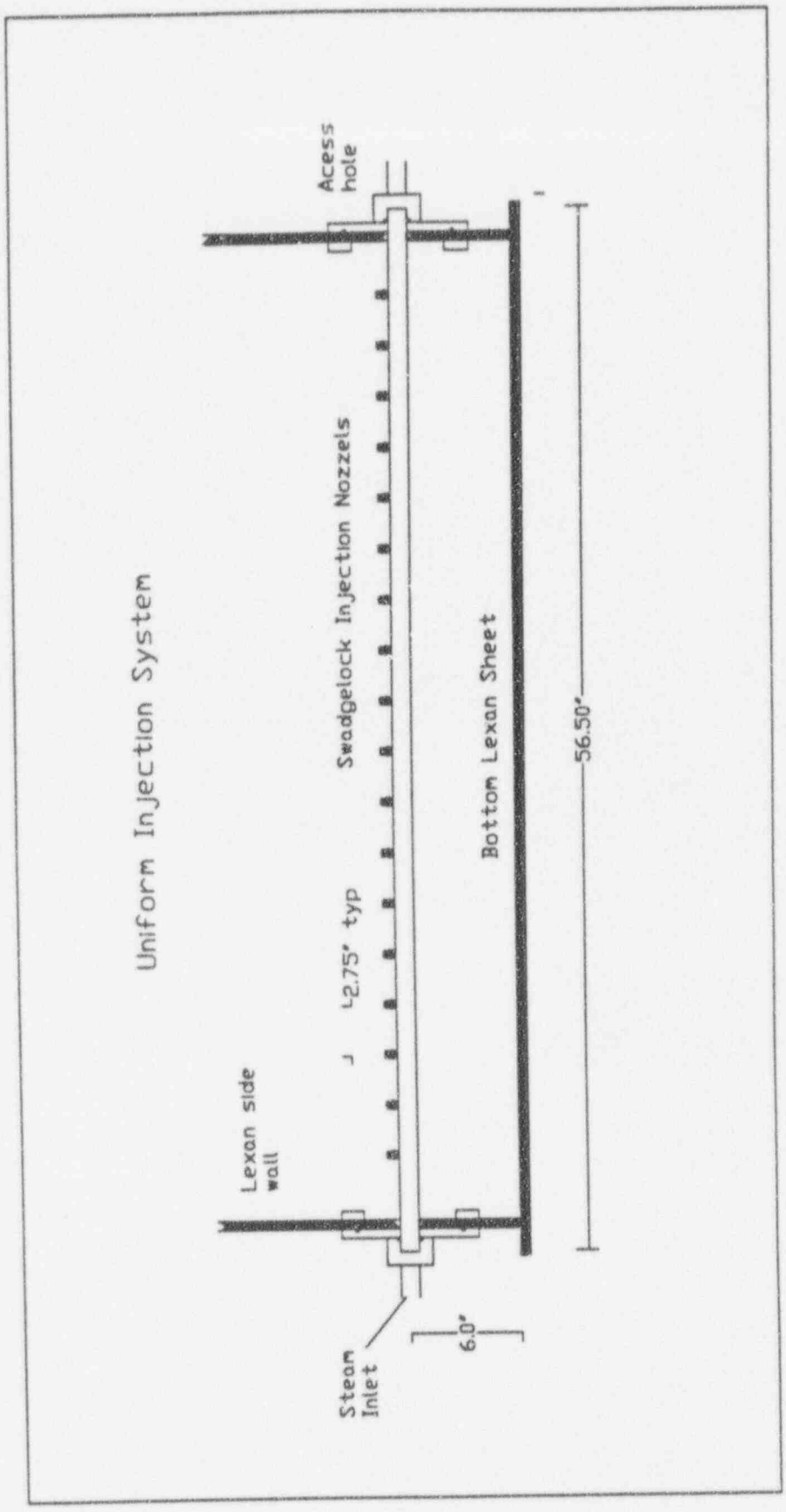

Figure 4.6 Uniform Injection System

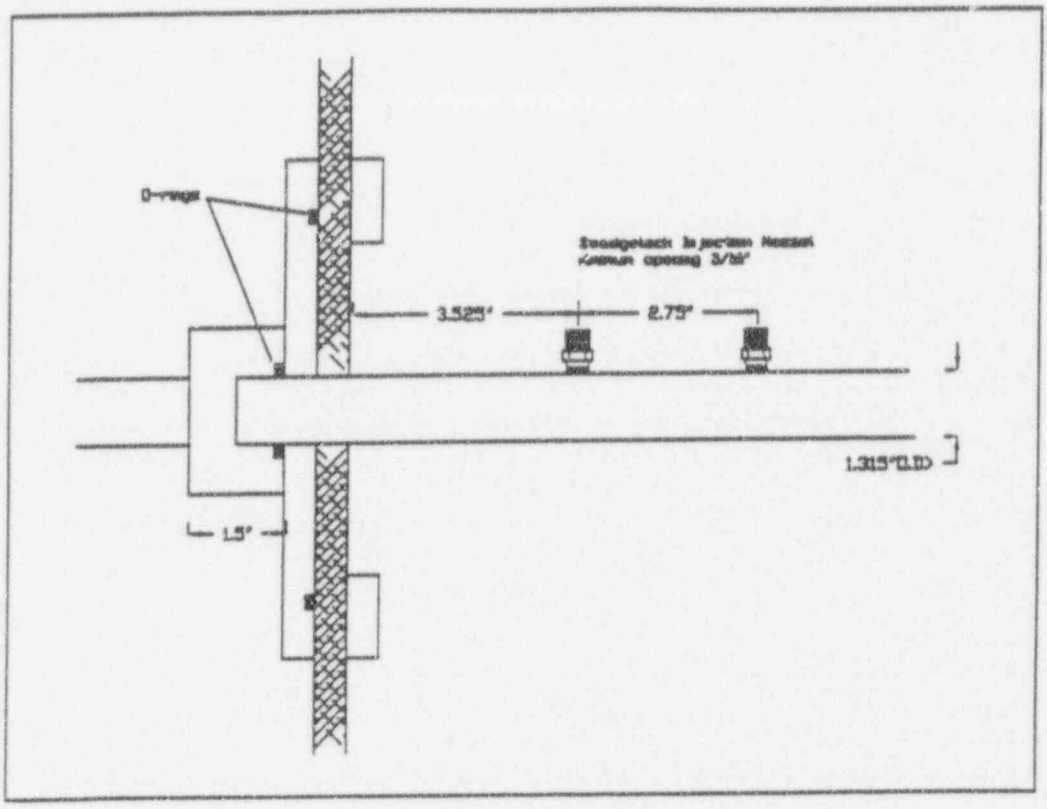

Figure 4.7 Steam Injection Nozzels

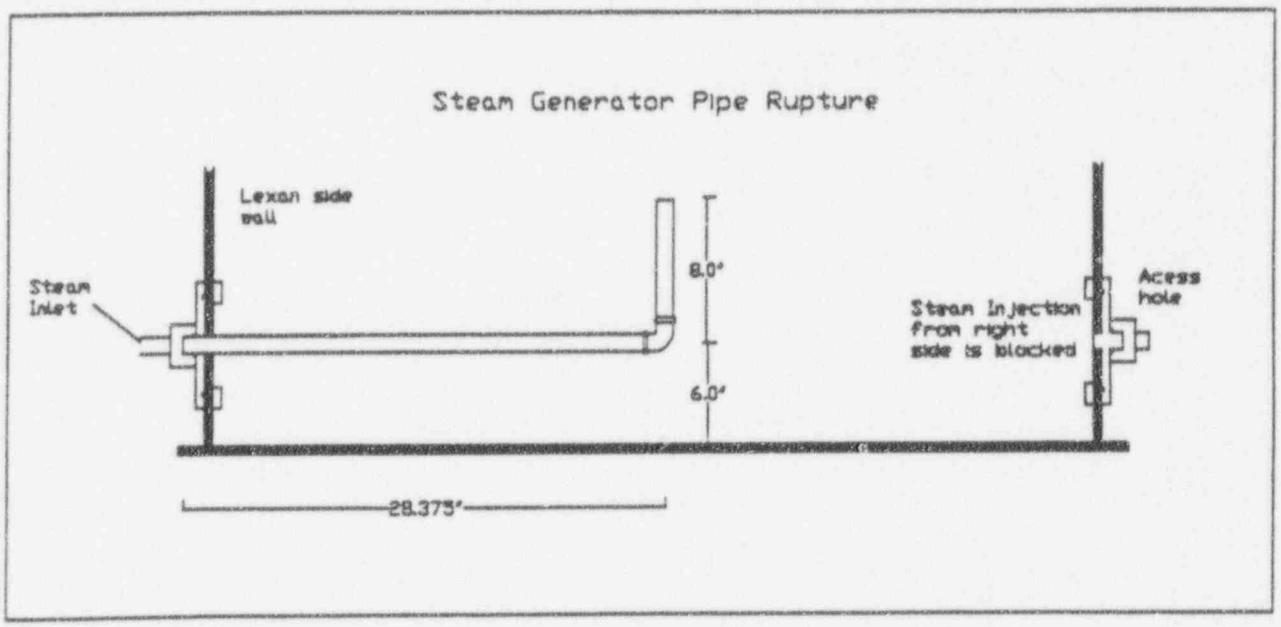

Figure 4.8 Steam Generator Pipe Rupture Injection System

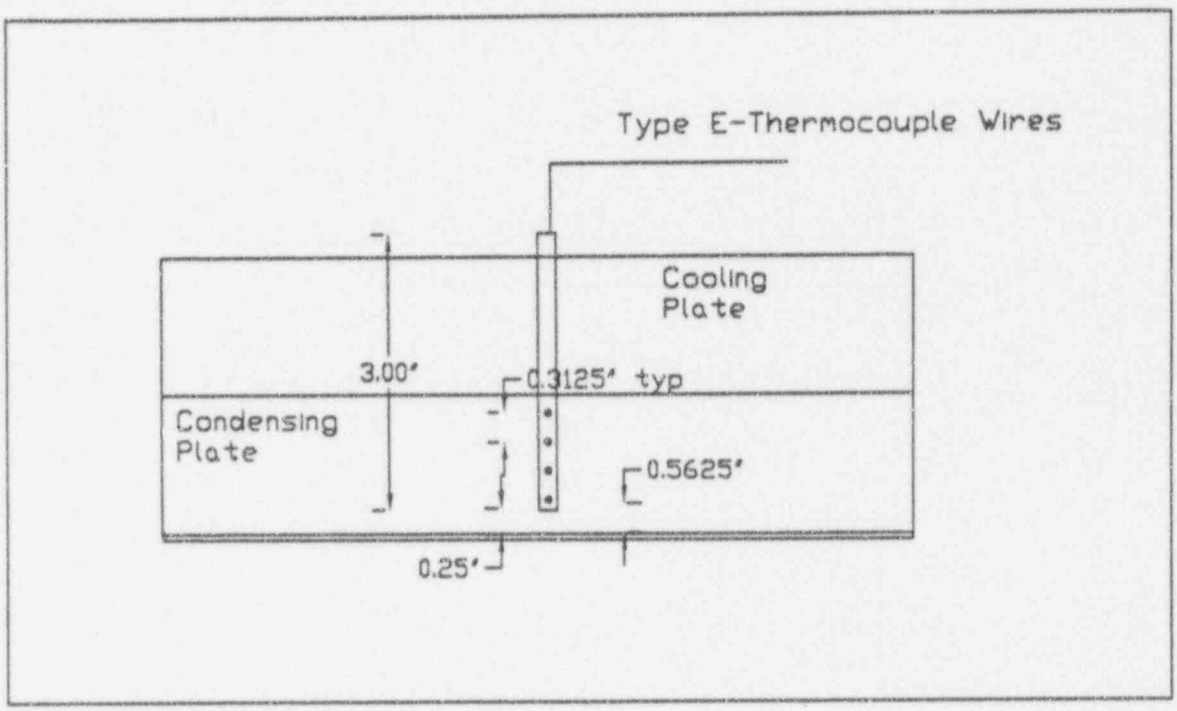

Figure 4.9 Heat Flux Meter Probes

junctions recorded with an error of less than 0.01". The thermocouples were then tested for accuracy at the National Standards Laboratory. This was done by placing the probes in a bath of mineral oil and measuring the temperature with a platinum thermometer while the millivolts produced by the junctions were recorded on a digital volt meter. These measurements were then compared to the IPTS-68 standards.

To determine the heat flux the HTFM's were set in holes drilled through the cooling plates into the aluminum condensing plate. An equation of a line defining the temperature distribution of the plate was found from the temperature measurements and positions of the thermocouples . The slope of this line is the temperature gradient in the aluminum plate and the y-intercept is the back plate temperature. Then using the following analysis we could determine the heat transfer coefficient at the location of the probe.

$$h = \frac{k\frac{dT}{dx}}{T_{mix} - T_{surf}} \qquad (8)$$

Assuming a linear temperature dependance the temperature of the plate is given by the equation

$$T_{alum}(X) = \frac{dT_{alum}}{dx}X + T_{back} \qquad (9)$$

A similar equation governs the temperature in the zinc coating layer. We included the existence of the coating, however we neglect any contact resistance between the aluminum and the zinc coating. With knowledge of the slope and intercept of a line through the aluminum plate we could calculate the surface temperature and with the corresponding measured mixture temperature we could calculate the heat transfer coefficient. The slope and intercept of the temperature distribution in the plate was found using a linear least squares fit to the recorded probe temperatures [12,13]. The specified error in the thermocouples reported by the manufacture (Omega Engineering) was +/- 1.0°C. This is the error in the

thermocouples absolute temperature reading, however we were concerned not with the absolute temperature but the difference in temperatures of the four thermocouples. If all four thermocouples are calibrated so that they read the same temperatures at zero heat flux then the resolution or a statistical standard deviation of the sampling of a ensomble of measurements can be used as the error in the linear least squares determination of the line. This was done by the program htf6.exe which is given in Appendix 2.

The second method of determination of the heat transfer coefficient was a coolant energy balance. Temperature controlled water was passed through a flow meter and then through the coolant channels in the coolant plates. The temperature of the water was measured with an E-type thermocouple at the inlet of the coolant plate and subsequently at the exit of the coolant plate. An energy balance on the liquid would yield the energy removed from the condensing plate and thus the heat transfer coefficient associated with the area under the coolant plate.

$$q_i'' = \frac{\rho_{cool} c_p (V \Delta T)}{A_i} \qquad (10)$$

$$h = \frac{q_i''}{T_{max} - T_{surf}} \qquad (11)$$

This method of determination of the heat transfer coefficient is different than the heat flux meter probes in that it is an area averaged heat transfer coefficient. Each coolant plate was used to obtain an average heat transfer coefficient where the HTFM's measure the heat transfer coefficient in the vicinity surrounding the probes. An error analysis of the above equations is given in Appendix 3.

4.5.1 Secondary measurement devices

The test section was also equipped with several temperature probes to measure axial variations in the test section fluid temperature. Figure 4.2 shows the locations of the temperature measurements. Swadglock fittings with a minimum opening of 1/2" were used to allow for easy installation of a variety of measurement probes. The probe holes located in the right hand corner next to the condensing plates were used as the mixture temperatures in the calculation of the heat transfer coefficient. These probes were located as close to the condensing plates as possible, considering the structural integrity of the Lexan sheets. These seven temperatures were recorded by the Keithley data acquisition system along with the HTFM and CEB temperature measurements. The remainder of the axial probes were connected to an Omega DP41-TC high performance temperature indicator.

A Vaisala series HMP 131Y humidity and temperature transmitter was used to measure the relative humidity in the test section. This probe's measurement of the RH is based on changes in the capacitance of a thin polymer film as it collects water. It has a 90% response time of 15sec in still air at 20°C with an error of +/-2 % RH. It also allows the simultaneous measurement of temperature with a platinum RTD sensor. The Vaisala probe junction box was connected to a Keithley DAS-8 data acquisition board inside a PC computer and the probe inserted in the test section through the same holes as the axial temperature probes so that a distribution of humidity levels could be obtained.

The steam mass flow rate was measured with two different techniques. The first method of measurement was an orifice flow meter Figure 4.10. It consisted of an ASME spec. square edge orifice. The area of the orifice opening was 2.7cm^2 with a two foot entrance pipe with area 17.719cm^2. Two 3/16" pressure taps were located on either side of the orifice and were connected to a 4025-B Capsuhelic deferential pressure gage. The mass flow rate could then be calculated from the equation:

$$\dot{m} = \rho < v > A C_d = C_d A_o \left(\frac{2\rho_g (P_1 - P_2)}{1 - \left(\frac{A_o}{A}\right)^2} \right)^{1/2} \qquad (12)$$

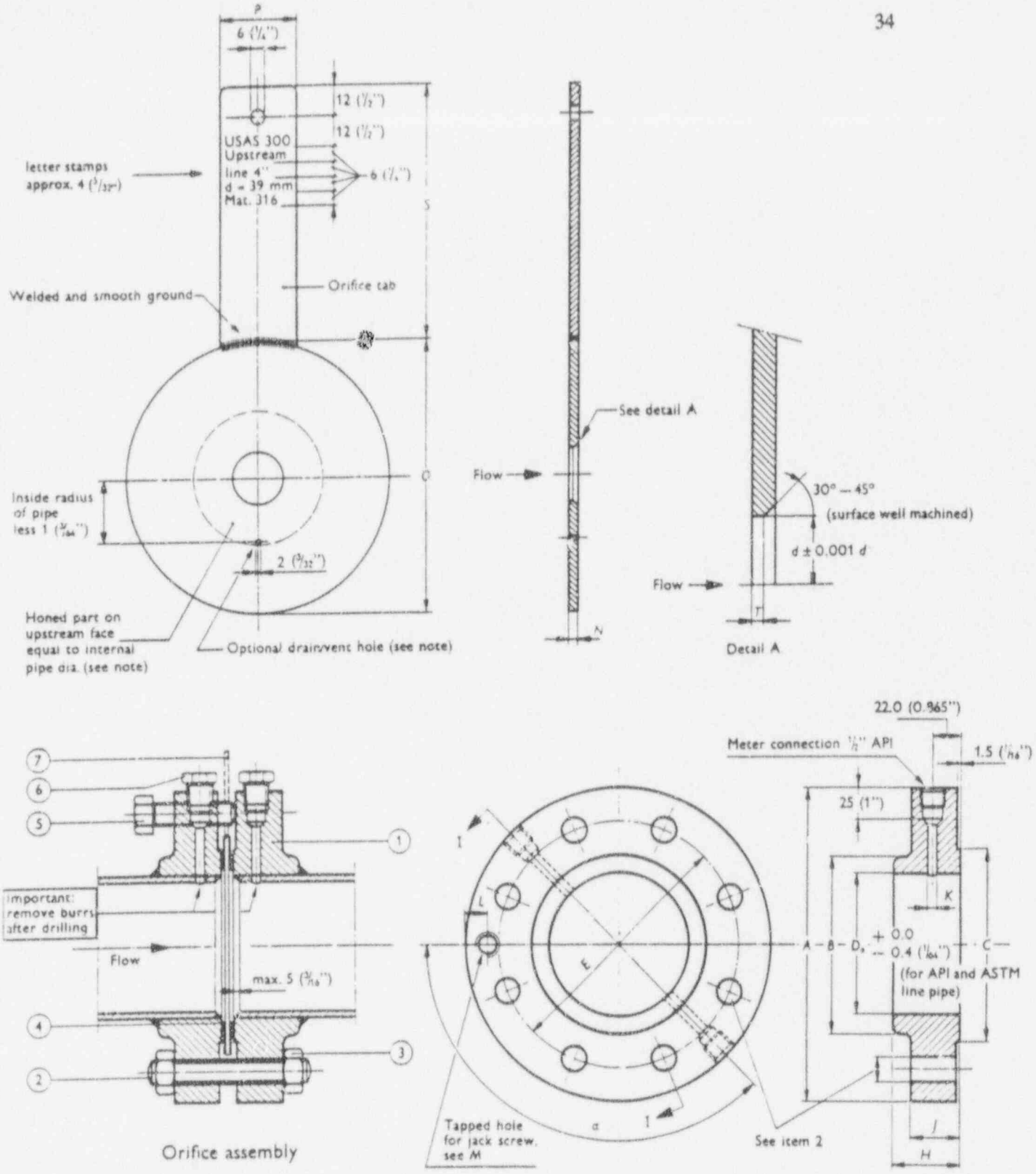

Figure 4.10 ASTM Orifice Flow Meter

(Shell Flow Meter Engineering Handbook)

The discharge coefficient was taken to be 0.61 which is the suggested value by Bird et.al [4]. The second method of measurement was an energy balance on the boiler cycle. After the test section reached a steady state temperature the boiler cycles were timed. If the power of the heater is known along with the time the heater is on one can determine the energy supplied to the steam. If this is known then the mass flow rate of the steam can be determined by the following equation:

$$\dot{m} = \frac{Qt}{((c_p(T_{sat}-T_{in})+ifg)t_{tot})} \qquad (13)$$

The pressure gage used to measure the pressure drop across the square edge orifice was used in only a few measurements since the silicon diaphragm was not able to handle the temperature and exposure of the steam for long periods and failed after a few uses. The second method agreed well with the measurements made by the orifice flow meter and was used throughout the experiments as the method of determination of the flow rate.

A Hontzsh vane wheel anemometer was used to record preliminary velocity measurements. The voltage proportional signal frequency of the meter is converted into a load independent voltage by a Hontzsch flow transducer powered by a 24 VDC Marter power processor . The voltage output from the transducer is read by a Nicolet 4175 Digital oscilloscope. The zero flow reading of the anemometer is 5.003volts therefore a high precision voltage calibrator was used as a DC offset to increase the resolution of the oscilloscope. The NIST traceable calibration of the velocity meter is given in Appendix 5.

4.6 Gas Sampling

A gas sampling device was constructed to determine the concentration of different gases that were present in the noncondensables. Figure 4.11 is the schematic of the gas sampling device used. Valve one is connected to a 1/2" copper tube, that was inserted in the test section through one of the axial

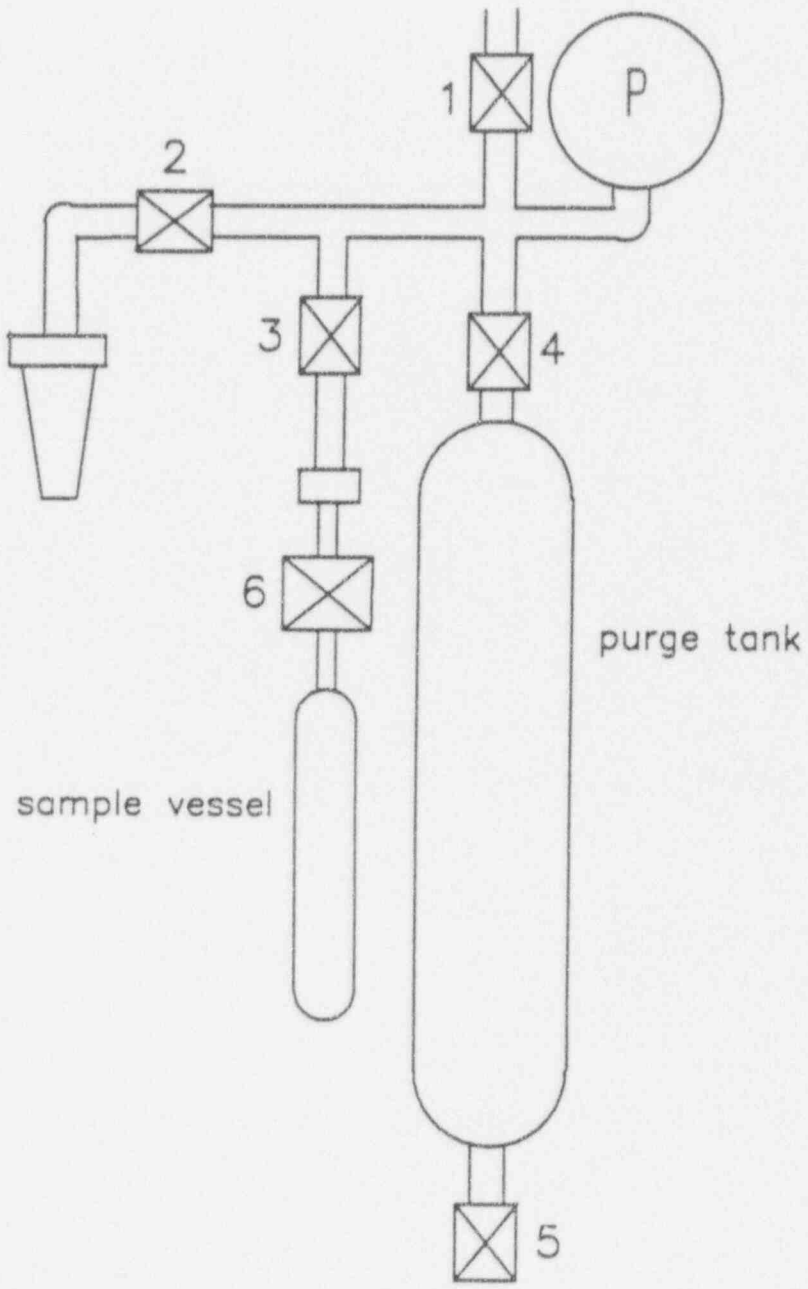

Figure 4.11 Gas Sampling Apperatus

temperature probe holes, to the rest of the sampling system. Valve two connected the sampling system to a vacuum pump so that the entire system could be purged of air prior to sampling. Valve four was connected to a purge tank so that a large volume of the gas could be taken into the sampling unit to ensure a uniform mixture. The actual sampling bottle was attached to valve three. The unit was wrapped with a heating tape which was connected to a temperature controller, so that the temperature of the whole sampling system could be raised to the test section conditions. Value five was used to drain any condensed liquid. The sample was then analyzed with a mass spectrometer.

4.7 Data Acquisition and Recording

A Keithley series 500 data acquisition system was used to collect the voltage signals from the majority of the temperature measurements. The Type-E thermocouple wire AWG-30 with a Teflon coating were connected to one of five Keithley AIM7 Thermocouple input modules. The AIM7 module allows the connection of 16 thermocouples to an isothermal block. A cold junction reference sensor is also connected to this isothermal block to allow accurate measure of its temperature. The voltage signals are routed to a global system amplifier which amplifies a ADM2 14 bit A/D converter. The AIM7 module has a gain of 100volts/volt and the global system amplifier was set to a gain of 10. This produces an overall amplification of 1000, giving an effective voltage input range of 20 millivolts. Both the sampling rate and the number of samples was controlled and recorded by a personal computer. The sampling of the temperatures was usually done at a sampling rate of 0.2hz where 30 samples were taken for each thermocouples. The temperature data was then sent to the data reduction program Htf6.exe where the temperatures and locations were used to determine the heat flux and the corresponding heat transfer coefficients.

Chapter 5

Air/Steam Experiments

5.1 Summary of Experimental Procedure

This was the first series of tests conducted in the experimental facility and as a result several tests were performed to ensure that everything functioned properly. The conditions of the outside environment were measured and recorded along with the time each test was conducted. The boiler was started and filled with distilled water from a large reservoir. Two pumps were used to fill the boiler a low pressure pump was needed to pump the water supply to a high pressure pump located on the boiler. Once the boiler reached its operating pressure of 25psig a throttling needle valve was opened to allow steam to flow into the test section. The coolant water supply was turned on and the flow meters and water temperature were set to maintain the surface temperature of the condensing plate at approximately 30°C. The Neslab HX-150 Refrigeration unit is rated to provide 4500W of cooling power at 20°C. This was found to be sufficient for test section temperatures of 60-80°C, however it was unable to remove sufficient energy at 85°C and 90°C to hold the plate temperature at the desired 30°C. Therefore building water was passed through the cooler in order to achieve a steady condensing plate temperature of 30°C and then was dumped down a drain. The tests were taken at atmospheric pressure due to the structural limitations of the Lexan sheets to handle higher pressures. To maintain the test section at atmospheric

pressure a ball valve located on the bottom of the test section was opened. This valve was connected to a hose which was inserted into a pool of water so that gas could only exit the test section atmosphere. The needle valve was adjusted until the test section temperature reached the desired temperature. After a sufficient time had elapsed (no less than a 1/2 hour) for the test section to reach a quasi-steady state data was collected. The Keithley 500 data acquisition system could only read one AIM7 temperature module at a time. This consisted of 16 thermocouple measurements. The thermocouple HTFM probes and the two thermocouples used in the measurements of the CEB were setup so each probes four temperature measurements would be measured at the same time. The sampling was usually done at a frequency of 0.2Hz with 30 temperature measurements taken for each thermocouple. Therefore it took 150 seconds to read each card. After each card was run the data had to be dumped to the hard drive of the personal computer. This took about one minute, therefore it took about 15 minutes to collect the complete set of heat transfer data. The data was then transferred to the data reduction program and examined to see if the plate surface temperature and test section temperatures were at the desired values. During each test the axial temperature at each grid location of the test section was measured along with the relative humidity. The boiler mass flow rate was also measured. The pressure differential of the Capsuhelic pressure gage was taken and the boiler cycles timed. The condensed steam in the test section was allowed to eject through the same ball valve that kept the test section at atmospheric pressure. After several tests were completed at a given test section temperature the steam flow rate was increased. This elevated the test section temperature to the next desired temperature and the procedure was repeated. Several tests were taken at temperatures of 60,70,80,85, and 90°C. Table 5.1 shows approximate mass flow rates needed to achieve the desired temperatures. Figures 5.1and 5.3 show the consistency in the heat transfer coefficients obtained at 70°C by the HTFM's and Figures 5.2 and 5.4 show the consistency of the CEB measurements. The labeling of the plots corresponds to the position of the HTFM meters as measured in centimeters. The coordinates of the horizontal plate heat transfer coefficient plots start from the left side

Test Section Temperature °C	Mass Flow Rate (kg/s)
60	0.00134
70	0.00238
80	0.00357
85	0.00422
90	0.00580

Table 5.1 Mass Flow Rate as a Function of Temperature

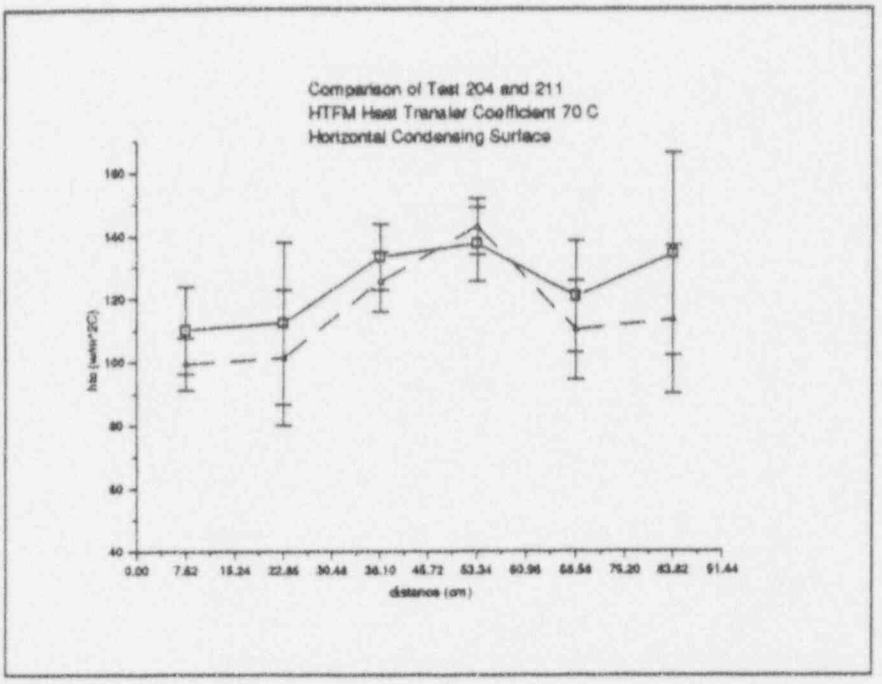

Figure 5.1 Consistency in HTFM (Horizontal)

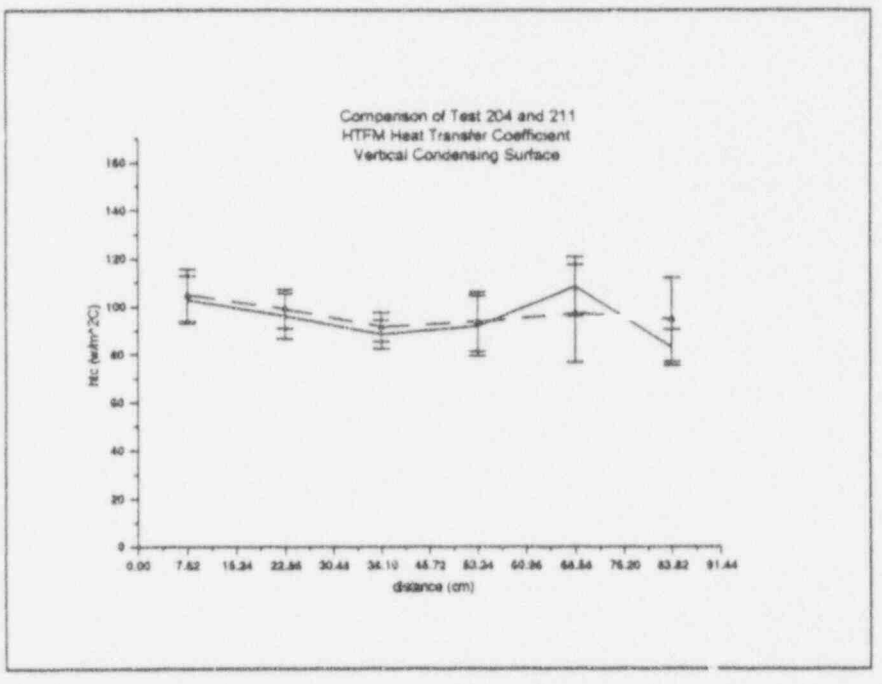

Figure 5.2 Consistency in HTFM(Vertical)

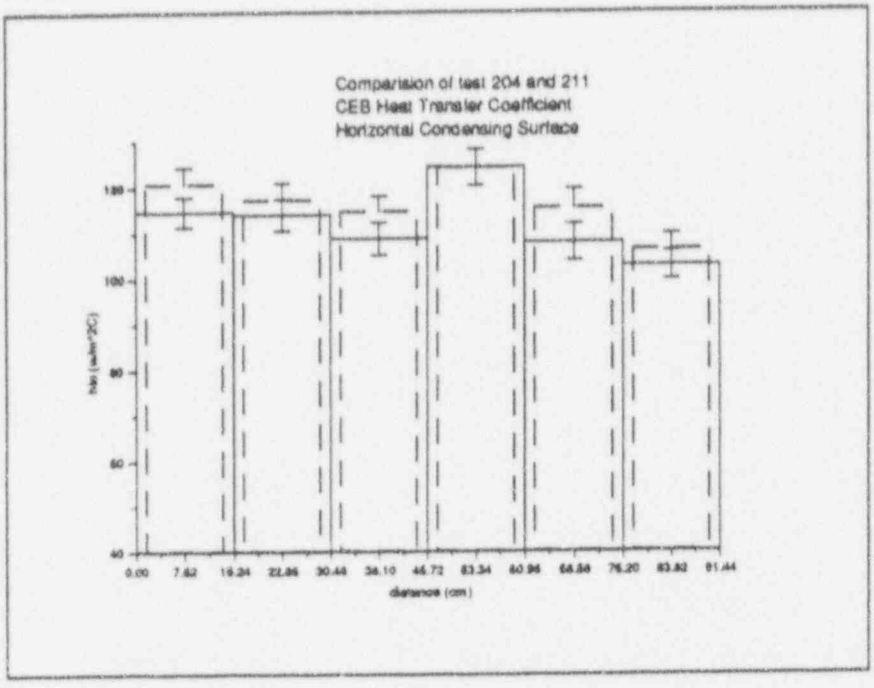

Figure 5.3 Consistency in CEB (Horizontal)

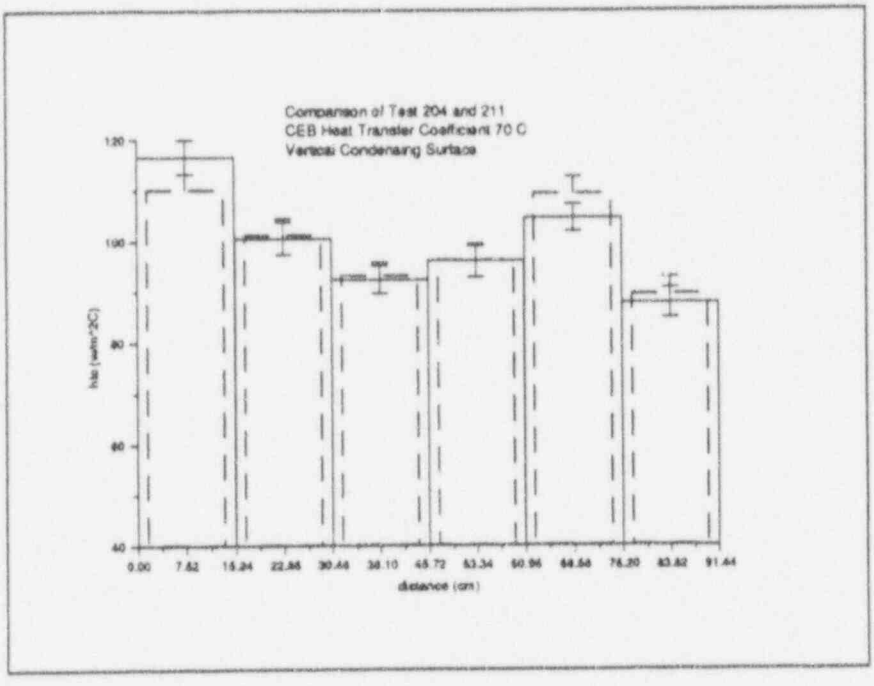

Figure 5.4 Consistency in CEB (Vertical)

of the condensing plate and end at the right hand corner of the test section where the horizontal plate meets the vertical condensing plate. The coordinates of the vertical plate heat transfer coefficient plots start in the corner of the two condensing plates and continue down the condensing surface.

5.2 Three Dimensional Effects Study

5.2.1 Description of test

One of the first experiments conducted was to determine whether there were any significant three dimensional effects present in the heat transfer coefficient. These tests are classified as the series 100. To study this the HTFM's were moved from the center hole of the condensing plate 6.25" from the Lexan front sheet to the outer locations 1" from the Lexan sheets. This test was done at 60°C.

5.2.2 Results Discussion

Figures 5.5 and 5.6 show the measured heat fluxes at the various positions. The back holes refer to the holes furthest from the Lexan face with the probe holes drilled in it. The front and back holes should produce relatively the same heat transfer coefficients due to symmetry arguments. The graph shows that the heat transfer coefficients measured when the HTFM's were in the center positions straddled the values of the heat transfer coefficients measured in the front and back locations. This suggests that there are no significant noticeable three dimensional effects in the heat transfer coefficient, and the test section can be treated primarily as a two dimensional slice. The data for 60°C produces the worst relative errors due to the fact that the temperature difference through the cross section of the aluminum condensing plate is low. This enhances the error in the difference of the successive temperature measurements and causes larger relative errors than the higher temperatures, yet no presence of three dimensionality seems to exist.

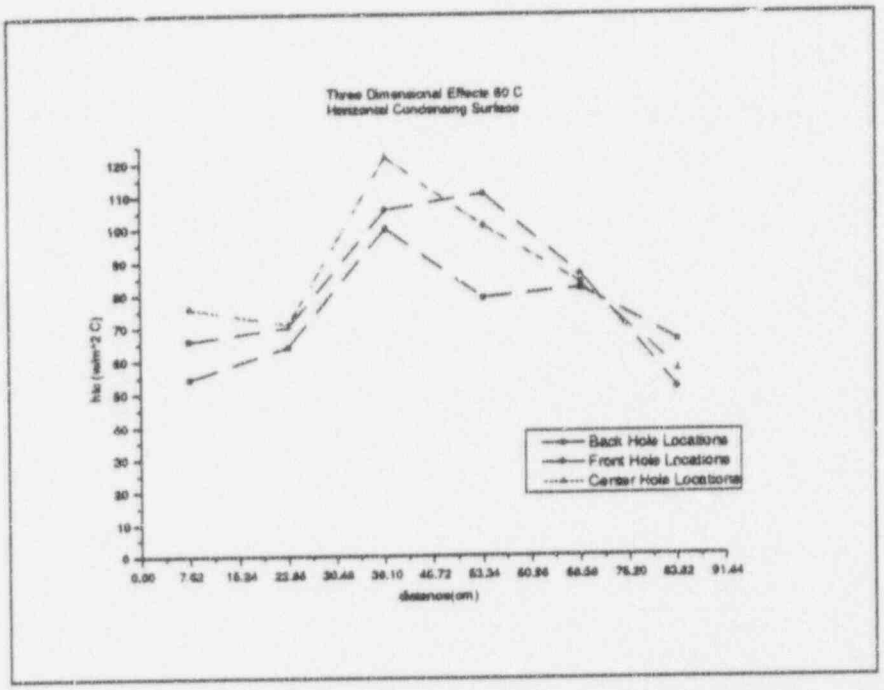

Figure 5.5 Three Dimensional Effects (Horizontal)

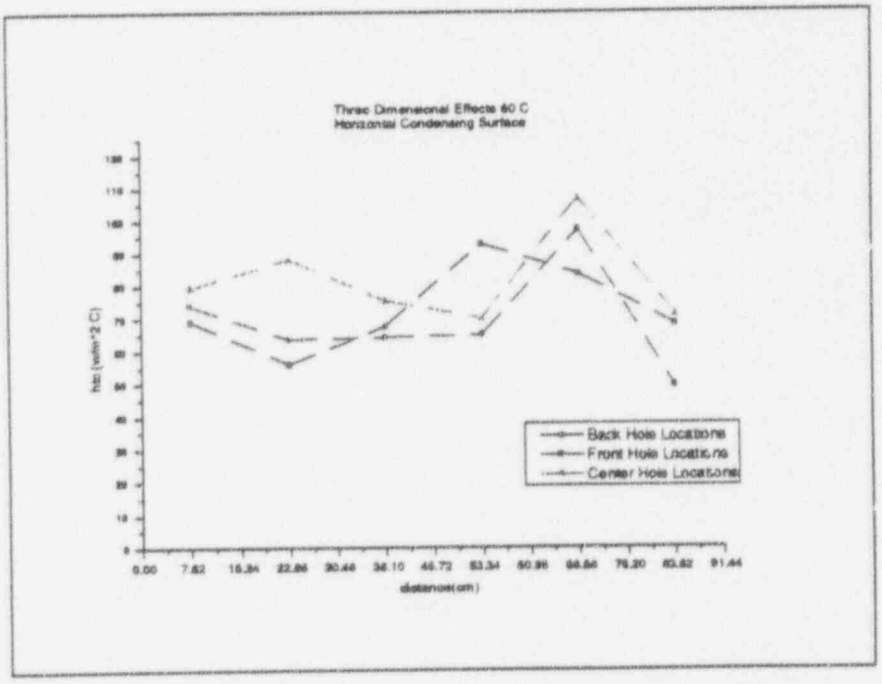

Figure 5.6 Three Dimensional Effects (Vertical)

5.3 Air/Steam at Various Temperatures (Uniform Injection)

5.3.1 Description of Test

The next series of tests, designated test series 200, were conducted to test the effects of the heat transfer coefficient with an increasing temperature difference between the test section atmosphere and the cooling plates. These air/steam tests were conducted with the uniform injection system shown in Figure 4.6.

5.3.2 Results/Discussion

Table 5.2 shows typical average values for the heat transfer coefficients at various temperatures measured by both the HTFM's and the CEB methods. The average values are given for both the vertical and the horizontal oriented condensing plates. Typical local heat transfer coefficients are given in graphical form in Figures 5.8 - 5.16 which have been taken from reference [5]. A definite trend in the heat transfer coefficients was observed. As we move along the vertical plate from the top of the test section down, the heat transfer coefficients decreased steadily until reaching coolant plate #10 or #11 (a distance of approximately 46 cm down from the corner of the test section see figure 5.17). At this point there is a slight increase in the heat transfer coefficient which usually continues across the last cooling plate. The behavior of the top (horizontal) plate seems to be more sporadic than that of the vertical side plate. The top plate has a consistently higher heat transfer coefficient than that of the vertical plate. There also seems to be a slightly larger discrepancy between the HTFM's and the CEB measurements in the horizontal plate. This increased heat transfer coefficient and the discrepancy in the two methods of measurement may be a result of droplet formation and the presence of rain from the top surface. Such a rough surface presented to the flow combined with the natural convective flow pattern may cause the difference, although analysis is still under way.

The inorganic zinc coating promotes filmwise condensation, however as noted by Huhtiniemi at angles of less than 1° and with velocities less than 1m/s droplets will form on the surface. Although, the

Test Section Temperature °C	HTFM Horizontal Plate (w/m^2C)	CEB Horizontal Plate (w/m^2C)	HTFM Vertical Plate (w/m^2C)	CEB Vertical Plate (w/m^2C)
60	88.23	82.32	70.53	71.07
70	115.24	112.04	95.24	99.79
80	209.5	195.32	168.4	173.32
85	229.84	238.15	178.02	201.74
90	296.28	303.17	230.66	267.45

Table 5.2 Typical Average Heat Transfer Coefficients

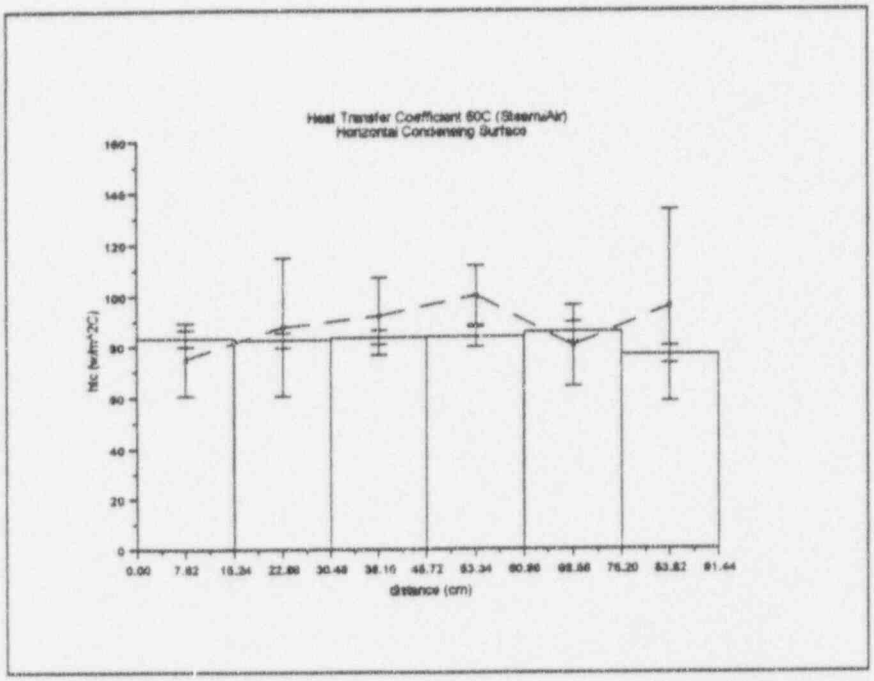

Figure 5.7 60 C Heat Transfer Coefficients (Horizontal)

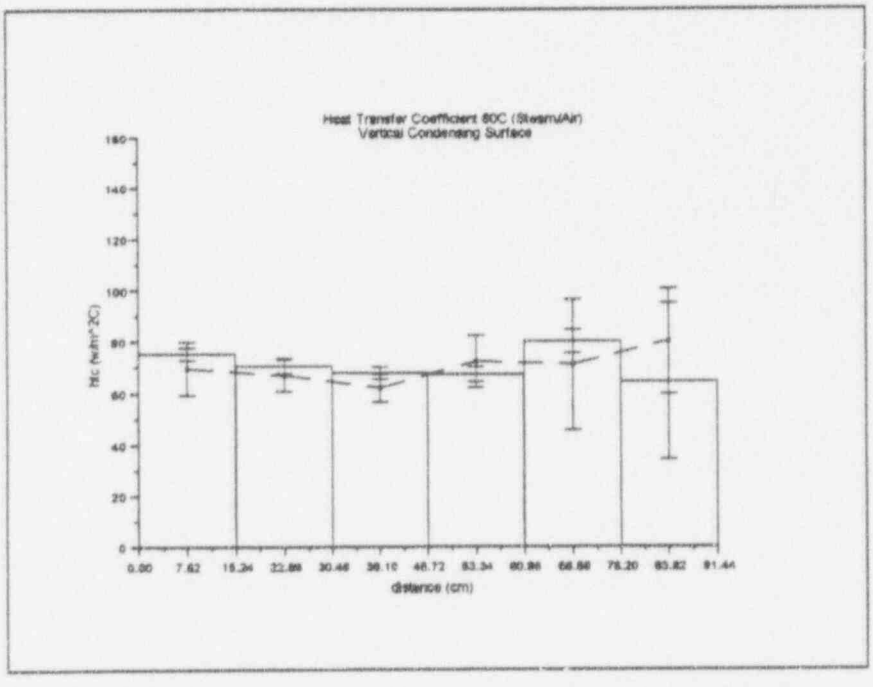

Figure 5.8 60 C Heat Transfer Coefficients (Vertical)

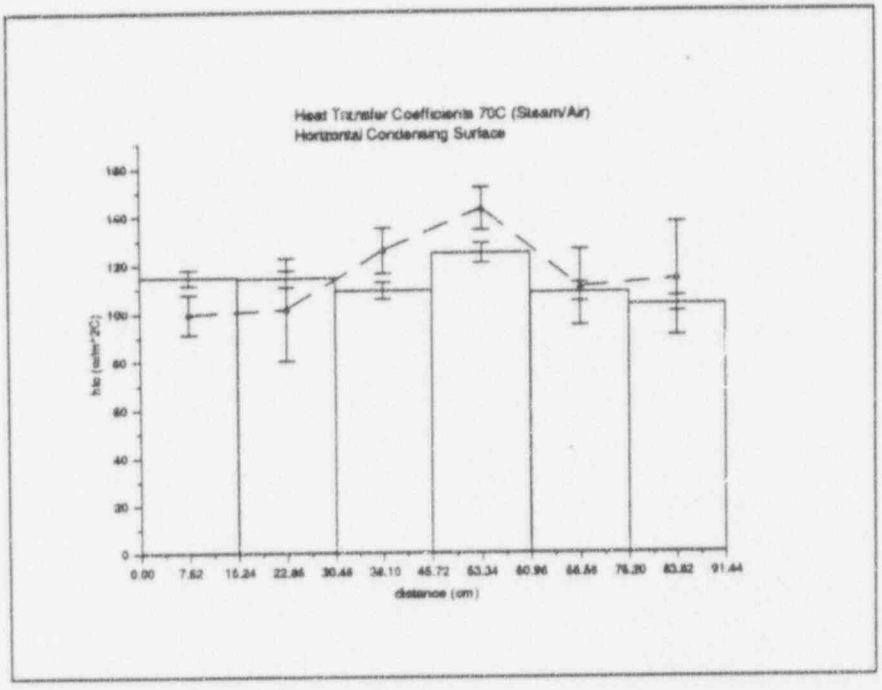

Figure 5.9 70 C Heat Transfer Coefficients (Horizontal)

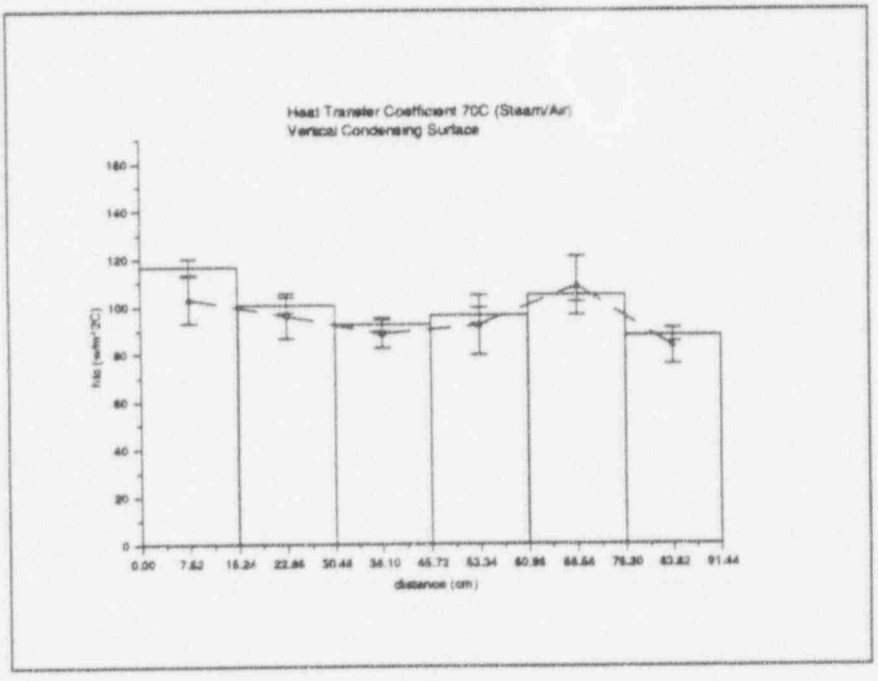

Figure 5.10 70 C Heat Transfer Coefficients (Vertical)

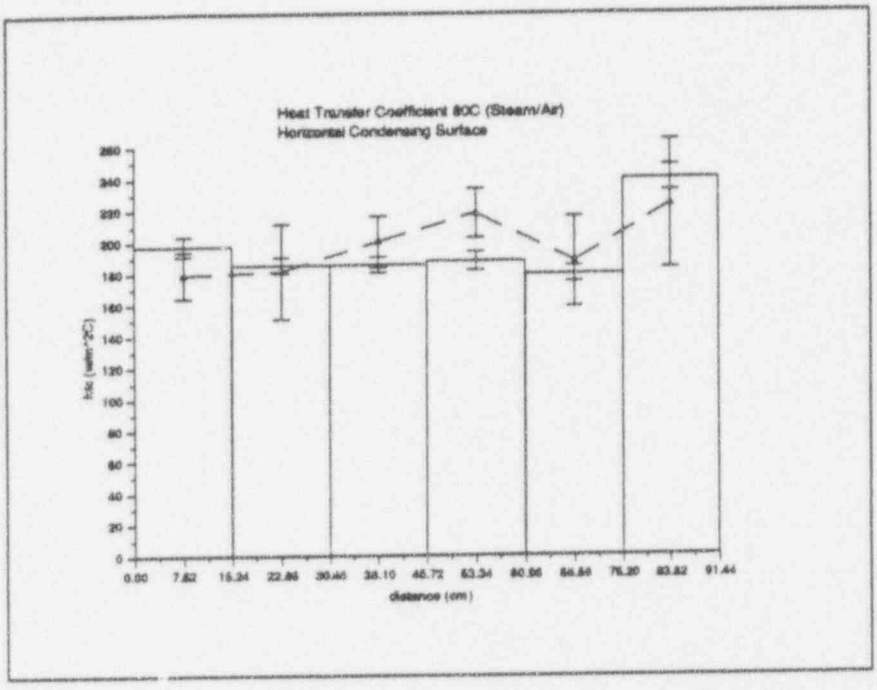

Figure 5.11 80 C Heat Transfer Coefficients (Horizontal)

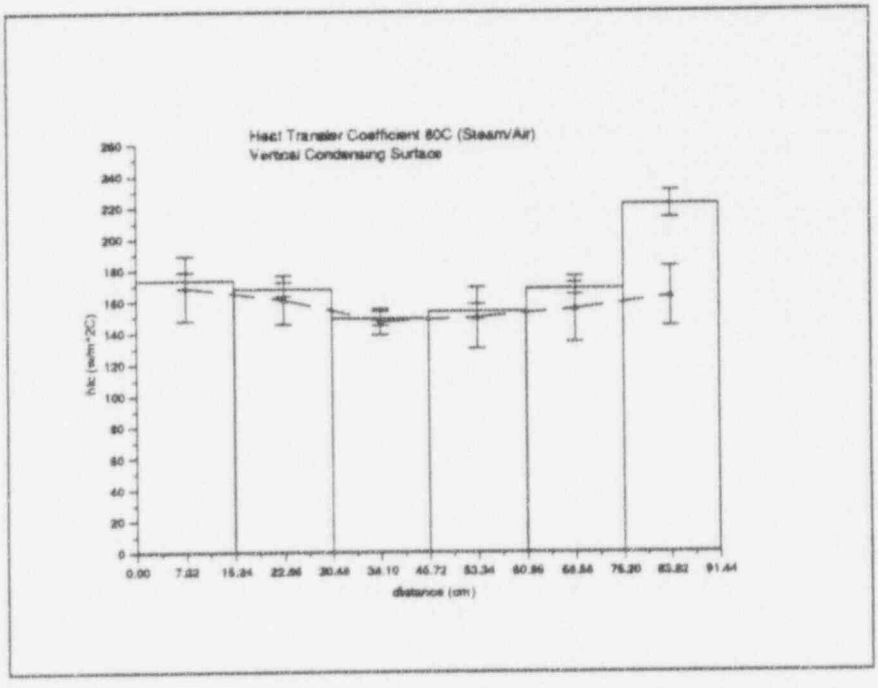

Figure 5.12 80 C Heat Transfer Coefficients (Vertical)

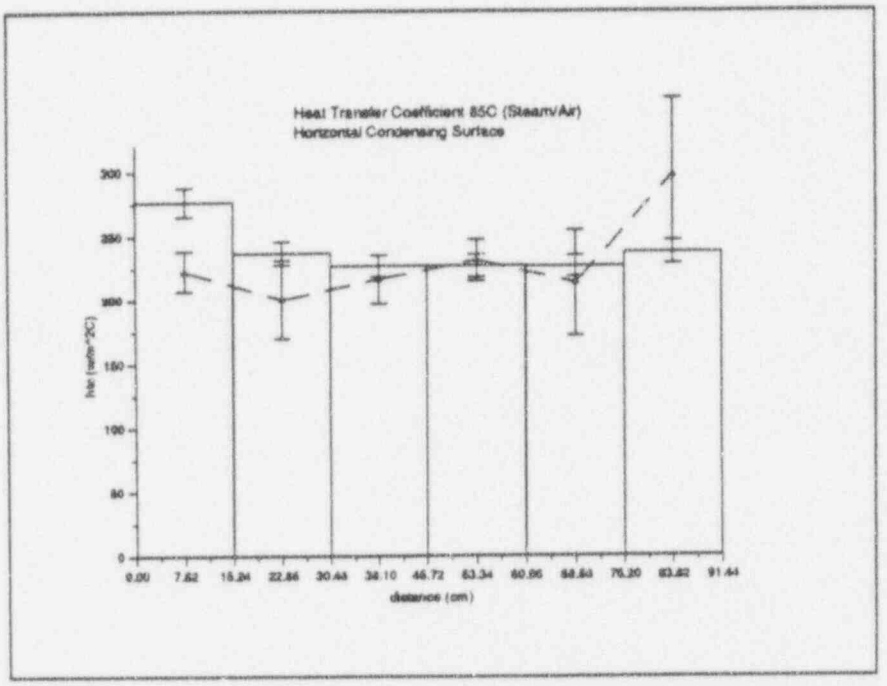

Figure 5.13 85 C Heat Transfer Coefficients (Horizontal)

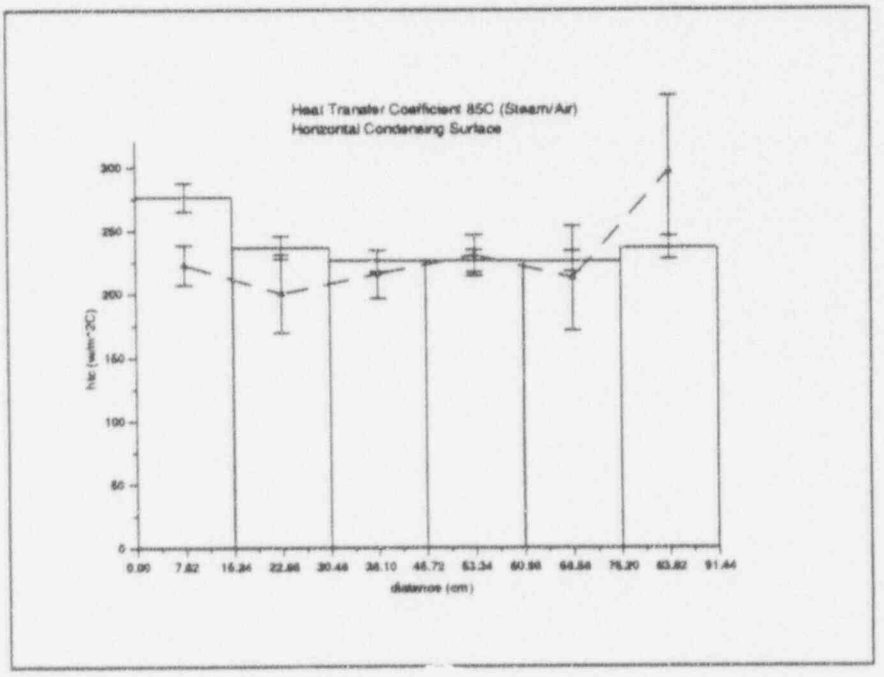

Figure 5.14 85 C Heat Transfer Coefficients (Vertical)

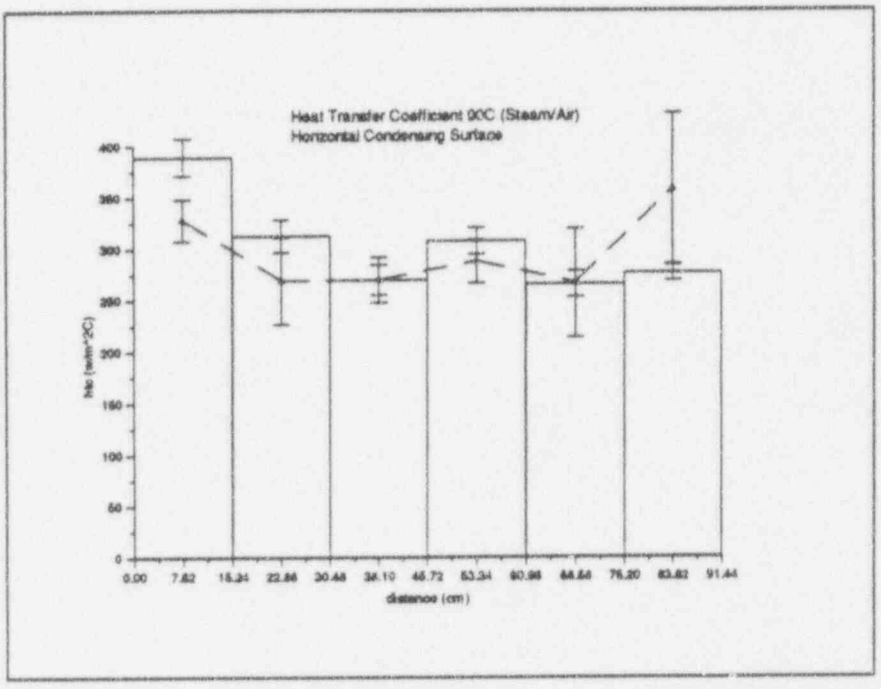

Figure 5.15 90 C Heat Transfer Coefficients (Horizontal)

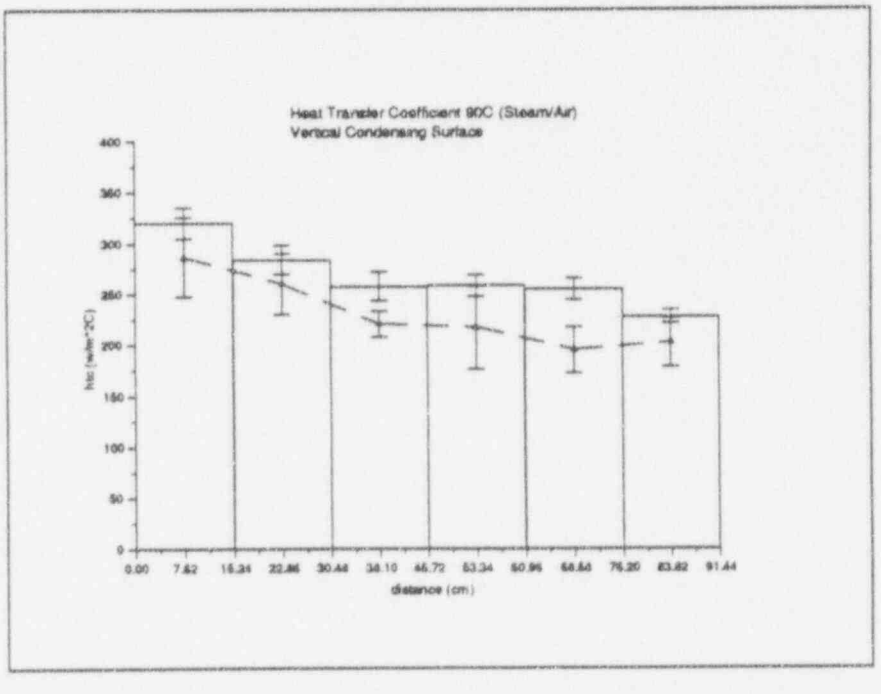

Figure 5.16 90 C Heat Transfer Coefficients (Vertical)

visual observation was obstructed by condensation on the Lexan side walls of the test section it was observed that there was significant droplet formation on the top condensing surface. There also appeared to be a liquid film on the plate accompanying the droplet formation. From visual observation the droplets were seen to vary in size from approximately 0.2cm to 0.5cm. The vertically inclined plate was observed to have pure filmwise condensation with no droplets present. The presence of the droplets could have many effects on the heat transfer coefficient of the horizontal surface. The droplets attached to the upper surface effectively increase heat transfer surface area which would result in the increased heat transfer coefficients observed on the top plate. There may also be an increase in the heat transfer due to the enhancement of turbulent mixing caused by the departure of the droplets. The random occurrence of the droplet formation and the rain droplet departure may have also contributed to the relatively unsteady nature in the heat transfer coefficient observed in the horizontal plate. The vertical plate heat transfer coefficient has very good agreement between the two methods of measurement as can be seen by Figure 5.3 and 5.4.

The data presented in figures 5.8 through 5.16 was also compared with other investigators of condensation in the presence of noncondensables, specifically Pernsteiner since his studies closely resembled the present work although at a much smaller scale. Pernsteiner investigated condensation on a vertical wall due to natural circulation. Although the test section geometry differs slightly, a relatively close agreement between his results and the current investigations was observed. As can be seen in Table 5.3 the average heat transfer coefficients in the current facility were slightly higher than those observed by Pernsteiner. This could be attributed to the larger test section geometries, because the present test section was significantly wider, mixed convection heat transfer mechanisms may have lead to the slight enhancement of the heat transfer coefficient. This effect was one of the primary reasons for the present test section and the hypothesis of enhancement of the heat transfer coefficient due to mixed convection was observed This effect also agrees with the observation by Westinghouse. Calculations were done with the correlations introduced in Chapter three and the results of the theoretical heat transfer

Test Section Temperature	Heat Flux Strip (w/m2C)	Coolant Energy Balance (w/m2C)
60.7	62	56
70.9	103	104
79.9	157	149
85.3	193	182
90.2	267	251

Table 5.3 Pernsteiner's Reported Results

Test Section Temperature °C	Heat Transfer Coefficient (w/m^2C)
60	70.15
70	104.43
80	159.47
85	202.39
90	267.7

Table 5.4 Theoretical Heat Transfer Coefficients

coefficients are given in Table 5.4. The horizontal plate heat transfer coefficients appear to be slightly higher than those calculated theoretically. This could be attributed to the raining effect observed on this surface as discussed previously. The vertical plate heat transfer coefficients, which exhibited pure filmwise condensation, seems to agree well with the theory.

5.4 Air/Steam at Various Temperatures (Steam Generator Rupture)

5.4.1 Description of Test

Test series 500 consists of a series of experiments designed to simulate a pipe rupture in the steam generator compartment of the AP600. The injection system was changed from the uniform injection system (Figure 4.6) to the injection system pictured in Figure 4.8. The right side of the steam inlet was plugged off and insulated so that no steam would exit and the test section would again be isolated from the environment. The test procedure was similar to the above mentioned procedure with the exception that preliminary velocity measurements were taken with a Hontzsch turbine anemometer. A 1.25" hole was drilled in the test section 16" from the vertical condensing plate and 2.5" below the horizontal condensing plate (between axial temperature locations 2 and 3) to provide for installation of the velocity meter. Figure 5.17 indicates the placement of the velocity meter with respect to the steam injection inlet. A 3" long aluminum flange was constructed and attached to the test section so that the Hontzsh velocity meter could be inserted. To allow the direction of flow to be determined a plate with degree measurements was attached to the flange and a pointer positioned on the velocity meter, so that the relative angle of the velocity meter would be known. Velocity measurements were taken at several different angles. Zero degrees corresponded to the turbine vane wheel parallel to the top condensing surface with the flow toward the vertical plate corresponding to the positive direction. The output of the meter was read from a Nicolet Oscilloscope as described in chapter 4.

5.4.2 Results/Discussion

The average values for the heat transfer coefficients are presented in Table 5.5. The heat transfer coefficients increased dramatically from those obtained with the uniform injection system especially at the higher temperatures of 85° C and 90°C. Table 5.6 gives an idea of the mass flow rates needed to achieve a given steady state temperature in this test series. Although sufficient testing or analysis has not been completed the enhancement in the heat transfer coefficient could be a result of the effect of a jet of steam impinging on the upper cooled condensing surface. In the uniform injection tests the steam would have dispersed more evenly and not created such a jet effect. The temperature profiles indicate that there is a plume of hot vapor in the vicinity of the injection, as would be expected Figure 5.18. Table 5.7 show the velocity measurements as a function of temperature and angle. Although these are preliminary velocity measurements they indicate that the horizontal flow is too small to be detected by the velocity meter (less than 0.5 ft/sec). Some oscillation was observed at angles of approximately 60° and 120°. This could be due to the inertia required to spin the turbine vane wheel. If the flow velocity is not fast enough there is not sufficient energy to overcome this inertia and the vane wheel may oscillate back and forth rather than spin in one direction, thus causing fluctuating voltage readings. When the velocity meter was rotated 90° so that the vane wheel was parallel to the vertical surface an upward velocity was seen to appear at 80°C, although it was only slightly above the velocity needed to overcome the inertia of the wheel. The velocity was observed to increase as the steady state temperature of the test section and correspondingly the mass flow rate was increased. This indicates that there may be some jet impingement on the upper condensing plate due to the modified steam injection system. These velocity measurements were mainly done to test the use of the meter and measurement techniques. Many more test will have to be conducted before a accurate determination of the velocity field can be obtained.

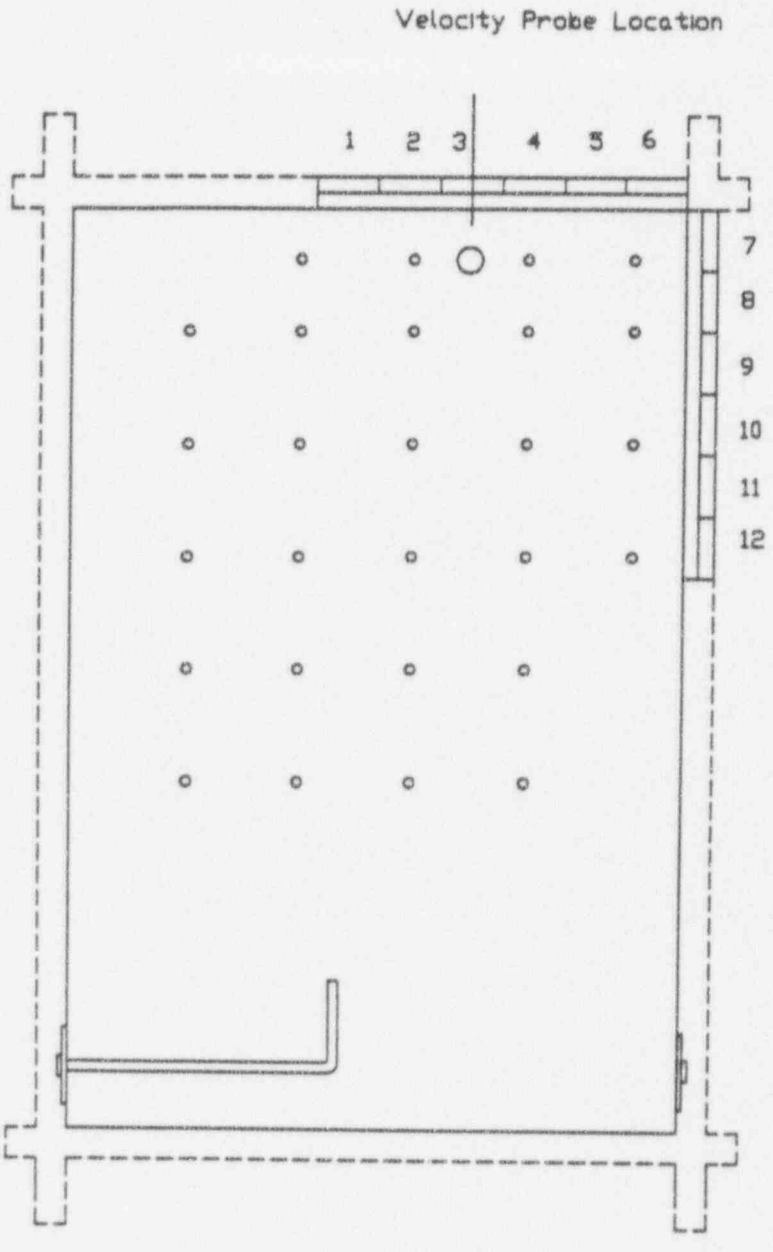

Figure 5.17 SGPR Location and Velocity Probe Location

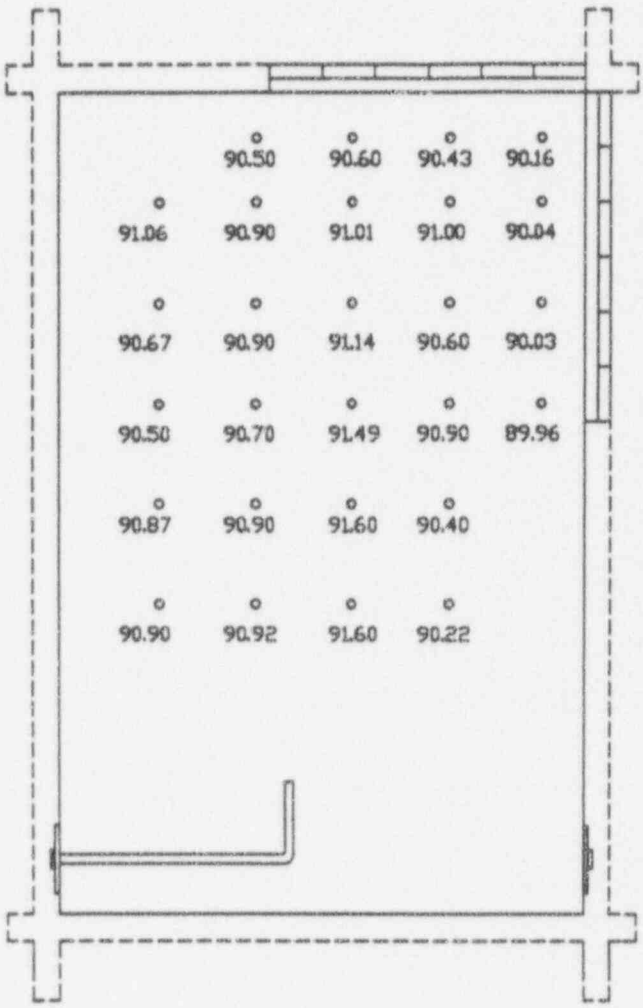

Figure 5.18 Temperature Distribution 90C SGPR

Test Section Temperature °C	HTFM Horizontal Plate (w/m^2C)	CEB Horizontal Plate (w/m^2C)	HTFM Vertical Plate (w/m^2C)	CEB Vertical Plate (w/m^2C)
60	97.43	85.66	79.1	72.92
70	154.26	141.46	112.15	112.75
80	174.19	179.53	139.44	123.52
85	317.98	300.28	210.48	233.53
90	512.73	488.82	371.3	387.47

Table 5.5 Heat Transfer Coefficients

Test Section Temperature °C	Mass Flow Rate (kg/sec)
60	0.00164
70	0.0022
80	0.00312
85	0.00467
90	0.00781

Table 5.6 Mass Flow Rates as a Function of Temperature

Angle °	Temperature 60	Temperature 70	Temperature 80	Temperature 85	Temperature 90
0	-----	-----	-----	-----	-----
40	-----	-----	-----	-----	-----
80	-----	-----	fluctuation	fluctuation around 0.5(ft/s)	fluctuation around 0.5(ft/s)
90	-----	-----	0.88(ft/s)	1.37(ft/s)	1.45(ft/s)
120	-----	-----	fluctuation	fluctuation	Sporadic around 0.88(ft/s)
180	-----	-----	-----	-----	-----

Table 5.7 Velocity Measurements

Chapter 6

Air/Helium/Steam Experiments

6.1Summary Description of Experimental Procedure

The procedure used in the series 300 experiments (air/helium/steam) was the same as that mentioned in chapter five with the air/steam experiments except that helium was added in various molar concentrations. The facility depicted in Figure 4.1 was modified slightly to allow the injection of a helium air mixture. Figure 6.1 is a schematic of the experimental apparatus containing the additional features. Building air and industrial quality helium (99.9% pure) was passed through two separate Dwyer RMC series air flow meters into a tee section, where the gases mixed prior to entering the test section. The flow meters were factory calibrated for air, therefore a correction factor for the different mass of helium was used:

$$Q_2 = Q_1 \sqrt{\frac{1}{s.g}}$$

where Q_2 is the actual flow corrected for the specific gravity, Q_1 is the observed flowmeter reading and s.g is the specific gravity of helium. The flow rates of the meters were adjusted so a particular molar percent of helium in air was entering the test section. A sufficient volume of the gas mixture was allowed to flow through the test section so that a uniform concentration existed. Gas samples were taken after the mixing tee and in the midsection of the test facility to ensure that the there was an even distribution of

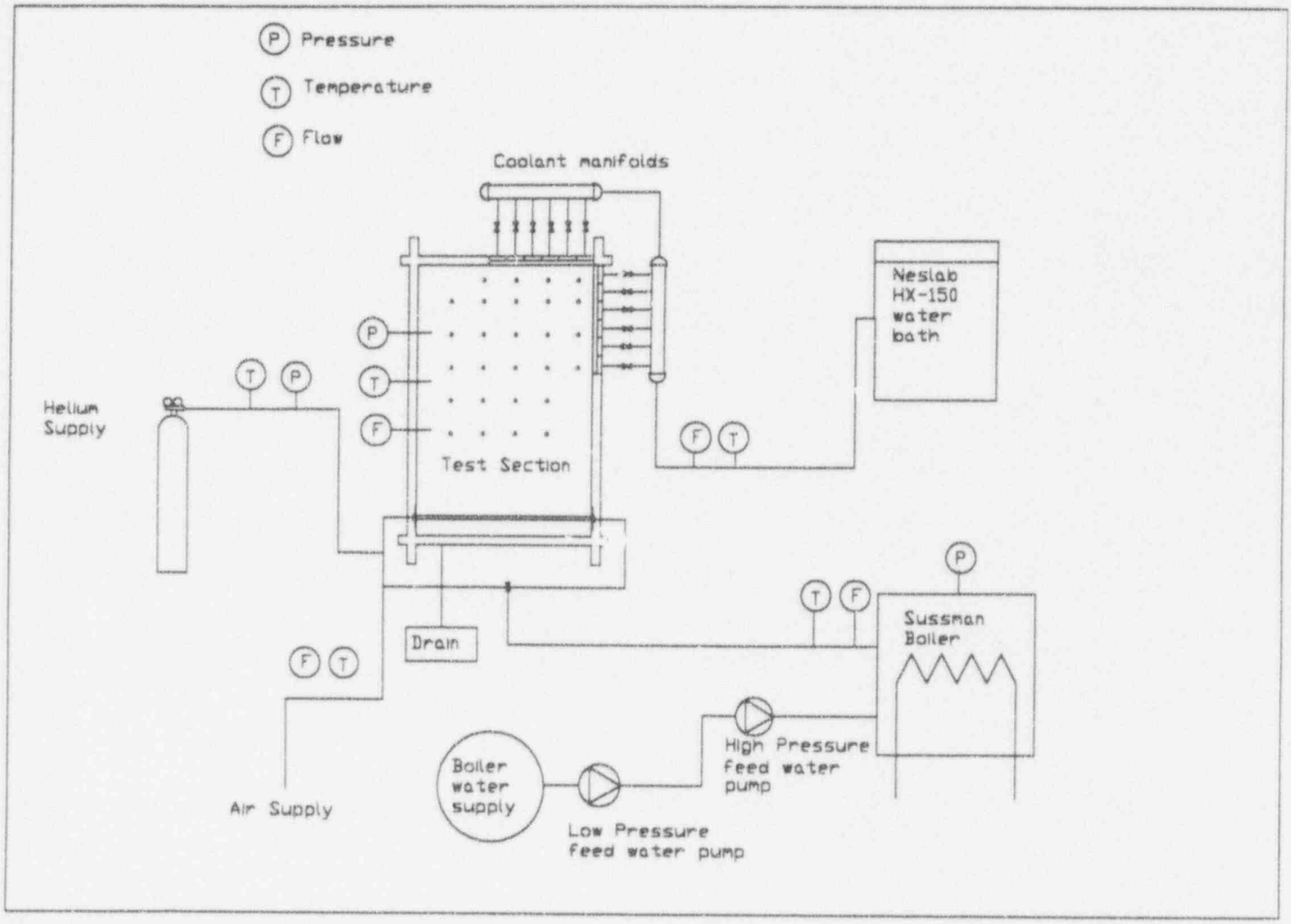

Figure 6.1 Esential Components of Helium Experiments

the gas mixture. The gas samples were analyzed on a mass spectrometer to ensure the proper mixture existed in the test section. Prior to taking a gas sample the gas sampling apparatus (discussed in chapter 4) was evacuated to a pressure of no more than 2 torr. The purge tank was filled with test section gas and a sample was taken. The two gas concentration measurement techniques (volume flow rate and mass spectrometer analyzed gas sample) yielded similar results that were within the error of the volume flow meters. The volume flow meters had the drawback that they were only able to measure the initial gas concentration therefore the gas sampling technique was needed to allow the sampling of the test section gas later in the test. After a molar percent of approximately 4,8,16, or 30 was achieved (as measured by the mass spec.) the boiler was turned on and steam allowed to enter through the throttling needle valve until one of the steady state temperatures was reached. Gas samples were taken at each of the separate steady-state temperatures so that the noncondensible gas mixture would be known.

This procedure produces slightly different results than what would occur in an actual accident scenario. The steam entering the containment atmosphere would react with the metal cladding material. This oxidizing reaction would replace some of the steam with hydrogen gas. In our experiments the amount of helium (substituted for hydrogen) to air ratio stays constant while the total noncondensible gas fraction decreases with increasing test section temperature. However, this difference in introduction of the light gas species does not effect the experimental results.

6.2 Results/Discussion

Table 6.1 shows the average heat transfer coefficients at various temperatures and helium concentrations. The local heat transfer coefficients can be found in reference 4. Figures 6.2 to 6.5 show the effects of the various concentrations of helium at a temperature of 70°C. A trend was seen in the heat transfer coefficients as the helium concentrations were increased from 0 to 30 percent molar. There appears to be a degradation in the heat transfer coefficient in the vicinity of cooling plates #5 and #11. This usually

occurred when the helium concentrations were above approximately 4% molar, however some tests with helium concentrations above this value did not exhibit this phenomena. Some air/steam only tests (series 200) were repeated after this phenomena was observed to check for possible systematic errors but none were found and the air/steam only tests compared well to previously measured tests. The origin of this degradation is not known, it is possible that it is some sort of random flow phenomena caused by light helium gas accumulation, or it could possibly be some yet undetected systematic error. Other than the unexplained dip in the heat transfer coefficient at plates #5 and #11 the air/helium/steam experiments produced heat transfer coefficients similar to the air/steam only experiments. This phenomena was also observed by Pernsteiner. He made an attempt to explain this similarity in helium and air experiments by considering that the increase in the diffusion coefficient with helium present was off set by a stratification of light gas next to the condensing plate. The increase of the diffusion coefficient of steam with the presence of helium increases the mass transfer coefficient and thus increases the heat transfer due to condensation/evaporation. He suggested that this increase of the heat transfer was suppressed by a stratification layer that may have formed next to the plate.

Test Section Temperature	Molar Fraction He	HTFM Horizontal	CEB Horizontal	HTFM Vertical	CEB Vertical
60	29.3	71.96	69.74	64.89	60.27
	17.2	78.1	77.13	69.37	65.76
	7.74	86.66	83.08	69.88	73.14
	3.8	78.77	79.05	69.57	73.28
70	27.9	94.73	96.61	87.41	79.62
	15	119.46	113.8	101.42	100.25
	7.13	126.99	112.82	101.59	101.34
	4.35	103.64	103.49	94.28	90.94
80	31.8	148.35	158.11	130.9	135.34
	14.18	183.77	171.95	152.6	145.75
	8.81	205.28	183.11	163.03	156.31
	3.68	203.62	184.64	162.52	150.34
85	29.7	182.9	217.39	162.61	180.26
	16.5	247.69	245.02	199.98	204.78
	8.8	194.6	224.74	216.49	201.2
	4.06	199.01	228.97	173.85	192.55
90	27.96	239.13	274.76	200.37	224.07
	16.38	315.83	310.62	252.54	261.67
	7.37	308.84	206.14	247.79	265.32
	4.06	239.82	249.51	190.48	205.17

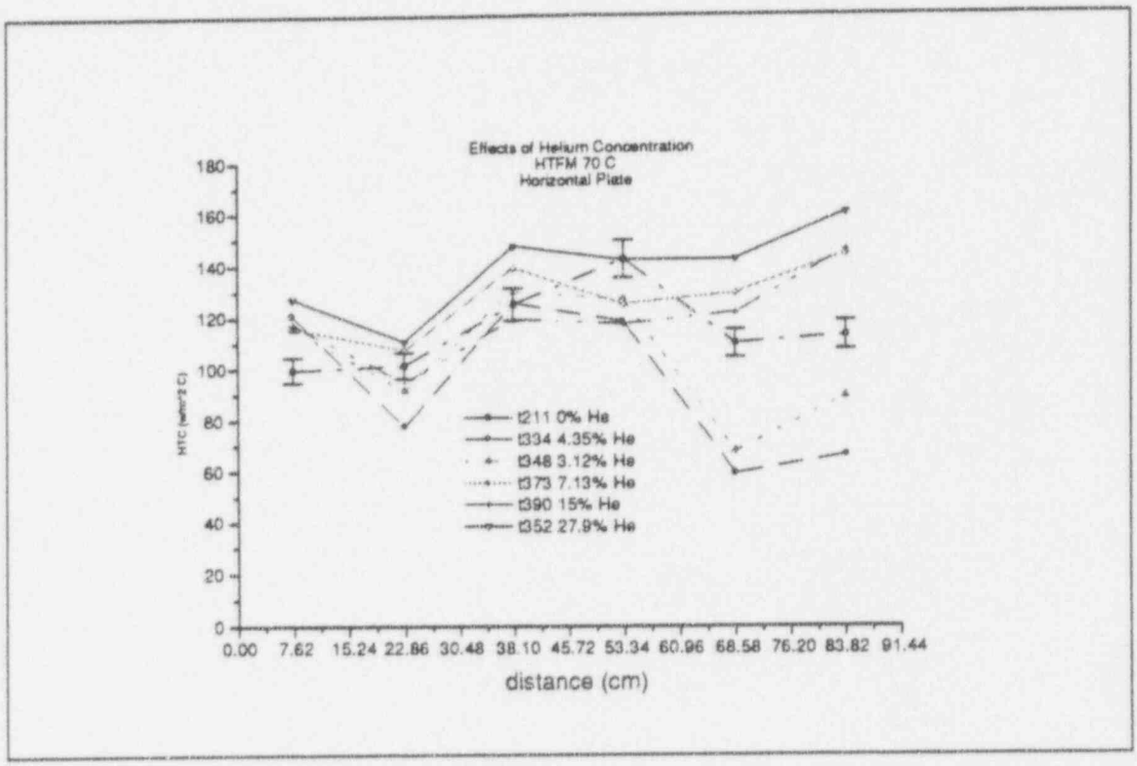
Effects of Helium Concentration
HTFM 70 C
Horizontal Plate
HTC (w/m^2 C)
180
160
140
120
100
80
60
40
20
0
0.00 7.62 15.24 22.86 30.48 38.10 45.72 53.34 60.96 68.58 76.20 83.82 91.44
distance (cm)
t211 0% He
t334 4.35% He
t348 3.12% He
t373 7.13% He
t390 15% He
t352 27.9% He

Figure 6.2

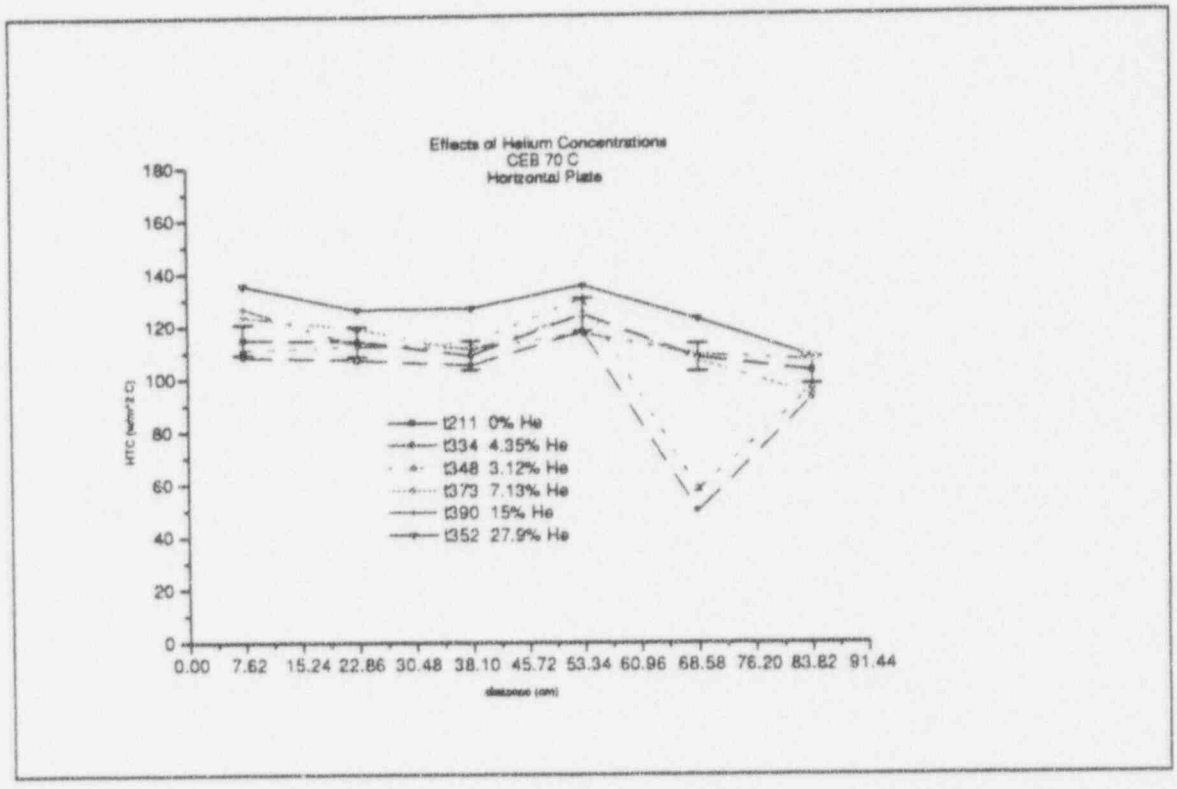
Effects of Helium Concentrations
CEB 70 C
Horizontal Plate
180
160
140
120
100
80
60
40
20
0
0.00 7.62 15.24 22.86 30.48 38.10 45.72 53.34 60.96 68.58 76.20 83.82 91.44
t211 0% He
t334 4.35% He
t348 3.12% He
t373 7.13% He
t390 15% He
t352 27.9% He

Figure 6.3

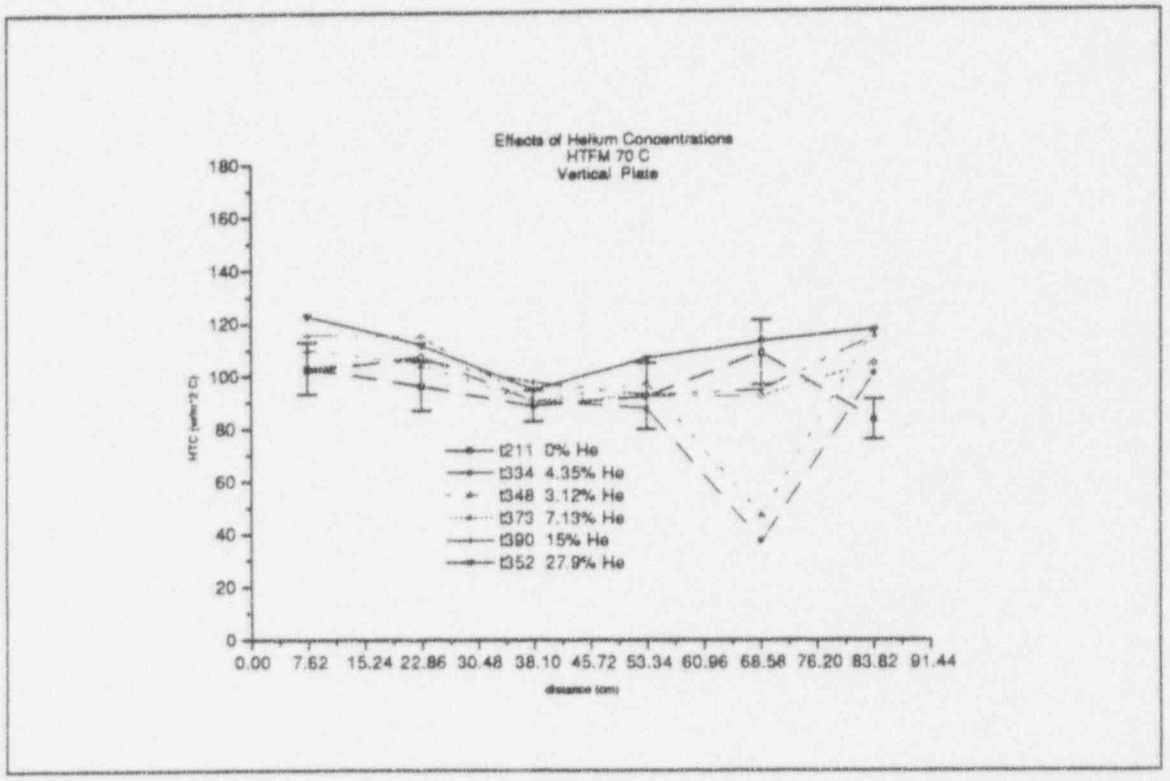
Effects of Helium Concentrations
HTFM 70 C
Vertical Plate
180
160
140
120
100
80
60
40
20
0
0.00 7.62 15.24 22.86 30.48 38.10 45.72 53.34 60.96 68.58 76.20 83.82 91.44
t211 0% He
t334 4.35% He
t348 3.12% He
t373 7.13% He
t390 15% He
t352 27.9% He

Figure 6.4

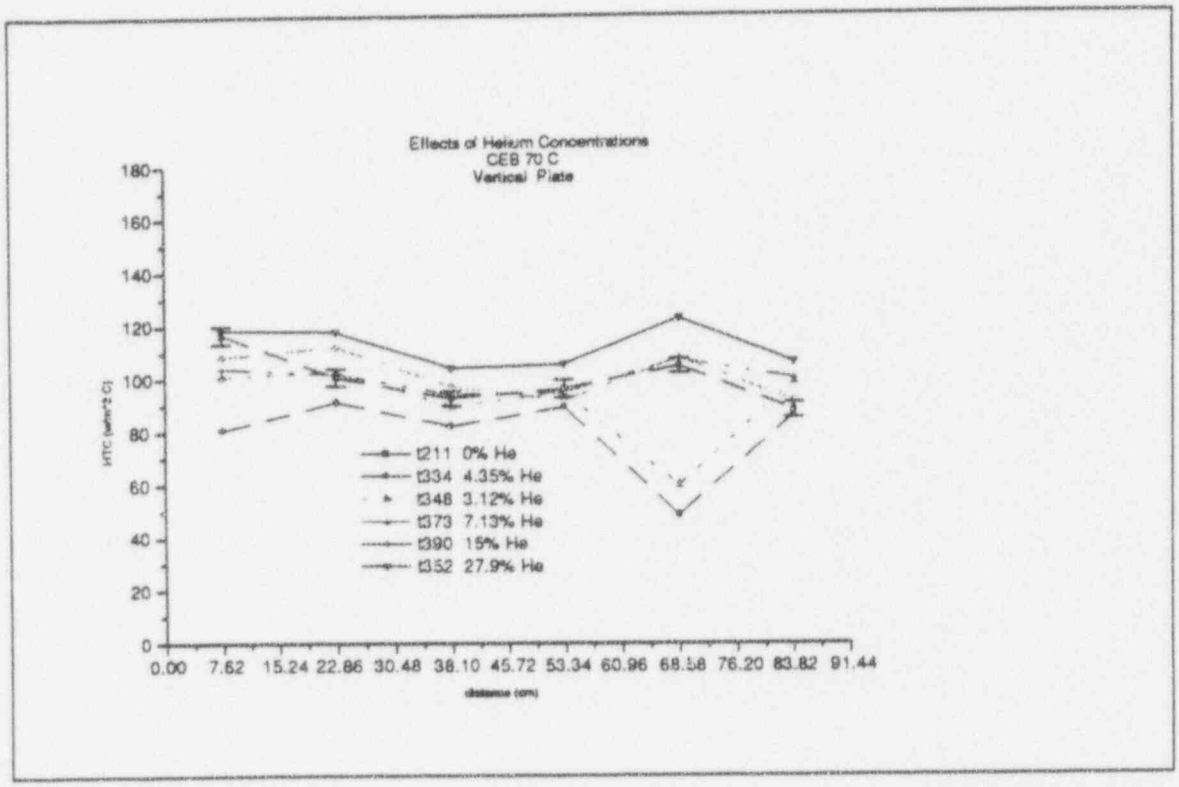
Effects of Helium Concentrations
CEB 70 C
Vertical Plate
180
160
140
120
100
80
60
40
20
0
0.00 7.62 15.24 22.86 30.48 38.10 45.72 53.34 60.96 68.58 76.20 83.82 91.44
211 0% He
334 4.35% He
348 3.12% He
373 7.13% He
390 15% He
352 27.9% He

Figure 6.5

Chapter 7

Observations

Experiments were conducted to determine the heat transfer coefficient, of steam in the presence of noncondensable gases, on a horizontal and vertical cooled condensing plate with a similar surface finish as the Westinghouse AP600 containment. Preliminary scoping tests seem to indicate the following:

- A slightly higher average heat transfer coefficient on the top condensing plate than on the vertical condensing plate was observed. This is assumed to be a result of the presence of droplets on the upper surface which results in an increased heat transfer area.

- Comparisons of air/helium/steam tests to the air/steam only tests did not show any significant change in the heat transfer coefficient for helium molar ratios between 4 and 30 percent except the reported degradation near plate #5 and #11. The presence of this degradation is unknown at the present time.

- The steam generator pipe break injection system showed increased heat transfer coefficients over the uniform injection system. This may be as result of a steam jet impinging on the surface of the upper plate. Unfortunately velocity measurements could not be obtained for the uniform injection series and only preliminary measurements were conducted with the SGPR injection system.

- Some work has been done to try to visualize the developed flow patterns in the test section, but the presence of condensate on the side walls has slowed the effort.

Bibliography

[1]Westinghouse Electric Corporation, *Tests of Heat Transfer and Water Film Evaporation From a Simulated Containment To Demonstrate the AP600 Passive containment Cooling System*, Westinghouse Report NSE-90-0013, Jan.1990

[2]Huhtiniemi I. K., *Condensation in the Presence of a Noncondensable Gas: The Effects of Surface Orientation*, PhD Thesis, University of Wisconsin, 1991

[3]Pernstiener A. P., *Condensation in the presence of noncondensable Gas: Effects of Helium Concentration*, Ms Thesis, University of Wisconsin, 1993

[4]Bird R. B., Stewart W. E., Lightfoot E. D., *Transport Phenomena*, John Wiley, 1960

[5]Anderson M. H., *Data Book of Condensation Experiments*, University of Wisconsin, 1994

[6]Incropera E.P., Dewitt D.P., *Introduction to Heat Transfer*, John Wiley, 1990

[7]*Shell Flow Meter Engineering Handbook*, edited by Preston T. S., 1968

[8]Glasstone, Laidler, Eyring, *Theory of Rate Processes*, McGraw-Hill, 1941

[9]Hirschfelder, *Molecular Theory of Gases and Liquids*, John Wiley, 1954

[10]Rohsenow W. M., *Heat, Mass, and Momentum Transfer*, Prentice-Hall, 1961

[11]Woodcock J., Spencer D. R., Kennedy M.D., Howe K. S., *Westinghouse - GOTHIC: A computer Code for Analyses of Thermal Hydraulic Transients for Nuclear Plant Containments and Auxiliary Buildings*, Westinghouse Report WCAP- 13412

[12] Shepherd J.P.G., *Data Analysis*, University of Wisconsin (River Falls), 1992

[13]Box G.E.P. *Statistics for Experimenters*, John Wiley 1978

[14]Suryanarayna N. V., Malchow G. L., *Film Condensation on Inclined Plane Surfaces*, Transactions of ASME, J. Heat Transfer, vol. 97(1), pp 79-82,1975

[15]Fox R. J., Nagasaki T., Hihikata K., Peterson P.F., *Heat Transfer and Stability Phenomena in Gas Loaded Condensers*, Dept. of Nuclear Engineering, University of California, Berkeley.

[16]Siddique M., Golay M. W., Kazimi M. S., *Local Heat Transfer Coefficients for Forced Convection Condensation of Steam in a Vertical Tube in the Presence of Air*, Dept. of Nuclear Engineering, MIT

[17]Kang H. C., Kim M.H., *Characteristics of Condensation heat Transfer with Wavy Interface in the Presence of Noncondensable Gas*, NURETH 6 Conference

[18]Barry J.J., *Effects of Interfacial Structure on Film Condensation*, PhD Thesis, University of Wisconsin, 1987

[19]Dallmeyer H., *Stoff-und Warmeubertragung bei der Kondensation eines Dampfes aus einem Gemisch mit einem nicht knodensieren Gas in laminarer und turbulenter Stromungsgrenzschicht*, VDI-Forschungs-Heft 539, pp. 5-24, 1970

[20]Dehbi A. A., *Analytical and Experimental Investigation of the Effects of Non-condensible Gases on Steam Condensation under Turbulent Natural Convection Condition*, PhD Thesis, Dept. of Nuclear Engineering, MIT, Jan. 1991

[21]Gerstmann j., Griffith P., *Laminar Film Condensation on the Underside of Horizontal and Inclined Surfaces*, Int. J. Heat Mass Transfer, vol 10, pp. 567-580, 1967

[22]Henderson C.L., Marchello J.M., *Film Condensation in the Presence of a Non-condensible Gas*, Transactions of ASME, J. Heat Transfer, vol. 91(3),pp. 447-50, 1969.

[23]Cho D. C., Stein R.P., *Steam Condensation on the Underside of a Horizontal Surface*, Proceedings of Third International Topical Meeting on Nuclear Power Plant Thermal Hydraulics and Operations, Nov. 1988

[24]Kroger D. G., Rohsenow W. M., *Condensation heat Transfer in the Presence of a Non-condensible Gas*, Int. J. Heat Mass Transfer, vol. 11 pp. 15-26, 1968

[25]Kutsuna H., Inoue K., Nakanishi., *Film Condensation of Bapo Containing Non-condensible Gas in a Horizontal Duct*, Int. Symposium on Heat transfer, beijing 1987

[26]Robinson J. A., Windebank S.R., *Measurement of Condensation Heat Transfer Coefficients in a Steam Chamber Using a Variable Conductance Heat Pipe*, Proc. 2nd UK National Conference on Heat Transfer, vol. 1, pp. 617-637, Sept. 1988

[27]Slegers L., Seban R.A., *Laminar Film Condensation of Steam Containing Small Concentrations of Air*, Int. J. heat Mass Transfer, vol. 13, pp. 1941-1947, 1970

[28]Spencer D.L., Chang K. I., Moy H. C., *Experimental Investigation of Stability Effects in Laminar Film Condensation on a Vertical Cylinder*, International Heat Transfer Conference, Paris, vol. 6, Paper CS 22.3,1970

Appendix 1

Thermophysical Properties

The procedure used to obtain the values of the thermophysical properties of the aluminium plate are presented along with the values used. This was done by Purdue University's Thermophysical Properties Research Laboratory.

TABLE OF CONTENTS

List of Tables

List of Figures

Thermophysical Properties of Al 2024

INTRODUCTION

Samples of Al 2024 were submitted for thermophysical property determinations. Specific heat (C_p) was measured using a differential scanning calorimeter. Bulk density (d) values were obtained form the sample's geometries and mass. Thermal diffusivity (α) was measured using the laser flash technique. Thermal conductivity (λ) values were calculated as the product of these quantities, i.e. $\lambda = \alpha C_p d$.

Specific heat is measured using a standard Perkin-Elmer Model DSC-2 differential scanning calorimeter (Figure 1) with sapphire as the reference material. The standard and sample were subjected to the same heat flux as a blank and the differential powers required to heat the sample and standard at the same rate were determined using the digital data acquisition system. From the masses of the sapphire standard and sample, the differential power, and the known specific heat of sapphire, the specific heat of the sample is computed. The experimental data are visually displayed as the experiment progresses (Figure 2). All measured quantities are directly traceable to NBS standards.

Thermal diffusivity is determined using the laser flash diffusivity method. In the flash method, the front face of a small disk shaped sample is subjected to a short laser burst and the resulting rear face temperature rise is recorded and analyzed. A highly developed apparatus (Figure 3) exists at TPRL and we have been involved in an extensive program to evaluate the technique and broaden its uses. The apparatus consists of a Korad K2 laser, a high vacuum system including a bell jar with windows for viewing the sample, a tantalum or stainless steel tube heater surrounding a sample holding assembly, a thermocouple or an i.r. detector, appropriate biasing circuits, amplifiers, A/D converters, crystal clocks and a minicomputer based digital data acquisition system capable of accurately taking data in the 40 microsecond and longer time domain. The computer controls the experiment, collects the

data, calculates the results and compares the raw data with the theoretical model.

RESULTS AND DISCUSSION

The diffusivity sample was 1.271 by 1.338 by 0.3806 cm and with a density of 2.769 gm cm^{-3}. Specific heat results are given in Table 1 and Figure 4. The specific heat was measured during three runs. The specific heat values measured during the first run increases rapidly with increasing temperature and exhibited peak near 235°C. The specific heat values measured during run two were smaller and the peak was about gone. The values measured in during run three were smaller yet and the peak had disappeared. Obviously the sample annealed during these runs.

Thermal diffusivity values are given in Table 2 and Figure 5. Using these results and the specific heat values from run three, thermal conductivity values are calculated in Table 3. The specific heat values from run three were used because the additional heat from the laser flash technique does not alter the annealing process so the "true" specific heat and not the "apparent" specific heat is involved. The conductivity values are plotted in Figure 6. The conductivity values increases from 1.22 to 1.69 W cm^{-1} K^{-1} between 23 and 250°C.

TABLE 1

Specific Heat Results

Temperature (C)	Run-1 (W-s/gm-K)	Run 2 (W-s/gm-K)	Run 3 (W-s/gm-K)
23.	0.8750	0.8750	0.8750
50.	0.9400	0.9200	0.9040
75.	0.9840	0.9480	0.9190
100.	1.0350	0.9790	0.9370
125.	1.0800	1.0030	0.9530
150.	1.1280	1.0200	0.9640
175.	1.2050	1.0340	0.9740
200.	1.2970	1.0530	0.9790
225.	1.4040	1.1090	0.9800
235.	1.4250	1.1160	0.9810
245.	1.4160	1.0800	0.9870
250.	1.3880	1.0510	0.9920

TABLE 2

Thermal Diffusivity Results

Temperature (C)	Diffusivity (cm^2 sec^{-1})
23.0	0.50502
50.0	0.53243
100.0	0.53840
150.0	0.57004
200.0	0.58822
250.0	0.61410

TABLE 3

Thermal Conductivity Calculations

Sample (No.)	Temp. (C)	Density ($gm\ cm^{-3}$)	Specific Heat ($W\text{-}s\text{-}gm^{-1}\ K^{-1}$)	Diffusivity ($cm^2\ sec^{-1}$)	Conduct. ($W\text{-}cm^{-1}\ K^{-1}$)	Conduct. (BTU *)	Temp (F)
A	23.0	2.769	0.8750	0.50502	1.22359	848.94	73.4
	50.0	2.769	0.9040	0.53243	1.33281	924.72	122.0
	100.0	2.769	0.9374	0.53840	1.39752	969.61	212.0
	150.0	2.769	0.9638	0.57004	1.52132	1055.50	302.0
	200.0	2.769	0.9779	0.58822	1.59270	1105.03	392.0
	250.0	2.769	0.9923	0.61410	1.68735	1170.70	482.0

* (BTU in $hr^{-1}\ ft^{-2}\ F^{-1}$)

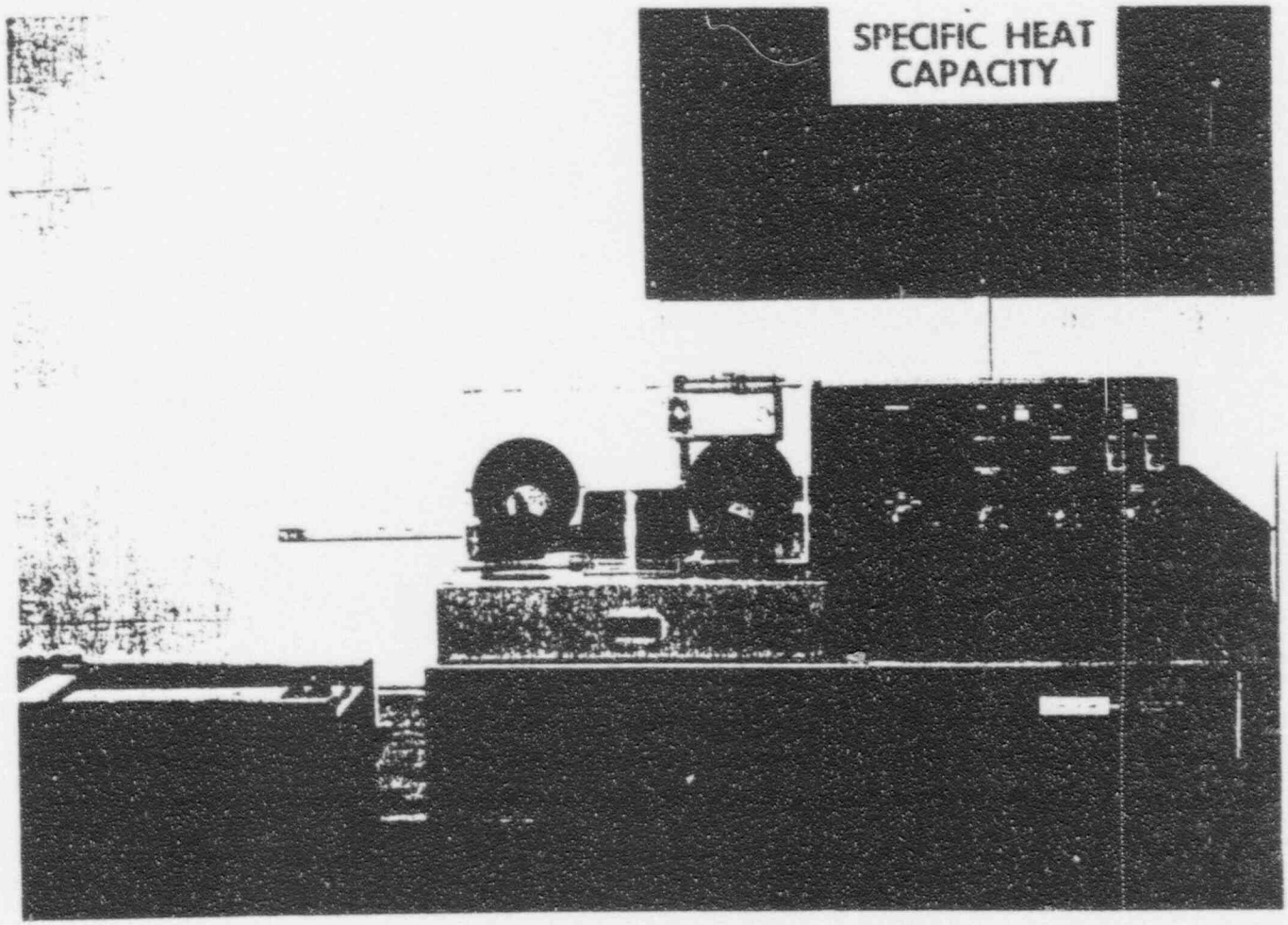

Figure 1. Differential Scanning Calorimeter

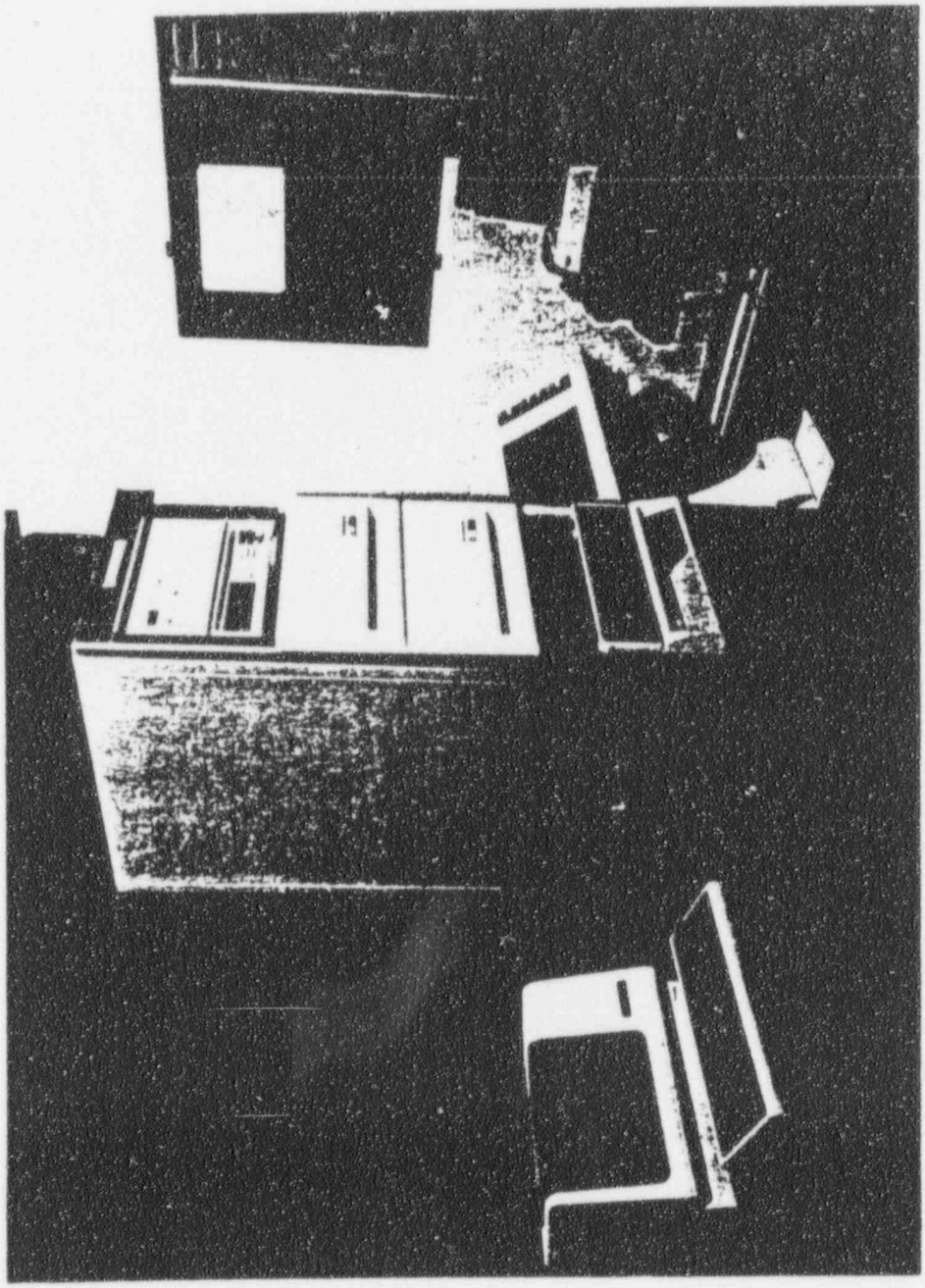

Figure 2. Digital Data Acquisition System

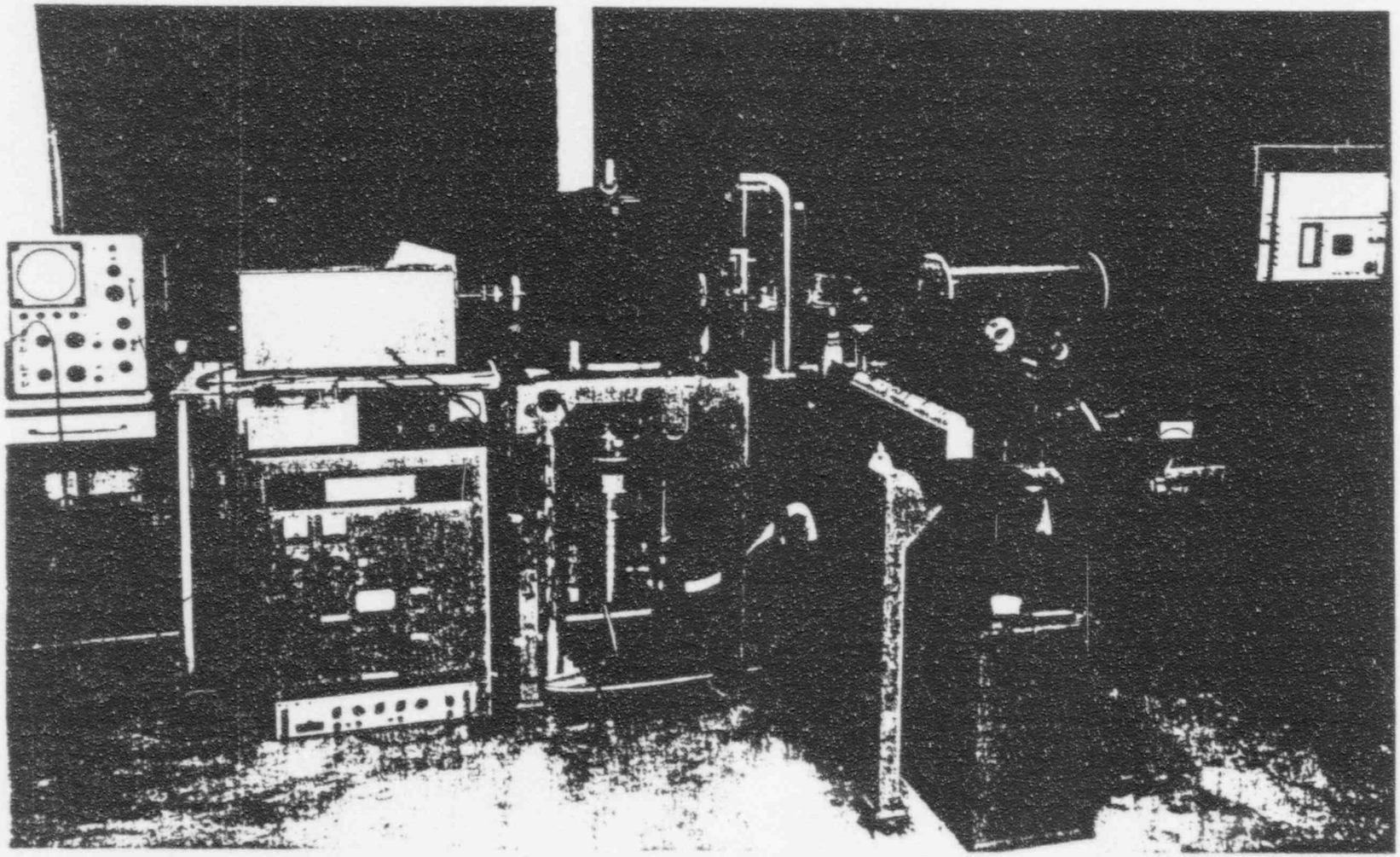

Figure 3. Flash Diffusivity Apparatus

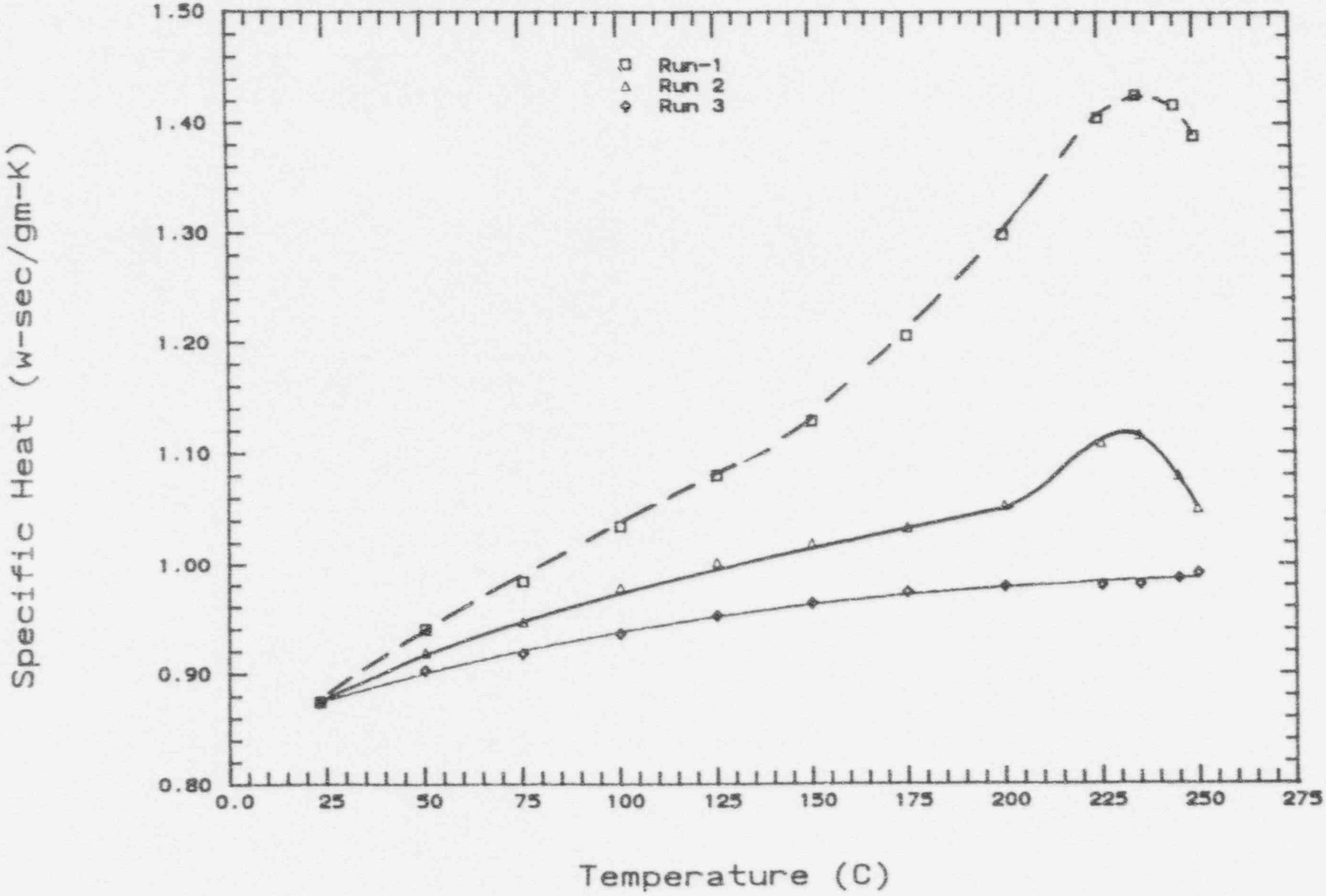

Figure 4 Specific Heat

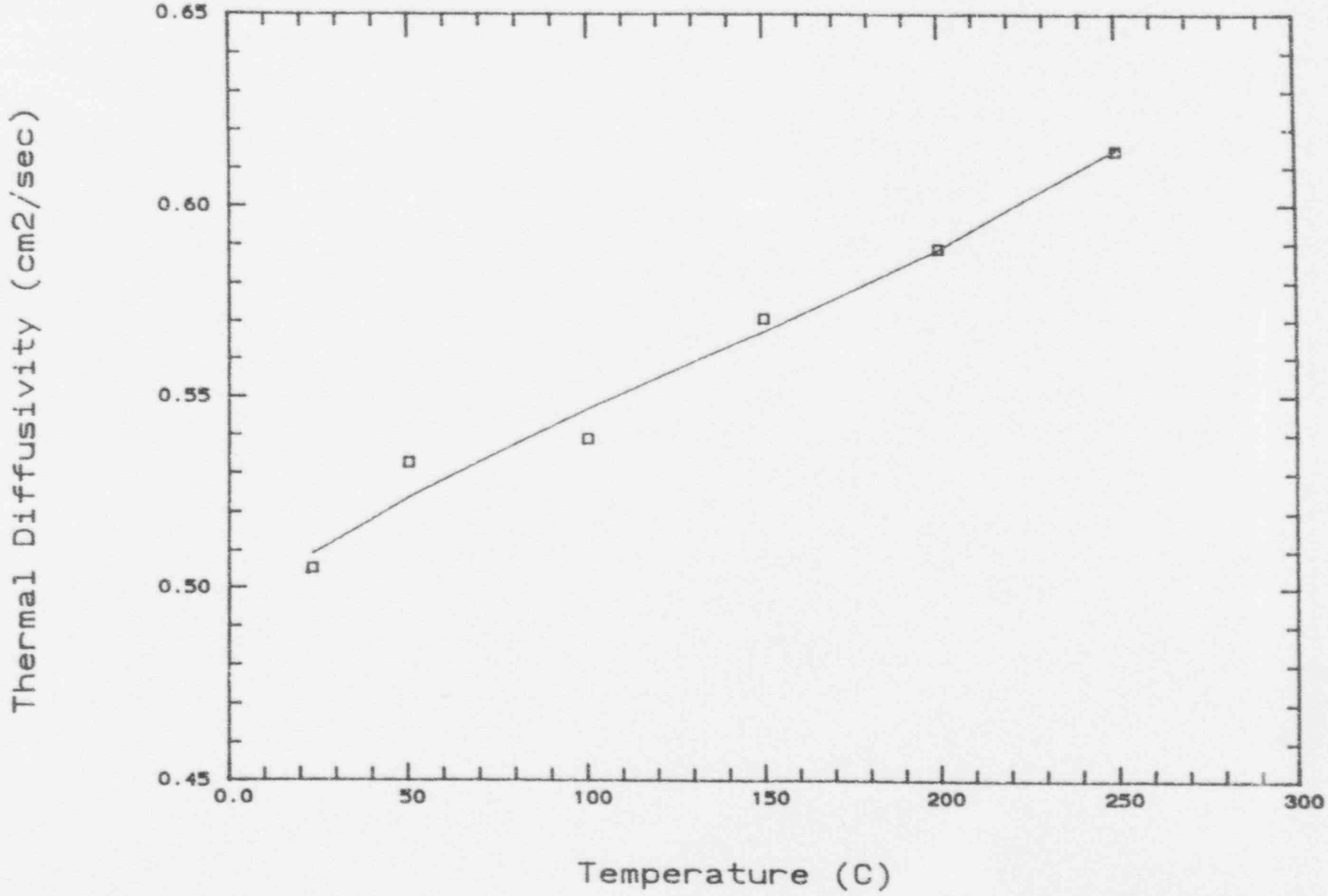

Figure 5 Thermal Diffusivity

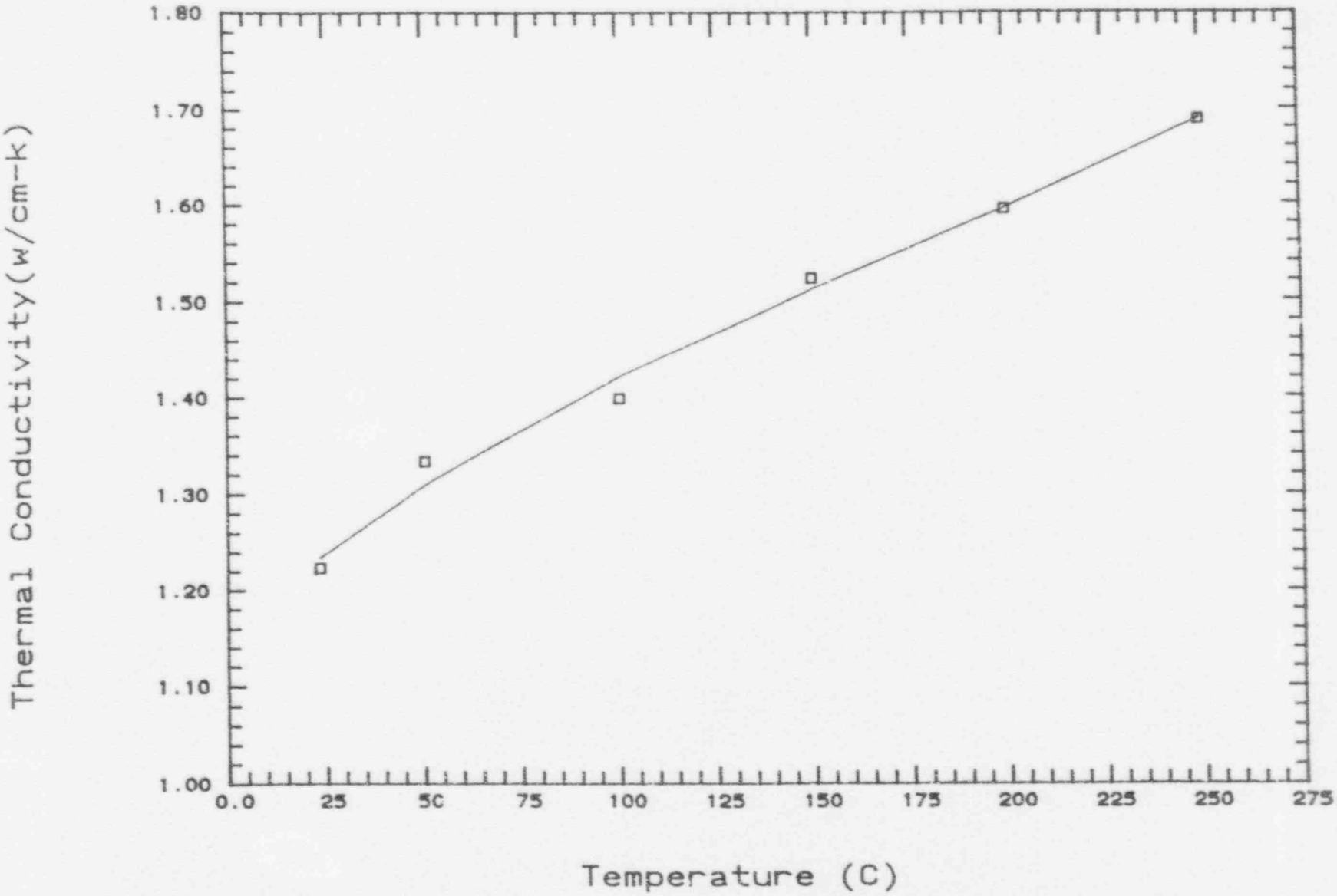

Figure 6 Thermal Conductivity

Appendix 2

Data Reduction Program

Appendix 2 consists of the data reduction program used in the analysis of the heat transfer data.

```
100     REM ------------------------------------------------------------------------
-
200     REM
300     REM     POSTTEST  - Surface Temperature Check
400     REM
500     REM     Version 3.1B      Oct 1989, for AP-600 B test series
600     REM
700     REM                       Feb 1990, the error estimates corr.
800     REM                       jun 1990, DAS-8 humidity, temp data
900     REM
1000    REM     (C)  Copyright  1987  J. J. Barry, modifications I.H.
1100    REM           10/8/93  M.H. Anderson (expansion to 12 heat flux meters, additio
n
1150    REM           of conductivity of CZn coating, 7 tmix temperatures
1200    REM ------------------------------------------------------------------------
-
1300    KEY OFF
1400    COLOR 15, 1, 1
1500    DIM x(12, 4), FS(12, 4), FTC$(12, 2), temp(12, 4), tc(12, 2), SD(12, 4), sdtc(1
2, 2), sigtc(12)
1600    DIM sigmatb(12), sigdtdx(12), hfmerr(12), sdt(12), sdtdeit(12), dtmixwall(12),
ceberr(12)
1700    DIM Tback(12), tsurf(12), Tinfac(12), hf(12), SERR(12), dtdx(12), htc(12)
1800    DIM flow(12), HFAVG(12), htcavg(12), LENGTH(12), VAIS(3), HUTE(3, 2), SDHUTE(3,
 2)
1850    DIM tmix(12), FTEM$(12), TMIXSTD(12), qerr(12), sdsurf(12), Tinerr(12), sigqceb
(12)
1900    nhfm = 12
2000    kal = 1.3179

2001    REM the value of the condictivity of the CZn was taking as
2002    REM the arthritic mean of the range given by the manufactures
2003    REM range (0.0159-0.0260 w/cmC) the error is the standard deviation

2010    kzn = .020913
2011    sigkal = .07178
2012    sigzn = .005
2015    dcarb = .09525
2100    PWIDTH = .1524
2105    sigflow = .038

2300    REM  Set thermocouple positions in all heat flux meters
2400    REM  measured from the backside of the condensing plates in mm
2505    REM  probe one position locations changed to test plate 12/12/93

2600    x(1, 1) = 29.733
2700    x(1, 2) = 21.733
2800    x(1, 3) = 13.733
2900    x(1, 4) = 5.733
3000    x(2, 1) = 30.036
3100    x(2, 2) = 21.908
3200    x(2, 3) = 13.907
3300    x(2, 4) = 5.906
3400    x(3, 1) = 29.82
3500    x(3, 2) = 22.2
3600    x(3, 3) = 14.199
3700    x(3, 4) = 6.198
3800    x(4, 1) = 29.794
3900    x(4, 2) = 21.26
4000    x(4, 3) = 13.869
4100    x(4, 4) = 6.096
4200    x(5, 1) = 30.585
4300    x(5, 2) = 22.228
4400    x(5, 3) = 14.671
4500    x(5, 4) = 6.645
4600    x(6, 1) = 29.299
4700    x(6, 2) = 21.59
4800    x(6, 3) = 13.881
4900    x(6, 4) = 5.893
5000    x(7, 1) = 31.433
5100    x(7, 2) = 23.533
5200    x(7, 3) = 15.964
5300    x(7, 4) = 7.887
5305    x(8, 1) = 29.527
5310    x(8, 2) = 21.958
5315    x(8, 3) = 14.203
5320    x(8, 4) = 6.164
5325    x(9, 1) = 30.622
5330    x(9, 2) = 23.106
5335    x(9, 3) = 15.13
5340    x(9, 4) = 7.155
5345    x(10, 1) = 30.531
5350    x(10, 2) = 22.428
5355    x(10, 3) = 15.062
5360    x(10, 4) = 7.086
5365    x(11, 1) = 28.905
5370    x(11, 2) = 20.904
5375    x(11, 3) = 13.119
5380    x(11, 4) = 5.042
5385    x(12, 1) = 30.053
5390    x(12, 2) = 22.281
5395    x(12, 3) = 14.31
5400    x(12, 4) = 6.312

6000    REM
6100    REM  Set number of t/c's per heat flux meter
6200    REM
6300
6400    ntc = 4
6500    LENGTH = .3048
6700    CLS
6800    PRINT "MIDTEST - Surface Temperature Check   Version 3B"
6900    PRINT
7000    PRINT
7300    INPUT "Enter the test number                : ", TESTNO!
7500    OPEN "coolant.dat" FOR INPUT AS #1
7600    FOR k = 1 TO nhfm
7700    INPUT #1, flow(k)
7800    flow(k) = flow(k) * 3.7853
7900    NEXT k
8000    CLOSE #1
8100    PRINT
8200    REM
8300    REM  read in data file names from setup file
8400    REM
8500    OPEN "posttest.inp" FOR INPUT AS #1
8600    LINE INPUT #1, A$ 'header record
8700    INPUT #1, ID$, ISLOT, CHAN%, A2D%, IGAIN, freq, NS, ICAL, FCAL$, FTEM$(1)'tmix1
8705    INPUT #1, ID$, ISLOT, CHAN%, A2D%, IGAIN, freq, NS, ICAL, FCAL$, FTEM$(2)'tmix2
8710    INPUT #1, ID$, ISLOT, CHAN%, A2D%, IGAIN, freq, NS, ICAL, FCAL$, FTEM$(3)'tmix2
8715    INPUT #1, ID$, ISLOT, CHAN%, A2D%, IGAIN, freq, NS, ICAL, FCAL$, FTEM$(4)'tmix3
8720    INPUT #1, ID$, ISLOT, CHAN%, A2D%, IGAIN, freq, NS, ICAL, FCAL$, FTEM$(5)'tmix3
8725    INPUT #1, ID$, ISLOT, CHAN%, A2D%, IGAIN, freq, NS, ICAL, FCAL$, FTEM$(6)'tmix4
8730    INPUT #1, ID$, ISLOT, CHAN%, A2D%, IGAIN, freq, NS, ICAL, FCAL$, FTEM$(7)'tmix4
8735    INPUT #1, ID$, ISLOT, CHAN%, A2D%, IGAIN, freq, NS, ICAL, FCAL$, FTEM$(8)'tmix5
8740    INPUT #1, ID$, ISLOT, CHAN%, A2D%, IGAIN, freq, NS, ICAL, FCAL$, FTEM$(9)'tmix5
8745    INPUT #1, ID$, ISLOT, CHAN%, A2D%, IGAIN, freq, NS, ICAL, FCAL$, FTEM$(10)'tmix6
8750    INPUT #1, ID$, ISLOT, CHAN%, A2D%, IGAIN, freq, NS, ICAL, FCAL$, FTEM$(11)'tmix6
```

```
8755      INPUT #1, ID$, ISLOT, CHAN%, A2D%, IGAIN, freq, NS, ICAL, FCAL$, FTEM$(12)'tmix
7
8798      INPUT #1, ID$, ISLOT, CHAN%, A2D%, IGAIN, freq, NS, ICAL, FCAL$, FSTEM$'steam
8800      INPUT #1, ID$, ISLOT, CHAN%, A2D%, IGAIN, freq, NS, ICAL, FCAL$, FTC$(1, 1)'cli
n-1
8900      INPUT #1, ID$, ISLOT, CHAN%, A2D%, IGAIN, freq, NS, ICAL, FCAL$, FTC$(1, 2)'clo
t-1
9000      INPUT #1, ID$, ISLOT, CHAN%, A2D%, IGAIN, freq, NS, ICAL, FCAL$, FTC$(2, 1)'cli
n-2
9100      INPUT #1, ID$, ISLOT, CHAN%, A2D%, IGAIN, freq, NS, ICAL, FCAL$, FTC$(2, 2)'clo
t-2
9200      INPUT #1, ID$, ISLOT, CHAN%, A2D%, IGAIN, freq, NS, ICAL, FCAL$, FTC$(3, 1)'cli
n-3
9300      INPUT #1, ID$, ISLOT, CHAN%, A2D%, IGAIN, freq, NS, ICAL, FCAL$, FTC$(3, 2)'clo
t-3
9400      INPUT #1, ID$, ISLOT, CHAN%, A2D%, IGAIN, freq, NS, ICAL, FCAL$, FTC$(4, 1)'cli
n-4
9500      INPUT #1, ID$, ISLOT, CHAN%, A2D%, IGAIN, freq, NS, ICAL, FCAL$, FTC$(4, 2)'clo
t-4
9600      INPUT #1, ID$, ISLOT, CHAN%, A2D%, IGAIN, freq, NS, ICAL, FCAL$, FTC$(5, 1)'cli
n-5
9700      INPUT #1, ID$, ISLOT, CHAN%, A2D%, IGAIN, freq, NS, ICAL, FCAL$, FTC$(5, 2)'clo
t-5
9800      INPUT #1, ID$, ISLOT, CHAN%, A2D%, IGAIN, freq, NS, ICAL, FCAL$, FTC$(6, 1)'cli
n-6
9900      INPUT #1, ID$, ISLOT, CHAN%, A2D%, IGAIN, freq, NS, ICAL, FCAL$, FTC$(6, 2)'clo
t-6
10000      INPUT #1, ID$, ISLOT, CHAN%, A2D%, IGAIN, freq, NS, ICAL, FCAL$, FTC$(7, 1)'cl
in-7
10100      INPUT #1, ID$, ISLOT, CHAN%, A2D%, IGAIN, freq, NS, ICAL, FCAL$, FTC$(7, 2)'cl
ot-7
10110      INPUT #1, ID$, ISLOT, CHAN%, A2D%, IGAIN, freq, NS, ICAL, FCAL$, FTC$(8, 1)'cl
in-8
10120      INPUT #1, ID$, ISLOT, CHAN%, A2D%, IGAIN, freq, NS, ICAL, FCAL$, FTC$(8, 2)'cl
ot-8
10130      INPUT #1, ID$, ISLOT, CHAN%, A2D%, IGAIN, freq, NS, ICAL, FCAL$, FTC$(9, 1)'cl
in-9
10140      INPUT #1, ID$, ISLOT, CHAN%, A2D%, IGAIN, freq, NS, ICAL, FCAL$, FTC$(9, 2)'cl
ot-9
10150      INPUT #1, ID$, ISLOT, CHAN%, A2D%, IGAIN, freq, NS, ICAL, FCAL$, FTC$(10, 1)'c
l1n-10
10160      INPUT #1, ID$, ISLOT, CHAN%, A2D%, IGAIN, freq, NS, ICAL, FCAL$, FTC$(10, 2)'c
lot-10
10170      INPUT #1, ID$, ISLOT, CHAN%, A2D%, IGAIN, freq, NS, ICAL, FCAL$, FTC$(11, 1)'c
l1n-11
10180      INPUT #1, ID$, ISLOT, CHAN%, A2D%, IGAIN, freq, NS, ICAL, FCAL$, FTC$(11, 2)'c
lot-11
10190      INPUT #1, ID$, ISLOT, CHAN%, A2D%, IGAIN, freq, NS, ICAL, FCAL$, FTC$(12, 1)'c
l1n-12
10195      INPUT #1, ID$, ISLOT, CHAN%, A2D%, IGAIN, freq, NS, ICAL, FCAL$, FTC$(12, 2)'c
lot-12
10200      INPUT #1, ID$, ISLOT, CHAN%, A2D%, IGAIN, freq, NS, ICAL, FCAL$, F$(1, 1)'hf-1
a
10300      INPUT #1, ID$, ISLOT, CHAN%, A2D%, IGAIN, freq, NS, ICAL, FCAL$, F$(1, 2)'   1
b
10400      INPUT #1, ID$, ISLOT, CHAN%, A2D%, IGAIN, freq, NS, ICAL, FCAL$, F$(1, 3)'   1
c
10500      INPUT #1, ID$, ISLOT, CHAN%, A2D%, IGAIN, freq, NS, ICAL, FCAL$, F$(1, 4)'   1
d
10600      INPUT #1, ID$, ISLOT, CHAN%, A2D%, IGAIN, freq, NS, ICAL, FCAL$, F$(2, 1)'hf-2
a
10700      INPUT #1, ID$, ISLOT, CHAN%, A2D%, IGAIN, freq, NS, ICAL, FCAL$, F$(2, 2)'   2
b
10800      INPUT #1, ID$, ISLOT, CHAN%, A2D%, IGAIN, freq, NS, ICAL, FCAL$, F$(2, 3)'   2
c
10900      INPUT #1, ID$, ISLOT, CHAN%, A2D%, IGAIN, freq, NS, ICAL, FCAL$, F$(2, 4)'   2d
11000      INPUT #1, ID$, ISLOT, CHAN%, A2D%, IGAIN, freq, NS, ICAL, FCAL$, F$(3, 1)'hf-3a
11100      INPUT #1, ID$, ISLOT, CHAN%, A2D%, IGAIN, freq, NS, ICAL, FCAL$, F$(3, 2)'   3b
11200      INPUT #1, ID$, ISLOT, CHAN%, A2D%, IGAIN, freq, NS, ICAL, FCAL$, F$(3, 3)'   3c
11300      INPUT #1, ID$, ISLOT, CHAN%, A2D%, IGAIN, freq, NS, ICAL, FCAL$, F$(3, 4)'   3d
11400      INPUT #1, ID$, ISLOT, CHAN%, A2D%, IGAIN, freq, NS, ICAL, FCAL$, F$(4, 1)'hf-4a
11500      INPUT #1, ID$, ISLOT, CHAN%, A2D%, IGAIN, freq, NS, ICAL, FCAL$, F$(4, 2)'   4b
11600      INPUT #1, ID$, ISLOT, CHAN%, A2D%, IGAIN, freq, NS, ICAL, FCAL$, F$(4, 3)'   4c
11700      INPUT #1, ID$, ISLOT, CHAN%, A2D%, IGAIN, freq, NS, ICAL, FCAL$, F$(4, 4)'   4d
11800      INPUT #1, ID$, ISLOT, CHAN%, A2D%, IGAIN, freq, NS, ICAL, FCAL$, F$(5, 1)'hf-5a
11900      INPUT #1, ID$, ISLOT, CHAN%, A2D%, IGAIN, freq, NS, ICAL, FCAL$, F$(5, 2)'   5b
12000      INPUT #1, ID$, ISLOT, CHAN%, A2D%, IGAIN, freq, NS, ICAL, FCAL$, F$(5, 3)'   5c
12100      INPUT #1, ID$, ISLOT, CHAN%, A2D%, IGAIN, freq, NS, ICAL, FCAL$, F$(5, 4)'   5d
12200      INPUT #1, ID$, ISLOT, CHAN%, A2D%, IGAIN, freq, NS, ICAL, FCAL$, F$(6, 1)'hf-6a
12300      INPUT #1, ID$, ISLOT, CHAN%, A2D%, IGAIN, freq, NS, ICAL, FCAL$, F$(6, 2)'   6b
12400      INPUT #1, ID$, ISLOT, CHAN%, A2D%, IGAIN, freq, NS, ICAL, FCAL$, F$(6, 3)'   6c
12500      INPUT #1, ID$, ISLOT, CHAN%, A2D%, IGAIN, freq, NS, ICAL, FCAL$, F$(6, 4)'   6d
12600      INPUT #1, ID$, ISLOT, CHAN%, A2D%, IGAIN, freq, NS, ICAL, FCAL$, F$(7, 1)'hf-7a
12700      INPUT #1, ID$, ISLOT, CHAN%, A2D%, IGAIN, freq, NS, ICAL, FCAL$, F$(7, 2)'   7b
12800      INPUT #1, ID$, ISLOT, CHAN%, A2D%, IGAIN, freq, NS, ICAL, FCAL$, F$(7, 3)'   7c
12900      INPUT #1, ID$, ISLOT, CHAN%, A2D%, IGAIN, freq, NS, ICAL, FCAL$, F$(7, 4)'   7d
12905      INPUT #1, ID$, ISLOT, CHAN%, A2D%, IGAIN, freq, NS, ICAL, FCAL$, F$(8, 1)'hf-8a
12910      INPUT #1, ID$, ISLOT, CHAN%, A2D%, IGAIN, freq, NS, ICAL, FCAL$, F$(8, 2)'   8b
12915      INPUT #1, ID$, ISLOT, CHAN%, A2D%, IGAIN, freq, NS, ICAL, FCAL$, F$(8, 3)'   8c
12920      INPUT #1, ID$, ISLOT, CHAN%, A2D%, IGAIN, freq, NS, ICAL, FCAL$, F$(8, 4)'   8d
12925      INPUT #1, ID$, ISLOT, CHAN%, A2D%, IGAIN, freq, NS, ICAL, FCAL$, F$(9, 1)'hf-9a
12930      INPUT #1, ID$, ISLOT, CHAN%, A2D%, IGAIN, freq, NS, ICAL, FCAL$, F$(9, 2)'   9b
12935      INPUT #1, ID$, ISLOT, CHAN%, A2D%, IGAIN, freq, NS, ICAL, FCAL$, F$(9, 3)'   9c
12940      INPUT #1, ID$, ISLOT, CHAN%, A2D%, IGAIN, freq, NS, ICAL, FCAL$, F$(9, 4)'   9d
12945      INPUT #1, ID$, ISLOT, CHAN%, A2D%, IGAIN, freq, NS, ICAL, FCAL$, F$(10, 1)'hf-1
0a
12950      INPUT #1, ID$, ISLOT, CHAN%, A2D%, IGAIN, freq, NS, ICAL, FCAL$, F$(10, 2)'   1
0b
12955      INPUT #1, ID$, ISLOT, CHAN%, A2D%, IGAIN, freq, NS, ICAL, FCAL$, F$(10, 3)'   1
0c
12960      INPUT #1, ID$, ISLOT, CHAN%, A2D%, IGAIN, freq, NS, ICAL, FCAL$, F$(10, 4)'   1
0d
12965      INPUT #1, ID$, ISLOT, CHAN%, A2D%, IGAIN, freq, NS, ICAL, FCAL$, F$(11, 1)'hf-1
1a
12970      INPUT #1, ID$, ISLOT, CHAN%, A2D%, IGAIN, freq, NS, ICAL, FCAL$, F$(11, 2)'   1
1b
12975      INPUT #1, ID$, ISLOT, CHAN%, A2D%, IGAIN, freq, NS, ICAL, FCAL$, F$(11, 3)'   1
1c
12980      INPUT #1, ID$, ISLOT, CHAN%, A2D%, IGAIN, freq, NS, ICAL, FCAL$, F$(11, 4)'   1
1d
12985      INPUT #1, ID$, ISLOT, CHAN%, A2D%, IGAIN, freq, NS, ICAL, FCAL$, F$(12, 1)'hf-1
2a
12990      INPUT #1, ID$, ISLOT, CHAN%, A2D%, IGAIN, freq, NS, ICAL, FCAL$, F$(12, 2)'   1
2b
12995      INPUT #1, ID$, ISLOT, CHAN%, A2D%, IGAIN, freq, NS, ICAL, FCAL$, F$(12, 3)'   1
2c
12997      INPUT #1, ID$, ISLOT, CHAN%, A2D%, IGAIN, freq, NS, ICAL, FCAL$, F$(12, 4)'   1
2d
13000      CLOSE #1
13100      REM
13200      REM  compute mean and stdev
13300      REM
13305      FOR k = 1 TO nhfm
13400            OPEN FTEM$(k) FOR INPUT AS #1
13500            GOSUB 27600
13600            XMEAN = dsum# / NS
13601            tmix(k) = XMEAN
13700            TMIXSTD(k) = (ABS((DVAR# / NS) - XMEAN ^ 2)) ^ .5
```

```
13705      NEXT k
13701      OPEN FSTEM$ FOR INPUT AS #1
13702      GOSUB 27600
13703      XMEAN = dsum# / NS
13704      TSTEAM = XMEAN
13800      TSTESTD = (ABS((DVAR# / NS) - XMEAN ^ 2)) ^ .5
13900      FOR k = 1 TO nhfm
14000         FOR j = 1 TO ntc
14100            OPEN F$(k, j) FOR INPUT AS #1
14200            GOSUB 27600
14300            XMEAN = dsum# / NS
14400            temp(k, j) = XMEAN
14500            SD(k, j) = (ABS((DVAR# / NS) - XMEAN ^ 2)) ^ .5
14600         NEXT j
14700      NEXT k
14800      FOR k = 1 TO nhfm
14900         FOR j = 1 TO 2
15000            OPEN FTC$(k, j) FOR INPUT AS #1
15100            GOSUB 27600
15200            XMEAN = dsum# / NS
15300            tc(k, j) = XMEAN
15400            sdtc(k, j) = (ABS((DVAR# / NS) - XMEAN ^ 2)) ^ .5
15500         NEXT j
15600      NEXT k
15700      REM
15800      REM  curve fitting - compute gradients, heat fluxes,
15900      REM       surface temperatures (and mean), and back temp.'s
15950      REM       linear least squares method
16000      REM
16100      tsurfa = 0!
16200      FOR k = 1 TO nhfm
16300         sumx = 0!
16400         sumx2 = 0!
16500         sumy = 0!
16600         SUMY2 = 0!
16700         SUMXY = 0!
16800         FOR j = 1 TO ntc
16900            sumx = sumx + x(k, j)
17000            sumx2 = sumx2 + x(k, j) ^ 2!
17100            sumy = sumy + temp(k, j)
17200            SUMY2 = SUMY2 + temp(k, j) ^ 2!
17300            SUMXY = SUMXY + x(k, j) * temp(k, j)
17400         NEXT j
17405         xbar = sumx / ntc
17410         ybar = sumy / ntc
17415         denom = sumx2 - ntc * xbar ^ 2
17500         dtdx(k) = (SUMXY - ntc * xbar * ybar) / denom
17501   REM these values are to calibrate the thermocouple probes
17502         IF (k = 1) THEN dtdx(k) = dtdx(k) + .00297
17503         IF (k = 2) THEN dtdx(k) = dtdx(k) + .004067
17504         IF (k = 3) THEN dtdx(k) = dtdx(k) - .002008768
17505         IF (k = 4) THEN dtdx(k) = dtdx(k) - .002261768
17506         IF (k = 5) THEN dtdx(k) = dtdx(k) + .001975948
17507         IF (k = 6) THEN dtdx(k) = dtdx(k) + .007618658
17508         IF (k = 7) THEN dtdx(k) = dtdx(k) + .001433858
17509         IF (k = 8) THEN dtdx(k) = dtdx(k) + 0!
17510         IF (k = 9) THEN dtdx(k) = dtdx(k) - .000432148
17511         IF (k = 10) THEN dtdx(k) = dtdx(k) + 0!
17512         IF (k = 11) THEN dtdx(k) = dtdx(k) - .0053
17513         IF (k = 12) THEN dtdx(k) = dtdx(k) + .0046637
17600         Tback(k) = ybar - dtdx(k) * xbar
17650
17700         hf(k) = kal * dtdx(k) * 100000!
17725         REM
17750         REM  take into acount the thermal conductivity of the CZn pain
17775         REM
17800         Tinfac(k) = 38.3705 * dtdx(k) + Tback(k)

17805         REM dcarb is the thicknesn of the carborinc coating
17810         REM kal and kzn are the conductivities of the aluminum and zinc

17850         tsurf(k) = dcarb * kal / kzn * dtdx(k) + Tinfac(k)
17900         tsurfa = tsurfa + tsurf(k)
17950         dtmixwall(k) = tmix(k) - tsurf(k)
18000         htc(k) = hf(k) / dtmixwall(k)
18100      NEXT k
18200      tsurfa = tsurfa / nhfm
18300      REM
18400      REM  compute fitting error & various statistical quantities
18500      REM
18600      FOR k = 1 TO nhfm
18700         var = 0!
18705         sum = 0!
19200         xsqrsum = 0!
19300         FOR j = 1 TO ntc
19400            TFIT = Tback(k) + x(k, j) * dtdx(k)
19500            var = var + (temp(k, j) - TFIT) ^ 2!
20000            xsqrsum = xsqrsum + x(k, j) ^ 2!
20005            sum = sum + x(k, j)
20100         NEXT j
20101         sigmatb(k) = SQR((var / ntc * xsqrsum) / (ntc * xsqrsum - sum ^ 2))
20105         sigdtdx(k) = SQR((var * ntc) / (ntc * xsqrsum - sum ^ 2))
20150      REM
20155      REM       standard error of estimate of the heat flux
20180      REM
20300         qerr(k) = hf(k) * SQR((sigkal / kal) ^ 2 + (sigdtdx(k) / dtdx(k)) ^ 2)
20302      REM error in interface temp used x=plate thickness, error in x=.50mm
20305         Tinerr(k) = SQR(sigmatb(k) ^ 2 + 38.3705 ^ 2 * sigdtdx ^ 2 + dtdx(k) ^ 2 * .
5 ^ 2)
20500      NEXT k
20600      REM
20700      REM  overall heat flux and average heat transfer coef.
20800      REM
20805      htcavv = 0
20810      htcavv = 0
20900      HTCAVh1 = 0!
21000      HTCAVh2 = 0!
21100      FOR k = 1 TO nhfm
21105       IF (k > 6) THEN GOTO 21605
21200       HFAVG(k) = flow(k) * 4182! * (tc(k, 2) - tc(k, 1)) / (60! * LENGTH * PWIDTH)
21300       htcavg(k) = HFAVG(k) / dtmixwall(k)
21400       HTCAVh1 = HTCAVh1 + htcavg(k)
21500       HTCAVh2 = HTCAVh2 + htc(k)
21600       IF (k < 7) THEN GOTO 21690
21605       HFAVG(k) = flow(k) * 4182! * (tc(k, 2) - tc(k, 1)) / (60! * LENGTH * PWIDTH)
21610       htcavg(k) = HFAVG(k) / dtmixwall(k)
21615       htcavv1 = htcavv1 + htcavg(k)
21620       htcavv2 = htcavv2 + htc(k)
21690      NEXT k
21700      REM  Coolant Energy Balance Average
21800      HTCAVh1 = HTCAVh1 / 6
21805      htcavv1 = htcavv1 / 6
21900      REM  Heat Flux Meter Average
22000      HTCAVh2 = HTCAVh2 / 6
22005      htcavv2 = htcavv2 / 6
22010      REM
22020      REM  now the error estimates for heat transfer coefficients
22030      REM  used propagation of errors for calculations pp 58-60 journal #1
```

```
22040     FOR k = 1 TO nhfm
22041     sdsurf(k) = SQR((dcarb / kzn * dtdx(k) * sigkal) ^ 2 + (kal / kzn * dcarb * dt
dx(k) * sigzn) ^ 2 + (dcarb * kal / kzn * sigdtdx(k)) ^ 2 + Tinerr(k) ^ 2)
22045     sdtdelt(k) = SQR(sdsurf(k) ^ 2 + TMIXSTD(k) ^ 2)
22050     hfmerr(k) = ABS(htc(k) * SQR((qerr(k) / hf(k)) ^ 2 + (sdtdelt(k) / dtmixwall(k
)) ^ 2))
22055     sigtc(k) = SQR(sdtc(k, 1) ^ 2 + sdtc(k, 2) ^ 2)
22060     sigqceb(k) = ABS(htcavg(k) * SQR((sigflow / flow(k)) ^ 2 + (sigtc(k) / (tc(k,
2) - tc(k, 1))) ^ 2 + 1.609E-05))
22065     ceberr(k) = ABS(htcavg(k) * SQR((sigflow / flow(k)) ^ 2 + (sigtc(k) / (tc(k, 2
) - tc(k, 1))) ^ 2 + 1.609E-05 + (sdtdelt(k) / dtmixwall(k)) ^ 2))
22080   NEXT k
22100   REM
22200   REM  output section
22300   REM
22400   OPEN "THERM" + RIGHT$(STR$(TESTNO!), (LEN(STR$(TESTNO!)) - 1)) + ".OUT" FOR OUT
PUT AS #2
23095   PRINT #2,
23100   PRINT #2, "  Test section temperature  Tmix:"
23105   FOR k = 1 TO nhfm
23110   IF (k = 3 OR k = 5 OR k = 7 OR k = 9 OR k = 11) THEN GOTO 23305
23200   PRINT #2, USING "                                                ##.##"; tmix(k);
23300   PRINT #2, USING " +/- ##.###"; TMIXSTD(k)
23305   NEXT k
23310   PRINT #2,
23340   PRINT #2, "     Steam temperature:                 ";
23350   PRINT #2, USING "###.##"; TSTEAM;
23360   PRINT #2, USING " +/- ##.###"; TSTESTD
23400   PRINT #2,
23500   PRINT #2, "  HEAT FLUX METER DATA:"
23600   PRINT #2,
23700   PRINT #2, "  HF meter   Tback     Tsurface              dT/dx                  Hea
t flux"
23800   FOR k = 1 TO nhfm
23900     PRINT #2, USING "   ##        ##.##     ##.## +/- #.###      #.#### +/- #.##
##     #####. +/- ###"; k; Tback(k); tsurf(k); sdsurf(k); dtdx(k); sigdtdx(k); hf(k); qe
rr(k)
24000   NEXT k
24100   PRINT #2,
24200   PRINT #2, "  COOLANT LOOP ENERGY BALANCE DATA:"
24300   PRINT #2,
24400   PRINT #2, "     C-loop      Tin       Tout       dT        Cool Flow      Heat
flux"
24500   FOR k = 1 TO nhfm
24600     PRINT #2, USING "        ##     ##.##         ##.##    #.####      #.##
    #####. +/- ###"; k; tc(k, 1); tc(k, 2); tc(k, 2) - tc(k, 1); flow(k) / 60; HFAVG(k);
 sigqceb(k)
24700   NEXT k
24800   PRINT #2,
24900   PRINT #2, "  TEMPERATURES"
25000   PRINT #2,
25100   PRINT #2, USING "     tsurf avg          =     ##.#"; tsurfa
25200   PRINT #2,
25300   PRINT #2, "          tc-a    tc-b    tc-c    tc-d"
25400   FOR k = 1 TO nhfm
25500     PRINT #2, USING "      ##   ##.##   ##.##   ##.##   ##.##"; k; temp(k, 1); t
emp(k, 2); temp(k, 3); temp(k, 4)
25600   NEXT k
25700   PRINT #2,
25800   PRINT #2, "  HEAT TRANSFER COEFFICIENTS"
25900   PRINT #2,
26000   PRINT #2, "  HF meter    HTC HFM's (W/m2-C)      HTC  CEB's (W/m2-C)      Diff.
 (%)"
26100   FOR k = 1 TO nhfm
26200     PRINT #2, USING "     ##     #####.## +/- ##.##       #####.## +/- ##.##
    ####.#"; k; htc(k); hfmerr(k); htcavg(k); ceberr(k); (htcavg(k) / htc(k) - 1) * 1
00!
26300   NEXT k
26400   PRINT #2,
26500   PRINT #2, USING "   Horizontal plate Average HTC Heat Flux Meters (HFM)        -
  #####.##"; HTCAVh2
26600   PRINT #2, USING "   Horizontal plate Average HTC Coolant Energy Balance (CEB)  -
  #####.##"; HTCAVh1
26605   PRINT #2, USING "   Vertical plate Average HTC Heat Flux Meters (HFM)          -
  #####.##"; htcavv2
26610   PRINT #2, USING "   Vertical plate Average HTC Coolant Energy Balance (CEB)    -
  #####.##"; htcavv1
26700   CLOSE #2
27400   END
27500   REM
27600   REM  statistics subroutine
27700   REM
27800   dsum# = 0#
27900   DVAR# = 0#
28000   INPUT #1, header$
28100   freq = VAL(MID$(header$, 43, 8))
28200   NS = VAL(MID$(header$, 51, 7))
28300   PRINT header$
28400   FOR I = 1 TO NS
28500      INPUT #1, time, TT
28600      dsum# = dsum# + TT
28700      DVAR# = DVAR# + TT * TT
28800   NEXT I
28900   CLOSE #1
29000   RETURN
29100   END
```

Appendix 3

Error Analysis Theory

The use of the Linear Least Squares Fit was used to determine the best slope and intercept of the line defining the heat flux. Since we have a slab geometry we can assume that the heat flux through the condensing surface is linear. Therefore we wish to find the best values for the equation of a line.

$$y = mx + b$$

If we assume that the distribution of the values obtained from the measurement of the temperatures in the plate are governed by Gaussian statistics then the best values of the slope (m) and the intercept (b) are given by the minimization of the following equation:

$$D^2 = \Sigma \frac{1}{\sigma_i^2}\left[y_i - (mx_i - b_i)\right]^2$$

where σ is a weighting factor. The above equation can then be minimized to find a pair of simultaneous equations which can be solved for the slope and the intercept. The equations for the best value of the slope and the best value of the y-intercept are as follows:

$$m = \frac{\sum_i^n x_i y_i - N\bar{x}_i\bar{y}_i}{\sum_i^n x_i^2 - N(\bar{x})^2}$$

$$y_{int} = b = \bar{y} - m\bar{x}$$

Where the bar over the x and y corresponds to the average values of x and y.

The errors in the slope and intercept can then be found using the matrix Inversion method of the linear least squares. The equation of the line can be written in matrix notation as follows:

$$|Y| = |X| \left| \frac{b}{m} \right|$$

where:

$$|Y| = \begin{vmatrix} \sum_i^n \frac{1}{\sigma_i^2} y_i \\ \sum_i^n \frac{1}{\sigma_i^2} y_i x_i \end{vmatrix}$$

and

$$|X| = \begin{vmatrix} \sum_i^n \frac{1}{\sigma_i^2} & \sum_i^n \frac{x_i}{\sigma_i^2} \\ \sum_i^n \frac{x_i}{\sigma_i^2} & \sum \frac{x_i^2}{\sigma_i^2} \end{vmatrix}$$

From these equations one can then find the following equations for the variance of the slope and intercept.

$$\sigma_b^2 = \frac{\sigma^2 \sum x_i^2}{N \sum x_i^2 - (\sum x_i)^2}$$

$$\sigma_m^2 = \frac{\sigma^2 N}{N \sum x_i^2 - (\sum x_i)^2}$$

Error in the heat transfer coefficient derived from the heat flux:

The equation for the heat flux is given by the equation:

$$q_i'' = k \frac{dT}{dx}$$

Now using the theory of Propagation or Combination of errors we can find the uncertainty in the heat flux:

$$\sigma_q = q'' \sqrt{(\frac{\sigma_k}{k})^2 + (\frac{\sigma_m}{m})^2}$$

Where again the slope or dT/dx of the best line is given by m. In the above analysis the uncertainty in the slope is essentially dependent on the statistical standard deviation of the temperature measurements. This can be assumed if we are concerned with the difference in the temperature measurements and if the absolute temperatures are the same when no heat flux is present. We are then effectively using the measured resolution of the thermocouple as the defining error in the heat flux. The term k in the above equation is the conductivity of the aluminum plate. The value and standard error for this was taken as 1.3179 +/- 0.72 w/cmK, however the absolute error in the heat flux is due to the error in the slope.

The heat transfer coefficient can be found from the heat flux with the following equation:

$$h = q''/\Delta T_{mix}$$

with an associated standard error given by:

$$\sigma_h = h \sqrt{(\frac{\sigma_q}{q})^2 + (\frac{\sigma_{\Delta T_{mix}}}{\Delta T_{mix}})^2}$$

where the error in ΔT_{mix} was obtained by similar combination of errors.

Error in the heat transfer coefficient derived from the coolant energy balance:

An energy balance on the coolant water results in the following equation:

$$q_i = \frac{\rho_{cool} Cp (V \Delta \dot{T}_{cool})_i}{A_i}$$

Since the maximum change in the density and heat capacity over the range of the temperature difference is only 0.2 percent, this was neglected. The heat transfer coefficient is given by the equation:

$$h = q'' / \Delta T_{mix}$$

with an associated error of

$$\sigma_h = h \sqrt{(\frac{\sigma_{\dot{V}}}{\dot{V}})^2 + (\frac{\sigma_{\Delta T}}{\Delta T})^2 + (\frac{\sigma_A}{A})^2 + (\frac{\sigma_{\Delta T_{mix}}}{\Delta T_{mix}})^2}$$

Where ΔT_{mix} is the bulk mixture temperature minus the plate surface temperature. ΔT is the temperature difference between the water inlet temperature and the water outlet temperature of the coolant plate. The errors associated with this was obtained from the standard deviation of the ensomble measured.

Appendix 4

Calibration of Turbine Meter

This appendix consists of the calibration of the Hontzsh turbine anomometer that was done by Colorado Engineering Experiment Station Inc.

CEESI

LABORATORY/OFFICE:
54043 County Rd. 37
Nunn, Colo. 80648
Phone: 303-897-2711
FAX: 303-897-2710

COLORADO ENGINEERING EXPERIMENT STATION INC.

CERTIFICATE OF CALIBRATION

This calibration is traceable to the

NATIONAL INSTITUTE OF STANDARDS AND TECHNOLOGY

Model: Hontzsch Serial Number: 20163

For: University of Wisconsin Order:

Data File: 94UOW1 Date: 1 July 1994 Disc: 0794-003

The uncertainty in indicated flowrate is estimated to be +/- 0.5 % of reading to 95% confidence.

The instrumentation used in the above calibration is traceable through standards calibrated under the following NIST test numbers:

737/228509, 215451, 202491, 184984, 213426, 209527, 222173, TN-249770, TN-250722, TN-246108, 811-249971, and 811/249886

This calibration was performed in accordance with PROC-010 rev 4 and MIL-STD 45662A.

This Calibration is: [x] As Found [ ] As Left

Calibration performed by: Roger Keeton

Dean M. Standiford
Asst. Quality Assurance Manager

Steve Caldwell For
Vice President

CEESI

LABORATORY/OFFICE:
54043 County Rd. 37
Nunn, Colo. 80648
Phone: 303-897-2711
FAX: 303-897-2710

COLORADO ENGINEERING EXPERIMENT STATION INC.

CERTIFICATE OF CALIBRATION

This calibration is traceable to the

NATIONAL INSTITUTE OF STANDARDS AND TECHNOLOGY

Model: Hontzsch Serial Number: 20163

For: University of Wisconsin Order:

Data File: 94UOW2 Date: 6 July 1994 Disc: 0794-003

The uncertainty in indicated flowrate is estimated to be +/- 0.5 % of reading to 95% confidence.

The instrumentation used in the above calibration is traceable through standards calibrated under the following NIST test numbers:

737/228509, 215451, 202491, 184984, 213426, 209527, 222173, TN-249770, TN-250722, TN-246108, 811-249971, and 811/249886

This calibration was performed in accordance with PROC-010 rev 4 and MIL-STD 45662A.

This Calibration is: [X] As Found [X] As Left

Calibration performed by: Roger Keeffe

Dean M. Standiford
Asst. Quality Assurance Manager

Steve Caldwell FOR
Vice President

CEESI

LABORATORY/OFFICE:
54043 County Rd. 37
Nunn, Colo. 80648
Phone: 303-897-2711
FAX: 303-897-2710

COLORADO ENGINEERING EXPERIMENT STATION INC.

Calibration of an Anemometer (forward flow)
Model: Hontzsch Serial Number: 20163
For: University of Wisconsin Order:
Data File: 94UOW2 Date: 6 July 1994 Disc: 0794-003
Inlet diameter: 12 inches Throat diameter: 3.248 inches
Test gas: AIR Standard density= .074915 lbm/cu-ft
at standard conditions of 529.69 deg R, and 14.696 psia
Mtr Vel: Meter calculated velocity(ft/sec), 13.124*Volts-65.62
Velocity: Actual mean velocity, ft/sec
Volts: Meter output in vdc
K Factor: Mtr Vel/Velocity
Press: Inlet static pressure in psia
Temp: Inlet temperature in degrees Rankine
Density: Inlet density in pounds mass per cubic foot
Zero reading at no flow: 5.00244

L	Volts	Velocity	Mtr Vel	K Factor	Density
1	9.355	52.769	57.155	1.083	0.06121
2	8.9719	48.066	52.127	1.084	0.06121
3	8.5528	42.969	46.627	1.085	0.06123
4	8.9308	47.517	51.588	1.086	0.06123
5	8.186	38.489	41.813	1.086	0.06124
6	7.8129	34.006	36.917	1.086	0.06124
7	8.184	38.485	41.787	1.086	0.06124
8	7.4428	29.522	32.059	1.086	0.06125
9	7.0711	25.046	27.181	1.085	0.06125
10	7.442	29.511	32.049	1.086	0.06126
11	6.705	20.576	22.377	1.088	0.06126
12	6.3367	16.139	17.543	1.087	0.06126
13	6.7049	20.568	22.375	1.088	0.06126
14	5.9761	11.729	12.810	1.092	0.06126
15	5.6326	7.4973	8.303	1.107	0.06125
16	5.9722	11.727	12.760	1.088	0.06124
17	5.4128	5	5.417	1.083	0.06123
18	5.254	3.1366	3.333	1.063	0.06120
19	5.4121	5.0004	5.408	1.082	0.06120

Average values for above results:
Press: 12.078 psia Density: .061238 lbm/cu-ft
Temp: 532.51 Deg R Viscosity: .0000010227 lbm/inch-sec
Compressibility factor: .99971

Post-it™ brand fax transmittal memo 7671 | # of pages ▸

To Mark Anderson	From Sean
Co. University of Wisconsin	Co.
Dept.	Phone # H.P. Model
Fax # 1-208-262-6707	Fax # 3440 1A

CEESI

LABORATORY/OFFICE:
54043 County Rd. 37
Nunn, Colo. 80648
Phone: 303-897-2711
FAX: 303-897-2710

COLORADO ENGINEERING EXPERIMENT STATION INC.

Calibration of an Anemometer (reverse flow)
Model: Hontzsch Serial Number: 20163
For: University of Wisconsin Order:
Data File: 94UOW1 Date: 1 July 1994 Disc: 0794-003
Inlet diameter: 12 inches Throat diameter: 3.248 inches
Test gas: AIR Standard density= .074915 lbm/cu-ft
at standard conditions of 529.69 deg R, and 14.696 psia
Mtr Vel: Meter calculated velocity(ft/sec), 13.124*Volts-65.62
Velocity: Actual mean velocity, ft/sec
Volts: Meter output in vdc
K Factor: Mtr Vel/Velocity
Press: Inlet static pressure in psia
Temp: Inlet temperature in degrees Rankine
Density: Inlet density in pounds mass per cubic foot
Zero reading at no flow: 5.001574

L	Volts	Velocity	Mtr Vel	K Factor	Density
1	.72795	51.773	-56.066	-1.083	0.06124
2	1.1012	47.301	-51.167	-1.082	0.06125
3	1.4692	42.85	-46.338	-1.081	0.06125
4	1.1484	46.705	-50.549	-1.082	0.06126
5	1.8823	37.86	-40.917	-1.081	0.06126
6	2.2462	33.453	-36.141	-1.080	0.06126
7	1.8841	37.852	-40.894	-1.080	0.06126
8	2.6067	29.05	-31.410	-1.081	0.06126
9	2.9706	24.655	-26.634	-1.080	0.06125
10	2.6068	29.047	-31.408	-1.081	0.06125
11	3.3277	20.268	-21.947	-1.083	0.06124
12	3.6856	15.905	-17.251	-1.085	0.06124
13	3.327	20.268	-21.956	-1.083	0.06123
14	4.0408	11.566	-12.588	-1.088	0.06123
15	4.3836	7.3977	-8.090	-1.094	0.06119
16	4.0403	11.569	-12.595	-1.089	0.06118
17	4.5939	4.9382	-5.330	-1.079	0.06116
18	4.7529	3.1004	-3.243	-1.046	0.06112
19	4.5941	4.9405	-5.327	-1.078	0.06111

Average values for above results:
Press: 12.1 psia Density: .061222 lbm/cu-ft
Temp: 533.62 Deg R Viscosity: .0000010243 lbm/inch-sec
Compressibility factor: .99971

Calibration Curve for Vaine Anemometer

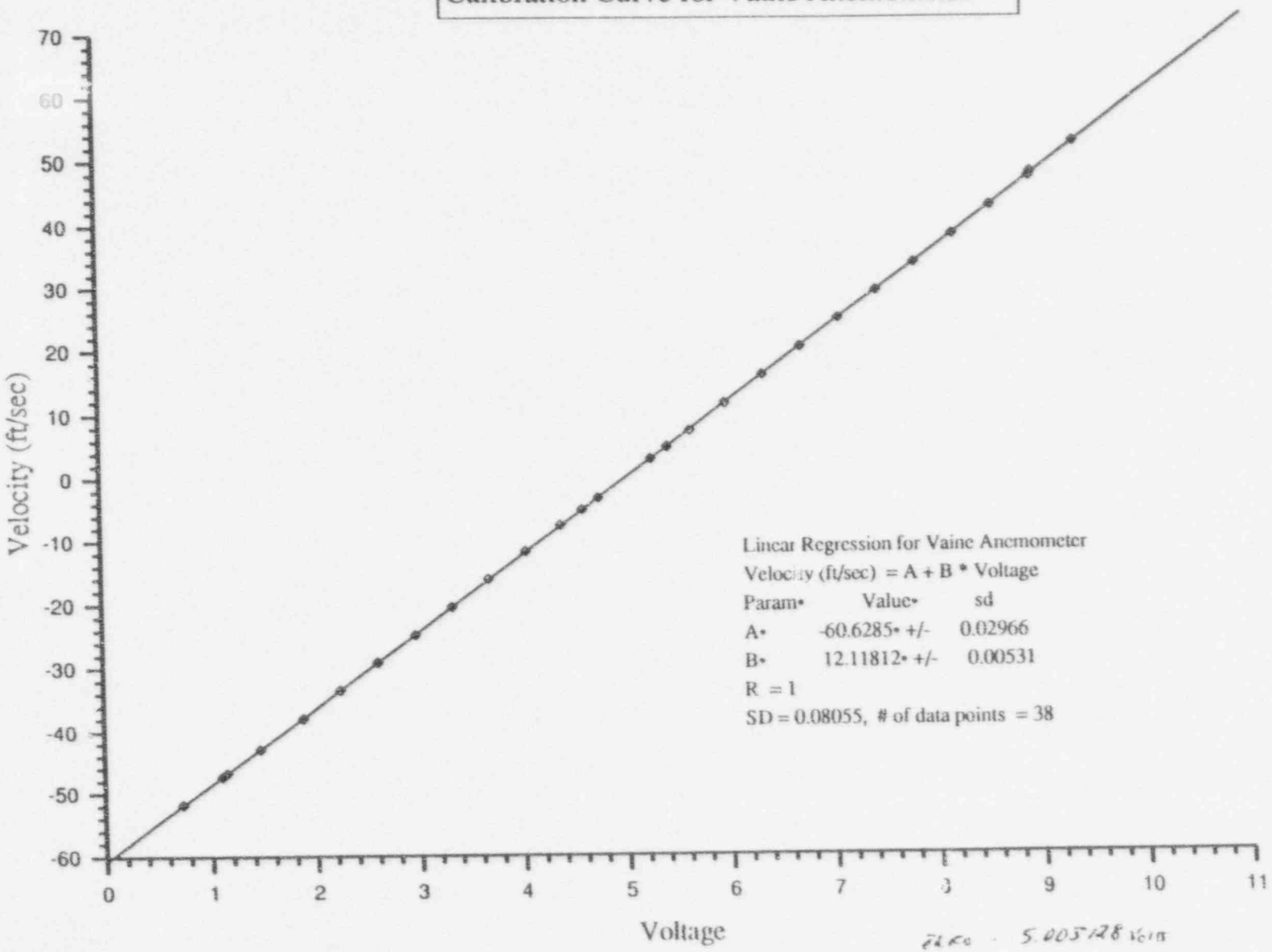

Linear Regression for Vaine Anemometer

Velocity (ft/sec) = A + B * Voltage

Param•	Value•	sd
A•	-60.6285• +/-	0.02966
B•	12.11812• +/-	0.00531

R = 1

SD = 0.08055, # of data points = 38

Full Scale = 5.005128 Volts

Appendix 5

Bibliography of Work Done at the University of Wisconsin

[1] M.H. Kim *Modeling of Condensation Heat Transfer in the Presence of Noncondensible Gas*, PhD Thesis 1986 [Modwl of Condensation H.T.- Correlation - 2D Model]

[2] J.J. Barry *Film Condensation in the Presence of Noncondensible Gas*, PhD Thesis 1988 [Experiments for Condensation on a Horizontal Surface]

[3] I.K. Huhtiniemi *Condensation in the Presence of Noncondensible Gas: Effect of Surface Orientation*, Prelim Thesis, 1990 [Ap600-1 Experiments and Initial AP600-2 Tests]

[4] I.K. Huhtiniemi *Condensation in the Presence of Noncondensible Gas:Effects of Surface Orientation* PhD Thesis 1992 [AP600-2 Experimental Test Series]

[5] A. Pernsteiner *Condensation in the Presence of Noncondensible Gas: Effect of Helium Concentration* MS Thesis 1993 [Helium- Air-Steam Tests with/without Forced Convection]

Refered Publications

[1] M.H. Kim, M.L. Corradini, *Modeling of Condensation Heat Transfer in a Reactor Containment* Nuclear Engineering Design, V118, 1990

[2] I Huhtiniemi, M.L. Corradini, *Condensation in the Presence of a Noncondensible Gas: Effect of Surface Orientation*, AIChE Symposium Series, No 269, Vol 85, S. B. Yilmaz, Ed. Aug. 1989

[3] I. Huhtiniemi, A. Pernsteiner, M. L. Corradini, *Steam Condensation in the Presence of Noncondensible Gas: Effect of Surface Orientation*, AIChE Symposium Series No. 283, Vol 87 S.B. Yilmaz, Editor July 1991

[4] I Huhtiniemi, A. Pernsteiner, M.L. Corradini, *Condensation in the Presence of Noncondensible Gases*, Nuclear Engr. Design (Accepted for publication in 1992)

[5] M.L. Corradini, *Natural convection Model for Condensation*, Internation Mtg. on Hydrogen Behavior, Albuquerque, NM Oct 1982

[6] M.L. Corradini, *Turbulant Condensation on a Cold Wall in the Presence of a Noncondensible Gas*, Second International Mtg on Nuclear Thermal- Hydraulics, Santa Barbra CA, Jan 1983

[7] M.H. Kim, M.L. Corradini, *Turbulent Condensation in a Noncondensible Gas*, ANS Proceedings of the Third International Meeting on Thermal-Hydraulics, Newport, RI Oct 1985

[8] J.J. Barry, M.L. Corradini, *Film Condensation in the Presence of Interfacial Waves*, ASME/AIChe National Heat Transfer Conference, Houston Tx July 1988

[9] I. Huntiniemi, J.J. Barry, M.L. Corridini, *Condensation in the Presence of Noncondensible Gas: The effects of Surface Orientation*, National Heat Transfer Conf. Philadelphia PA Aug 1989

[10] I. Huntiniemi, A Pernsteiner, M.L. Coradini, *Steam Condensation in the Presence of Noncondensible Gas: Effect of Helium*, National Heat Transfer Conference, Minneapolis MN July 1991

[11] A. Pernsteiner, I.K. Hyhtiniemi, M.L. Corradini, *Condensation in the Presence of Noncondensible Gases: Effects of Helium*, Proc of NURETH-5 Mtg, Salt Lake City UT Sept.1992